ESTIMATION OF THE THREE-DIMENSIONAL ANISOTROPIC SPATIAL COVARIANCE OF LOG PERMEABILITY USING SINGLE-HOLE AND CROSS-HOLE PACKER TEST DATA FROM FRACTURED GRANITES

by

Joseph Scott Depner

A Thesis Submitted to the Faculty of the

DEPARTMENT OF HYDROLOGY AND WATER RESOURCES

In Partial Fulfillment of the Requirements
For the Degree of

MASTER OF SCIENCE
WITH A MAJOR IN HYDROLOGY

In the Graduate College

THE UNIVERSITY OF ARIZONA

1 9 8 5

STATEMENT BY AUTHOR

This thesis has been submitted in partial fulfillment of requirements for an advanced degree at The University of Arizona and is deposited in the University Library to be made available to borrowers under rules of the Library.

Brief quotations from this thesis are allowable without special permission, provided that accurate acknowledgment of source is made. Requests for permission for extended quotation from or reproduction of this manuscript in whole or in part may be granted by the head of the major department or the Dean of the Graduate College when in his or her judgment the proposed use of the material is in the interests of scholarship. In all other instances, however, permission must be obtained from the author.

SIGNED: Joseph S. Depner

APPROVAL BY THESIS DIRECTOR

This thesis has been approved on the date shown below:

Shlomo P. Neuman
Professor of Hydrology
and Water Resources

10/30/85
Date

This thesis is dedicated to

my parents.

ACKNOWLEDGMENTS

This thesis was completed while I was employed as a research assistant by the Department of Hydrology and Water Resources, under the Nuclear Regulatory Commission contract NRC-04-78-275. I am grateful to Dr. Shlomo P. Neuman and Dr. Eugene S. Simpson, the principal investigators for the NRC project, for providing me with this excellent opportunity.

I would like to extend special thanks to my advisor, Dr. Shlomo Neuman, for his undying patience and guidance. I would also like to thank Dr. Don R. Davis and Dr. Tom Maddock III who, as members of my committee, made many helpful suggestions. Others who generously gave their time and assistance are Javier Samper, Dr. Don E. Myers, Steve Silliman, and Todd Rasmussen. Finally, I am indebted to my typist, Sally Adams. Her attitude while typing the more than 200 equations of this thesis was the very embodiment of the phrase "Perseverance furthers."

TABLE OF CONTENTS

TABLE OF CONTENTS--Continued

TABLE OF CONTENTS--Continued

LIST OF ILLUSTRATIONS

LIST OF ILLUSTRATIONS--Continued

LIST OF TABLES

ABSTRACT

The log permeability spatial covariance function is usually estimated by semivariogram analysis of local log permeability measurements. In the presence of statistical anisotropy, however, this method is sometimes impractical because it requires a large number of measurements. In this thesis, a methodology is developed which overcomes this difficulty by combining results from both small-scale and large-scale field tests. In particular, data from single-hole packer tests conducted in vertical boreholes drilled into granite near Oracle, Arizona, are combined with cross-hole test results to determine the three-dimensional covariance structure of the local log permeability field. The combination is based on a theoretical relationship between the effective permeability tensor of a rock mass and the spatial variability of local log permeabilities within the rock mass.

CHAPTER 1

INTRODUCTION

1.1 Purpose and Scope

To understand and predict the behavior of a hydrogeologic system, it has been traditional to adopt a deterministic approach based on physical principles. This approach requires:

(1) Identifying the variable(s) of interest (dependent variable(s))

(2) Identifying the independent variable(s)

(3) Identifying the governing physical laws and expressing them mathematically

(4) Specifying the appropriate initial and boundary conditions

(5) Estimating the spatial distribution of the physical parameters and (6) Solving the resulting problems by analytical, numerical, or analog methods.

The usefulness of the deterministic approach is limited because it provides no systematic method of treating either (1) the uncertainty associated with parameter estimates due to spatial variability and experimental error, (2) uncertainties in the initial and boundary conditions, or (3) the uncertainty associated with the resulting predictions of the dependent variable(s).

An alternative approach is to supplement the deterministic formulation with a stochastic analysis. This can be done in various

ways depending on the particular problem to be solved. For a review see Neuman (1982). For this study I shall focus on the statistical characterization of spatial variability of log permeability.

A statistical characterization of spatial variability can be accomplished by assuming that log permeability is a stochastic process characterized by a mean and a spatial covariance function and/or a semivariogram. The most common use of semivariograms is in connection with the stochastic interpolation technique known as kriging (Journel and Huijbregts, 1978; Delhomme, 1979; Gambolati and Volpi, 1979). Other uses include the analytical and numerical solution of stochastic differential equations (e.g., Bakr and others, 1978; Gutjahr and others, 1978; Dagan, 1979; Gutjahr and Gelhar, 1981; Gelhar and Axness, 1983a), deriving expressions for effective (deterministic) parameters (e.g., Gutjahr and others, 1978; Dagan, 1979; Gelhar and Axness, 1983a; Winter, Neuman and Newman, 1984), estimating such parameters, and studying the distribution of high-permeability channels in rocks (Silliman, 1985).

Because the log permeability covariance and/or semivariogram functions are generally direction dependent (anisotropic), their estimation requires a large amount of data. That is, many permeability measurements at points with various relative orientations are necessary. In most field applications the number of available data points is limited. Thus, it is necessary to develop covariance inference techniques that work with limited data. According to Gelhar (1985): "We need to find better methods of estimating input covariance

parameters including improvements in statistical methodology as well as an indirect method approach based on geologic information or bulk hydraulic properties." This thesis is an attempt to develop, demonstrate and better understand the application of an indirect method to the problem of log permeability covariance estimation. Specifically, it is an effort to show how information on bulk or effective permeability in three dimensions can be used to derive information about statistical anisotropy when the latter cannot be determined by standard geostatistical methods.

To demonstrate the technique, small-scale (single-hole) log permeability data and larger-scale directional (cross-hole) permeability data from a fractured granitic rock mass near Oracle, Arizona were analyzed. A brief description of the Oracle site, the field tests, and the procedures used to interpret the data is given in the remainder of this chapter.

In Chapter 2, I establish the general statistical framework, into which fit the spatial covariance function and the geostatistical methodology for its estimation. The concept of geometric statistical anisotropy and its quantitative description through the use of integral scales is especially important to the developments in following chapters. Chapter 3 is an application of the stochastic theory presented in Chapter 2 to steady-state, heterogeneous ground-water flow systems. The goal of this chapter is to derive, in detail, approximate analytical expressions for the large-scale effective permeability tensor, in terms of the statistical parameters of the local log permeability

field. Most of these results (except the section on geometric anisotropy) are due to Gelhar and Axness (1983a).

In Chapter 4, I apply the stochastic theory which was introduced in Chapters 2 and 3 to the log permeability field at the Oracle site. The log permeability field is shown to be statistically anisotropic, and the data base is shown to be insufficient for covariance estimation by geostatistical analysis alone. Using information obtained by statistical analysis of the two types of data introduced in Chapter 1, and the expressions derived in Chapter 3, the covariance is estimated. Chapter 5 contains my conclusions.

1.2 The Oracle Site

The Oracle field site is located on the northern edge of the Santa Catalina mountains, about 8 kilometers from the town of Oracle, Arizona (Figure 1.1). The site lies on a gentle, northeast-facing slope at an elevation of approximately 1300 meters m.s.l. (Hsieh, Neuman and Simpson, 1983).

At the site, eight boreholes have been drilled into the bedrock, a fractured, Precambrian, biotite quartz monzonite known as the Oracle granite (Jones, 1983). The granite is blanketed by a sandy soil, which extends to a depth of approximately 2 meters. The upper 13 meters of the granite is weathered. Dikes of various composition have been found to intersect the granite, at or near the site (Jones, 1983). More exhaustive geological descriptions and historical interpretations can be found in Banerjee (1957) and Jones (1983).

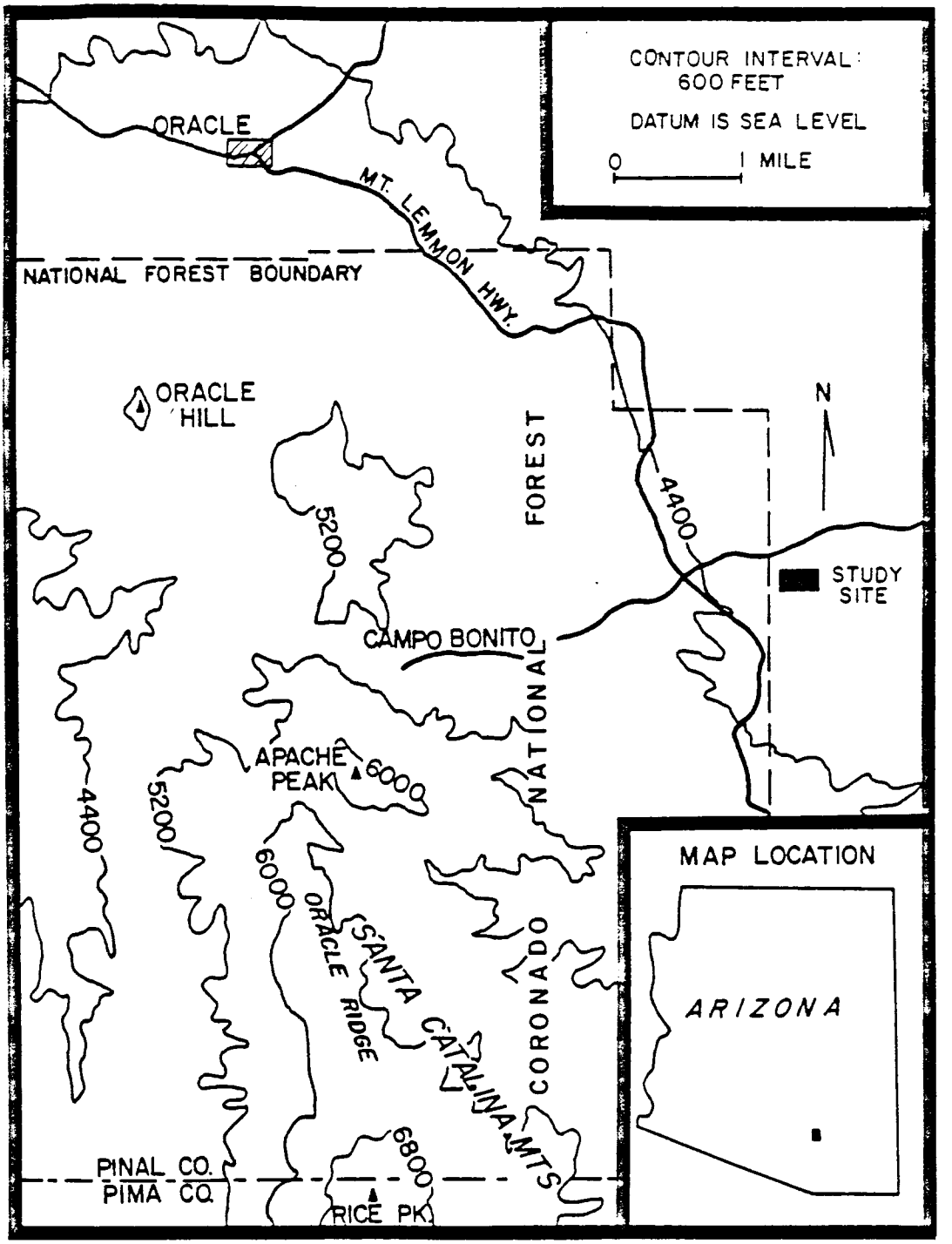

Figure 1.1. Location of the Oracle Field Site. (After Jones and others, 1985)

Figure 1.2 shows the spatial arrangement of the boreholes, in plan view. The boreholes are nearly vertical and range in depth from 76 to 91 meters, and in diameter from 0.10 to 0.17 meters. A detailed summary of borehole specifications can be found in Jones (1983) and in Jones and others (1985).

A suite of geophysical and hydraulic tests has been conducted at the site (see Jones and others, 1985). Of particular importance in this study are the hydraulic tests described in the following section.

1.3 Hydraulic Tests

Both types of hydraulic tests described herein were conducted well below the water table, which lies at a depth of approximately 12 meters. Therefore the physical interpretation of the test results was restricted to that of fully-saturated flow.

The measurements obtained in both types of test were interpreted so as to yield effective values of permeability. In other words, the permeabilities estimated from individual single-hole tests and the directional diffusivities estimated from individual cross-hole tests, can be thought of as average or effective values for the volumes of rock tested. In addition, the results of the cross-hole tests were analyzed statistically (Hsieh and others, 1985) to estimate the effective permeability tensor at the site.

More detailed descriptions of both the single-hole and cross-hole tests can be found in Hsieh and others (1983). In particular, that report contains a detailed description of the injection and monitoring equipment and the field procedures used in the data

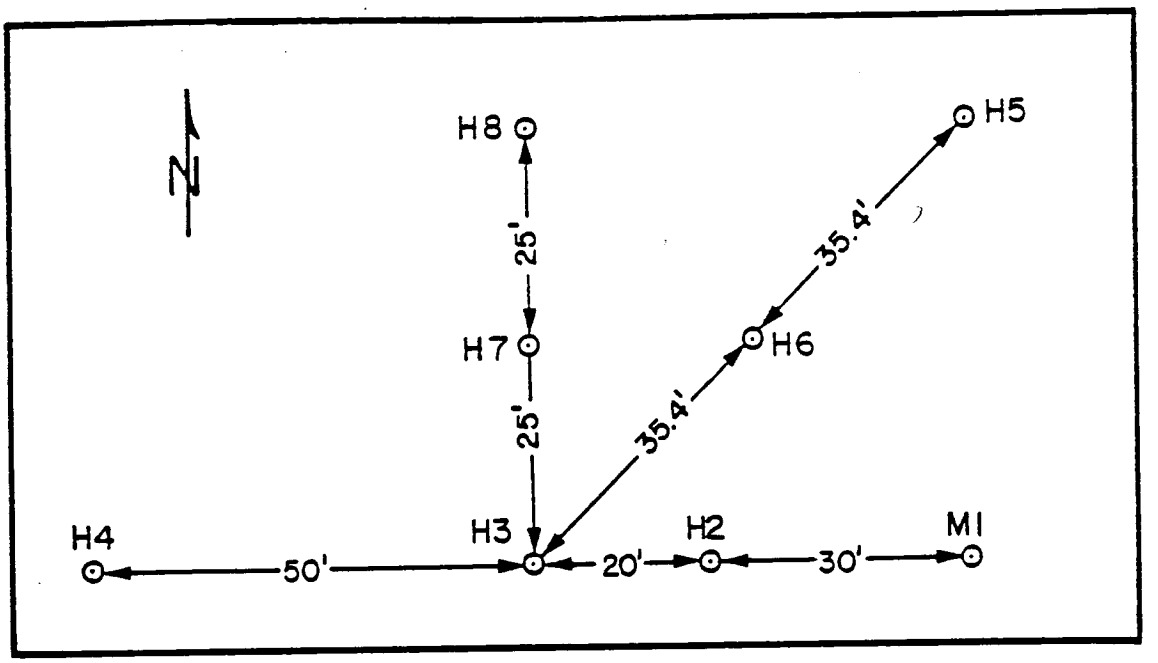

Figure 1.2. Map View of Boreholes at the Oracle Site. (After Flynn, 1985)

collection. An updated version of the theory is given by Hsieh and Neuman (1985), and an updated interpretation of the cross-hole test results is presented by Hsieh and others (1985).

1.3.1 Single-Hole Packer Tests

Two main types of single-hole injection tests were conducted at the site: continuous injection and slug tests (open hole/pressurized). Only the results of the continuous injection tests will be analyzed in this thesis. The results of these tests were interpreted to estimate saturated, effective permeabilities. Each permeability estimate corresponds only to the volume of rock in the immediate vicinity of the test zone. As a consequence of the geometry of the straddle-packer assembly (Figure 1.3) and of the near-vertical orientation of boreholes at the site, these results are expected to be biased toward the corresponding local horizontal permeabilities.

The continuous injection tests were conducted by injecting water at a constant pressure into a region of the borehole that had been isolated between two inflated packers. This region is called the test zone. At the Oracle site the same straddle-packer assembly was used for all of the single-hole tests, so that the length of the test zone, $\ell = 3.8$ meters, remained constant. The pressure in the test zone, measured by transducer, was continually monitored during each test. The pressure that was recorded after the flow rate had appeared to stabilize was converted to hydraulic head. Permeability was then calculated using expression (1.5), given below.

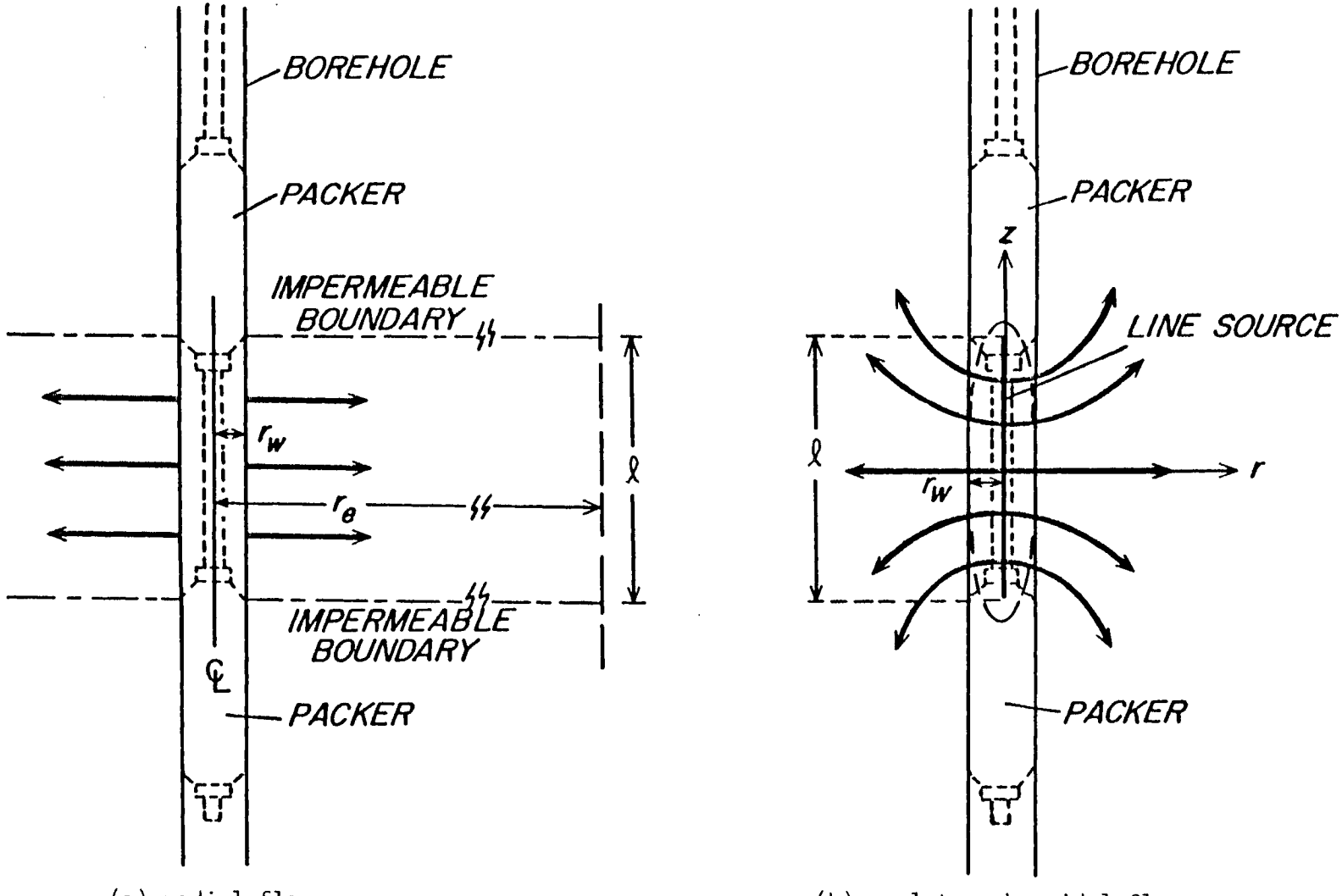

(a) radial flow

(b) prolate spheroidal flow

Figure 1.3. Single-Hole Packer Test. (After Hsieh and others, 1983)

For steady radial flow the governing flow equation is

$$\frac{d}{dr}\left(r\,\frac{dH}{dr}\right) = 0 \tag{1.1}$$

where r is the radial distance from the axis of the borehole and H is hydraulic head. The boundary conditions are

$$\begin{aligned} H &= H_w && \text{at } r = r_w \\ r\,\frac{dH}{dr} &= \frac{Q}{2\pi K \ell} && \text{at } r = r_w \end{aligned} \tag{1.2}$$

where H_w is the hydraulic head at the wellbore, r_w is the radius of the wellbore, Q is the volumetric rate of injection into the wellbore, K is the permeability in the radial direction, and ℓ is the length of the test interval. Figure 1.3a shows the experimental arrangement corresponding to these conditions.

Solving (1.1) subject to (1.2) yields the Thiem equation:

$$H_w - H = \frac{Q}{2\pi K \ell} \ln\left(\frac{r}{r_w}\right) \tag{1.3}$$

Beyond a certain radius of influence, r_e, the hydraulic head increase is assumed to be negligible:

$$H = H_o \qquad \text{at } r = r_e \tag{1.4}$$

where H_o is ambient hydraulic head. Substituting (1.4) into (1.3) and solving for K gives

$$K = \frac{Q}{2\pi \ell \Delta H_w} \ln\left(\frac{r_e}{r_w}\right) \tag{1.5}$$

where

$$\Delta H_w = H_w - H_o \tag{1.6}$$

If r_e is assumed to be known, equation (1.5) can be used to calculate K from the results of the single-hole tests. In fact, r_e was taken to be equal to ℓ, the length of the test interval, for the following reason. An alternative interpretation of the tests is based on the assumption of prolate ellipsoidal flow (Figure 1.3b), rather than radial flow. A useful approximation is (Hsieh and others, 1983)

$$K \cong \frac{Q}{2\pi\ell\Delta H_w} \ln \frac{\ell}{r_w} \quad \text{when } \ell >> 2r_w \tag{1.7}$$

Note that when $r_e = \ell$, (1.5) becomes identical to (1.7). Indeed, cross-hole test results confirm that the pressure response in neighboring boreholes 6 to 9 meters away, due to injection, is negligible (Hsieh and others, 1983).

Throughout the tests, borehole pressures were also monitored in the zones immediately above and below the packers. This was done primarily with the hope that such information would aid in the detection of vertical leakage out of the test zone, between the wall of the borehole and an improperly sealed packer. For instance, the pressure in the upper zone (above the test zone) might continue to increase after the pressure in the test zone appears to stabilize. One could then conclude that vertical leakage was occurring from the test zone to the borehole above the upper packer.

However, when vertical fractures intersect the borehole, as often happens at the Oracle site, the interpretation is ambiguous. Clearly, a pressure increase in the upper zone can be interpreted to indicate that upward flow is occurring, causing the water level in the borehole above the test zone to rise. But should this flow be interpreted as leakage, to be subtracted from the measured injection rate, or as a normal consequence of prolate spheroidal flow (Figure 1.3b)? Hsieh and others (1983) chose to treat the pressure increase as a possible consequence of leakage and therefore discarded test results from boreholes M1 and H3. Acoustic televiewer logs showed both of these boreholes to have extensive intersections with vertical fractures.

In this study, the results of over 100 single-hole tests performed by Paul Hsieh and Gary Stiles were analyzed in two ways. In the first method, the volumetric rate of leakage from the test interval was estimated and subtracted from the measured injection rate. The resulting corrected injection rate was then used to calculate the permeability, K. These are the leakage-corrected data. In the second method, borehole pressure increases outside of the test interval were ignored.

The rate of leakage to the upper borehole was estimated from the raw pressure data as follows. A pressure increase in the borehole immediately above the upper packer was assumed to coincide with a change in static water level. Since this portion of the borehole was unconfined, compressibility effects (of water) were ignored. The

leakage rate was estimated by

$$Q_{leak} \cong \frac{\pi r_w^2 \Delta p}{\rho g \Delta t} \qquad (1.8)$$

where r_w is the radius of the borehole, Δp is the pressure increase measured in the borehole above the upper packer over a time period of duration Δt, ρ is the density of water and g is the acceleration of gravity.

The ambient water level in the wells was usually above the bottom of the casing, so the inner radius of the casing was substituted for r_w. Typically, a duration of t = 5 minutes (the last 5 minutes of the test) was used for the calculation.

In the event of leakage to the borehole below the lower packer, a rough estimate of the total leakage was made by doubling that calculated for the upper borehole. Realistically, in this case the leakage is expected to be less than that corresponding to an equivalent pressure increase in the upper borehole (equation 1.8), because the packer assembly creates confined conditions below the lower packer. Therefore this method may overestimate leakage rates, and consequently underestimate permeabilities.

For most of the test intervals, two or three tests were conducted using different injection rates. The leakage correction was applied to the results of each test. Usually, the results of the low injection-rate test were selected to represent the interval, for two reasons. First, the low flowrate test often showed little evidence of

leakage. Second, at lower injection rates, there is less chance of causing non-linear flow conditions. Regardless, for most intervals tested the permeabilities calculated for the low and high flowrates did not differ greatly.

Out of 102 intervals tested, the results of 3 were discarded after making the leakage correction because the corrected injection rate was negative or so near zero as to be outside the range of reasonable accuracy of the instruments. In only 14 of the remaining 99 intervals did the leakage correction cause a perceptible change in the estimated permeability, which was calculated to within one significant figure.

The non-corrected and the leakage-corrected permeabilities are listed in Appendices A and B, respectively. The coordinates given are for the mid-point of the test interval. As in the remainder of this thesis, the working coordinate system is defined in the following way. The origin is the top of the casing for well H4. The x or x_1 axis extends horizontally due east from the origin, while the y or x_2 axis extends horizontally due north. The z or x_3 axis extends vertically upward from the origin. θ and ϕ are angular coordinates, used to specify the orientation of vectors. They are defined in the manner which is conventional for spherical coordinates.

The sample statistics for the two sets of log permeability data are presented in Table 1.1. Note that the statistics are for the base ten logarithms of the permeabilities measured in meters per second. Values in parentheses are the equivalent statistics in the natural

Table 1.1. Sample Statistics of Measured Base Ten Log Permeabilities, Single-Hole Tests. (Permeability in m/sec; equivalent statistic in natural log permeability in parentheses following)

	Non-Corrected	Leakage-Corrected	Jones (1983)
Number of Samples	102	99	102
Minimum	-10.2	-10.1	-10.3
Maximum	-5.22	-5.22	-5.60
Mean	-7.97 (-17.9)	-7.87 (-18.1)	-8.04 (-18.5)
Variance	1.53 (8.10)	1.30 (6.88)	0.83 (4.40)
Skewness	0.19	0.24	0.26

logarithms of the permeabilities. Relative frequency histograms for the two data sets are shown in Figure 1.4. Both histograms are asymmetric, though that of the leakage-corrected data is slightly more so than that of the non-corrected data. Note that the effect of the leakage correction, as shown by comparison of the two histograms, is to shift some of the "mass" of the log permeability data from the upper range ($\log_{10}K > -7.095$) to the middle range ($-8.345 < \log_{10}K < -7.095$), thus decreasing the sample mean and increasing the skewness. The relative frequencies of measurements in the lower range ($\log_{10}K < -8.345$) remain essentially unchanged. An exception is the interval at the extreme low end. Here there is a slight decrease in relative frequency corresponding to those few corrected measurements that were discarded because they were believed to be of questionable accuracy.

Cumulative frequency plots for the two log permeability data sets, on normal probability paper, are shown in Figures 1.5 and 1.6. The overall shape of the two curves is similar. In neither case do the experimental points appear to fall on a straight line. Instead, the points tend to curve slightly downward at the lower end, and slightly upward at the upper end, of log permeability. There is also an abrupt increase in cumulative frequency followed by a leveling off, at about $\log_{10}K = -7$. This corresponds to the single highest frequency class of the histograms in Figure 1.4. The main difference in the two plots is their behavior at the upper range of log permeability ($-6.3 < \log_{10}K$). Though both turn upward, indicating that the positive tail of the corresponding distribution is not as tapered as the tail of a normal

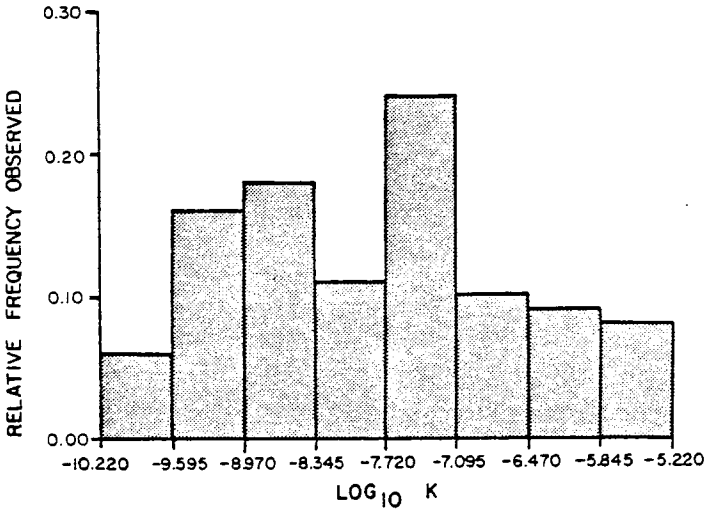

(a) Non-Corrected Data

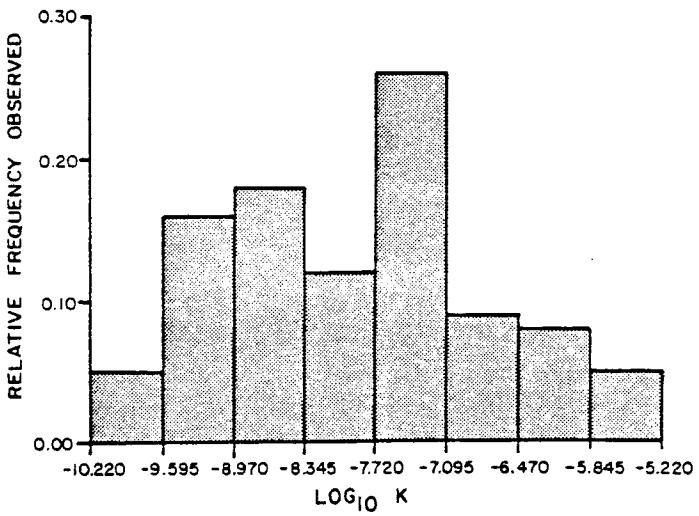

(b) Leakage-Corrected Data

Figure 1.4. Histograms of Base Ten Log Permeabilities. (Permeability in m/sec)

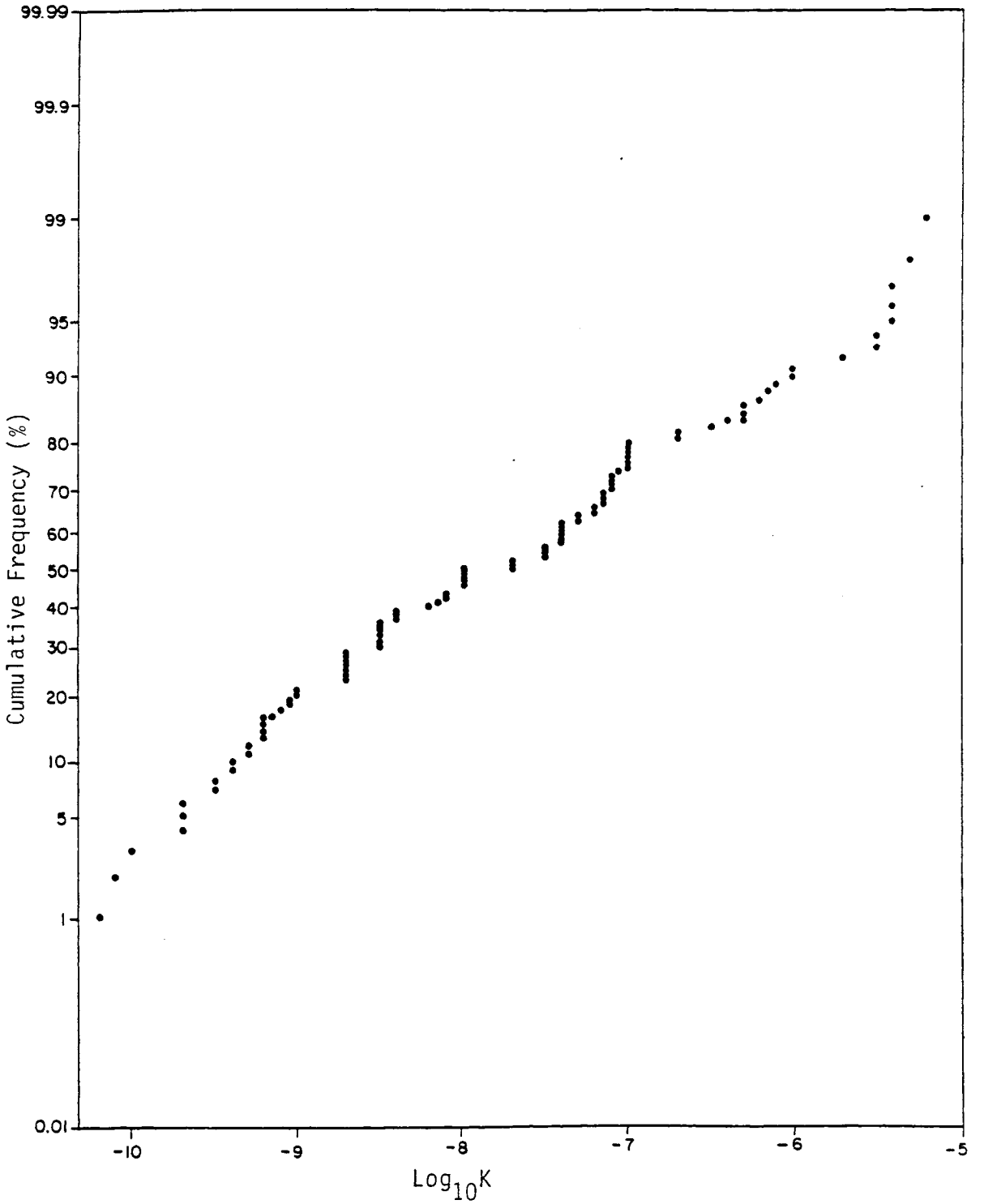

Figure 1.5. Cumulative Frequency Plot of Non-Corrected Base Ten Log Permeabilities, on Normal Probability Paper.

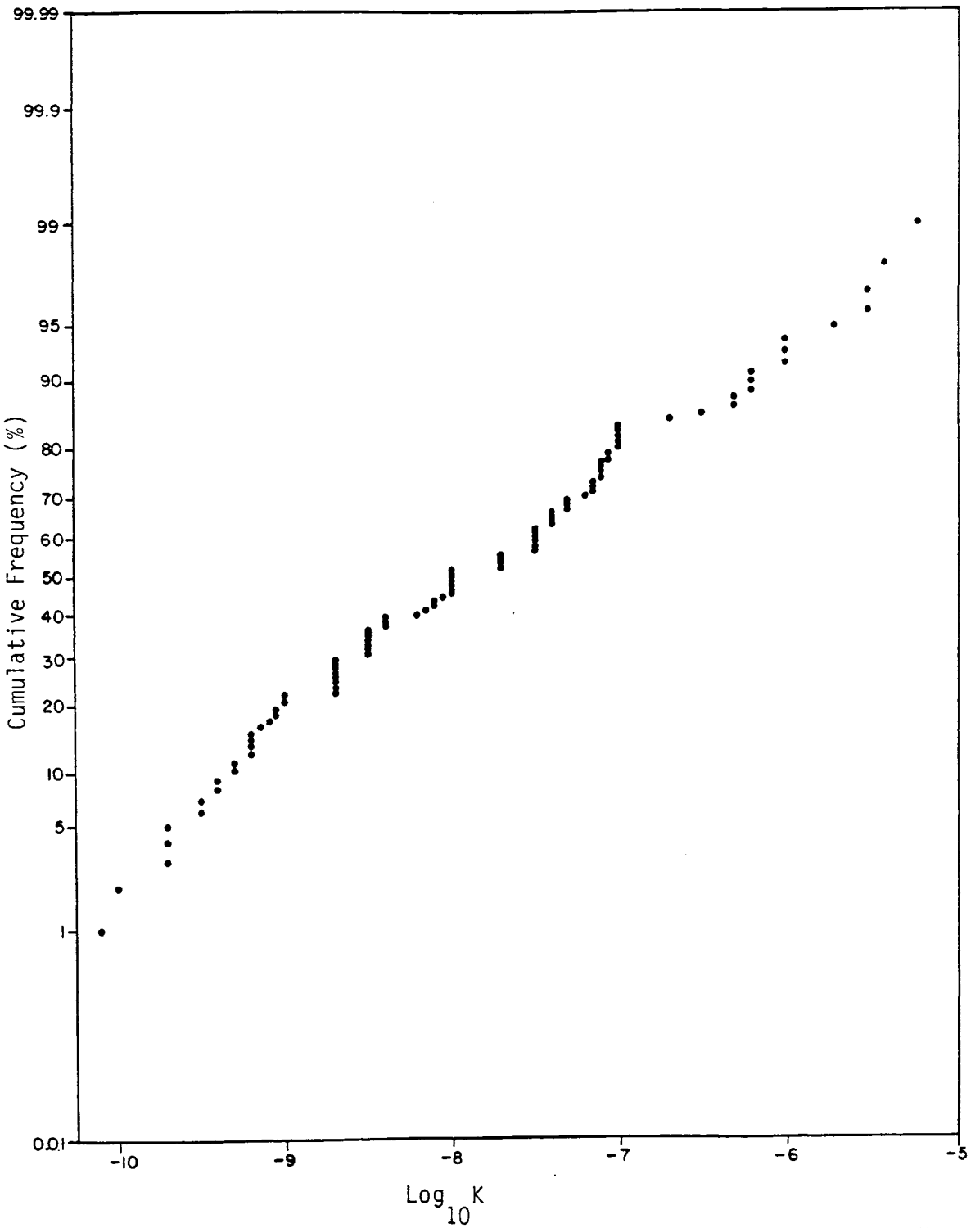

Figure 1.6. Cumulative Frequency Plot of Leakage-Corrected Base Ten Log Permeabilities, on Normal Probability Paper.

distribution, the non-corrected data curve increases faster than the leakage-corrected data curve. The difference is easily explained by comparing the high log permeability ($-7.095 < \log_{10}K$) intervals of the two histograms in Figure 1.4. The relative frequency of the non-corrected log permeabilities is nearly uniform over these intervals, while the frequency of the leakage-corrected data shows more taper with increasing log permeability.

It is tempting to interpret the statistics of these two log permeability data sets as extremes, between which the true statistics are likely to fall. Though this is obviously true of the mean, it is not necessarily true of the higher order moments. Furthermore, it may be noted that there is a greater difference in the sample variances of the two data sets than in the sample means. The sample variances differ by 1.22 while the means differ by only 0.20, about one-sixth as much. If instead we were to compare the relative differences between the two sets of sample statistics, by normalizing the differences listed above, the contrast is even more noticeable. The relative difference in sample variances is

$$\frac{8.11 - 6.89}{(8.11+6.89)/2} = 0.16$$

while the relative difference in sample means is

$$\frac{-18.1 - (-17.9)}{(-18.1-17.9)/2} = 0.011$$

The latter is about one-fifteenth of the former. All of this points to one thing. There is more uncertainty associated with estimates of the variance of log permeability than with estimates of the mean.

In addition to the two data sets described above, a third set was reported in Jones (1983) and in Jones and others (1985). Jones apparently interpreted the single-hole test results more subjectively, and therefore obtained even lower log permeability estimates than the leakage-corrected estimates described above. For comparison with the other two data sets, the statistics of this data set are also listed in Table 1.1. The data reported by Jones (1983) will not be used in this thesis.

1.3.2 Cross-Hole Packer Tests

Cross-hole injection tests were conducted in over 20 zones connecting boreholes H2, H3 and H6. The tests were conducted by Paul Hsieh and Gary Stiles. Water was injected into a packed-off interval in one borehole and the pressure response was monitored in another packed-off interval in a neighboring borehole (Figure 1.7). By matching the pressure response curve to a type-curve, a directional diffusivity was calculated. This diffusivity corresponds to the vector whose origin is at the center of the injection interval and whose end-point is at the center of the monitoring interval. Then, by least-squares, an ellipsoid was fitted to the entire collection of calculated directional diffusivities. Using this information, the three effective principal directions and corresponding principal permeabilities were

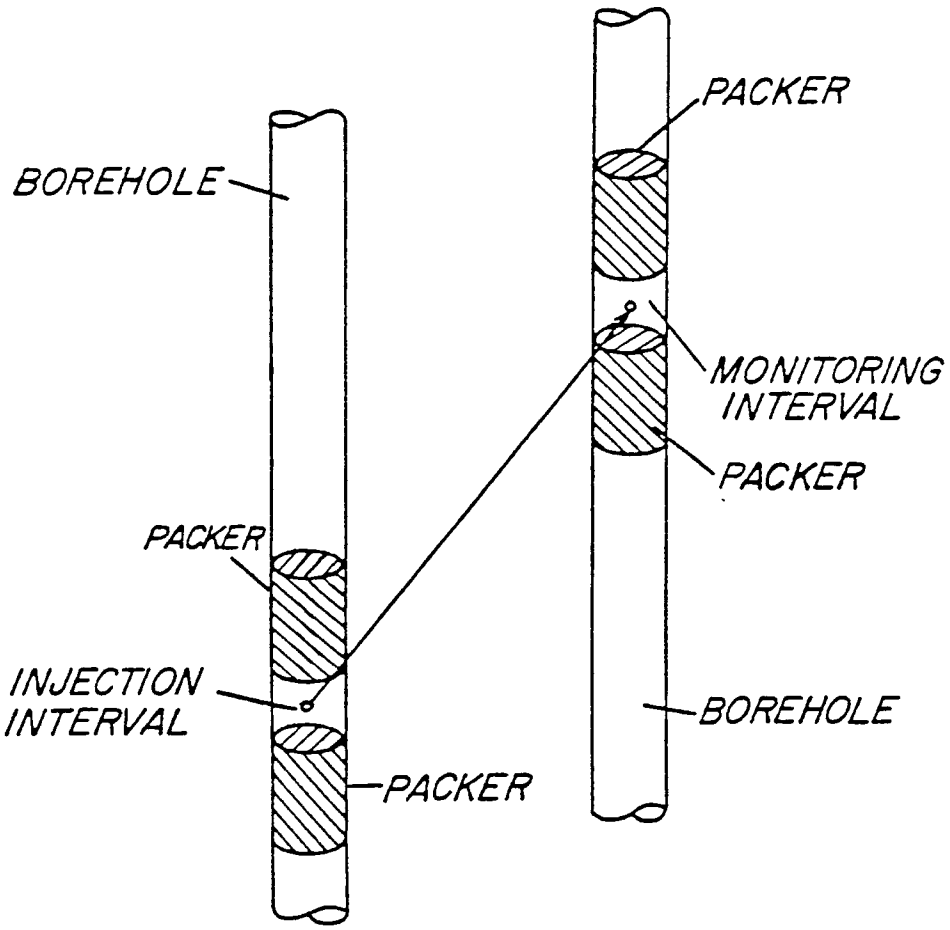

Figure 1.7. Cross-Hole Packer Test. (After Hsieh and others, 1983)

calculated. A complete description of the analysis is given by Hsieh and others (1985).

The permeability ellipsoid was estimated by both ordinary least-squares and weighted least-squares (Hsieh and others, 1985). Thus, two estimates of the permeability tensor are available. The two estimates, summarized in Table 1.2, are seen to be quite similar. Hsieh and others (1985) have shown that the orientation of the principal axes is strongly influenced by the fracture sets at the site, as mapped by Jones (Jones and others, 1985).

Table 1.2. Results of Least-Squares Analysis of Cross-Hole Test Data. (From Hsieh and others, 1985)

Method	Estimated Principal Directions Bearing	Plunge	Estimated Principal Hydraulic Conductivity
Ordinary Least-Squares	248°	32°	6.5×10^{-8} m/s
	340°	4°	1.7×10^{-8}
	77°	58°	1.8×10^{-7}
Weighted Least-Squares	247°	51°	6.9×10^{-8}
	342°	4°	2.2×10^{-8}
	75°	39°	1.6×10^{-7}

CHAPTER 2

STOCHASTIC CHARACTERIZATION OF SPATIAL VARIABILITY

2.1 The Random Field

Earth materials are formed by the complex interaction of natural geologic processes. Typically these processes act nonuniformly in space as well as in time. As a result, a material's physical characteristics may vary from one point in space to another, in a manner which is not straightforward. For example, the spatial variation of a hydrologic parameter like permeability is not easily quantified or predicted from available field data but rather is characterized by an apparent randomness. The term "random" is used here to imply that there is a considerable degree of uncertainty associated with the parameter's spatial distribution due to (1) a lack of experimental data, (2) an incomplete understanding of the collective underlying geologic processes and (3) measurement error. The apparent randomness suggests that a stochastic approach may be most appropriate to characterize the spatial variability.

A concept from mathematics which is particularly well suited for the stochastic characterization of spatial variability is that of a random field. The terms random field, random function, random process and stochastic process are considered equivalent (Priestley, 1981) and are used interchangeably. A random field is simply a collection of jointly distributed random variables defined on a two- or higher-

dimensional parameter space. In general, the parameter space may be either continuous or discrete. A spatial random field has one (univariate) or more (multivariate) random variables associated with every unique location in its domain or parameter space. An example of a univariate spatial random field defined on a three-dimensional continuous parameter space is given by the random variable porosity, as a function of location.

Consider one particular realization of each random variable in a univariate spatial random field. Collectively, these realizations form a univariate function of the spatial coordinates, called a sample function. This sample function constitutes one realization among a collection or ensemble of many possible realizations of the random field. If the spatial domain is continuous, then every realization of the field consists of the particular realizations of an infinite number of random variables. Therefore, the ensemble contains an uncountable number of possible realizations. This is true regardless of whether the random field is univariate or multivariate, two- or three-dimensional, whether it consists of continuous, discrete or mixed random variables and whether it is of finite or infinite extent. For the remainder of this study though, only real, continuous-valued random fields defined on a three-dimensional, continuous parameter space are considered.

2.2 Simplifying Assumptions

To effect a complete statistical description of a random field requires knowledge of the joint probability density (or mass) function

of its constituent random variables or equivalently, knowledge of all of the moments of the joint density (mass) function. Realistically, this information is impractical if not impossible to obtain. In practice, certain simplifying assumptions must be made. These assumptions are discussed below.

2.2.1 Neglect of Higher Order Moments

Commonly, the assumption is made that only the first and second moments of the joint probability density (or mass) function are important in characterizing the statistical structure of the random field. Strictly, this only holds for fields in which the random variables' joint density function is Gaussian. However, this is not to say that the field is assumed to be jointly Gaussian. While it is recognized that the statistical characterization provided by estimates of the first- and second-order moments is necessarily incomplete if the field is non-Gaussian, the higher-order moments are sometimes neglected as a matter of operational convenience. A similar practice will be followed in this study.

2.2.2 Stationarity

An additional assumption lends tractability to the task of moment estimation. It is the assumption of stochastic stationarity. The concept of stationarity exists in varying degrees. The most restrictive form is complete or strict stationarity. A spatial random field is strictly stationary if its corresponding joint probability density (mass) function is invariant under a simple translation of

coordinates. A less restrictive form is n^{th}-order stationarity. A stochastic process is n^{th}-order stationary if all of its joint moments, of order n and lower, are dependent only on the displacement vector(s) and not on the actual coordinates. Since only the first and second moments will be treated explicitly in this study, most of the applicable theory will rely on the assumption of second-order or wide-sense stationarity. This type of field is said to be statistically homogeneous or weakly stationary.

2.2.3 Ergodicity

To estimate the moments of the probability density (mass) function of a single independent random variable generally requires that experiments be performed repeatedly to obtain many realizations. Then from this large collection of experimental outcomes, the moments are estimated. By analogy, since a random field is a collection of random variables, it seems logical to require that many different realizations of the field be sampled for moment estimation. This is impossible, of course, because only one realization of the field really exists, that being the actual aquifer or geologic environment under consideration. To circumvent this problem, the hypothesis of ergodicity is adopted.

An ergodic field is one in which ensemble averages can be replaced by spatial averages. In other words, a random field is ergodic if spatial averages from a single realization converge to the corresponding ensemble averages as the sample size increases. In

effect then, the moments of the joint probability density (mass) function can be inferred from a single realization of an ergodic field.

The ergodic hypothesis has been a subject of concern for several reasons. First, the estimation of the moments seems an impossible task without it. Second, because the random field is a conceptual abstraction existing only in the human mind, the ergodic assumption is necessarily unverifiable (Matheron, 1971; Huijbregts, 1985). Despite, and perhaps because of this apparent dilemma, the ergodic problem is dismissed as irrelevant to the practical concerns of a stochastic analysis, though admittedly it remains unresolved.

2.3 Moments

2.3.1 Definitions

The mean or expectation of a random process is given by the Stieltjes integral

$$\overline{f}(\underline{x}) = E[f(\underline{x})] = \int_{-\infty}^{+\infty} f(\underline{x})\, dP[f(\underline{x})] \qquad (2.1)$$

where f is the random quantity of interest, $\underline{x} = (x_1, x_2, x_3)$ denotes the corresponding three-dimensional location vector in the continuous parameter space and $P[f(\underline{x})]$ is the cumulative distribution function of the random variable $f(\underline{x})$. Then if $P[f(\underline{x})]$ is differentiable,

$$\overline{f}(\underline{x}) = \int_{-\infty}^{+\infty} f(\underline{x})\, p[f(\underline{x})]\, df(\underline{x}) \qquad (2.2)$$

where $p[f(\underline{x})]$ is the probability density function associated with the random variable $f(\underline{x})$ and is given by

$$p[f(\underline{x})] = \frac{dP[f(\underline{x})]}{df(\underline{x})} \tag{2.3}$$

For fields which are at least first-order stationary, the mean is independent of spatial position:

$$\overline{f}(\underline{x}) = \overline{f} \tag{2.4}$$

Such a field is said to be without drift. A field may exhibit a drift or spatial trend. Although estimation of the drift from limited field data tends to be rather problematic, for theoretical considerations, it is assumed to be possible. Then the residual, as it is called, is given by the increment

$$f'(\underline{x}) = f(\underline{x}) - \overline{f}(\underline{x}) \tag{2.5}$$

The residuals themselves constitute a zero-mean, first-order stationary random field:

$$E[f'(\underline{x})] = 0 \tag{2.6}$$

The spatial covariance function describes the degree of linear association or information sharing between two random variables of the field, as a function of their locations. When it exists, it is given by

$$C(\underline{x},\underline{x}+\underline{h}) = E[f'(\underline{x})f'(\underline{x}+\underline{h})] \tag{2.7}$$

where E is the expectation operator and $\underline{h}$ is referred to as the spatial separation vector, lag vector or displacement vector. The covariance is generally dependent on both the magnitude and the orientation of the separation vector. The condition for existence of the covariance, is that the variance be finite. The variance of the field is simply the value of the covariance function corresponding to zero separation:

$$\sigma^2(\underline{x}) = C(\underline{x},\underline{x}) \tag{2.8}$$

Note that it is generally dependent upon the spatial coordinates, $\underline{x}$. An alternative interpretation is that $\sigma^2(\underline{x})$ is the variance of the random variable $f(\underline{x})$:

$$\sigma^2(\underline{x}) = \mathrm{Var}[f(\underline{x})] \tag{2.9}$$

For second-order stationary random fields, the covariance is written

$$C(\underline{x},\underline{x}+\underline{h}) = C(\underline{h}) \tag{2.10}$$

Although it is still generally dependent on both the magnitude and the orientation of the separation vector, it is independent of location. In this case the variance is constant:

$$\sigma^2 = C(\underline{o}) \tag{2.11}$$

It is important not to confuse covariance with overall stochastic dependence. Random variables may be highly dependent stochastically, but if the dependence is not linear, they may not display

appreciable covariance (Benjamin and Cornell, 1970). In order to illustrate the linear memory or linear aspect of information sharing described by the covariance function, consider the following example. Let $f(\underline{x})$ be a homogeneous, zero-mean, random field. Suppose the value corresponding to a particular realization of the random variable $f(\underline{x}_0)$, $\underline{x}_0$ fixed, is known and that we wish to estimate without bias the unknown value $f(\underline{x}_0+\underline{h})$, $\underline{h}$ fixed, by a multiple of the known value $f(\underline{x}_0)$, such that the mean square error is minimized. A general rule for determining the weight b can be established as follows. Consider the problem of estimating $f(\underline{x}+\underline{h})$ from $f(\underline{x})$ in a manner similar to that described above. Let the estimate be given by

$$\hat{f}(\underline{x}+\underline{h}) = bf(\underline{x}) \quad (\underline{x},\underline{h} \text{ fixed; b nonstochastic}) \tag{2.12}$$

Then the mean square error is

$$\begin{aligned} MSE &= E\{[f(\underline{x}+\underline{h}) - \hat{f}(\underline{x}+\underline{h})]^2\} \\ &= E\{[f(\underline{x}+\underline{h}) - bf(\underline{x})]^2\} \end{aligned} \tag{2.13}$$

The weight b can be determined simply by minimizing the quantity MSE, treating b as a variable. To do this, first differentiate MSE with respect to b and set equal to zero:

$$\frac{\partial(MSE)}{\partial b} = 0 \tag{2.14}$$

Solving for b gives

$$b = \frac{E[f(\underline{x}+\underline{h})\ f(\underline{x})]}{E[f^2(\underline{x})]} \tag{2.15}$$

This result can be expressed generally

$$b = C(\underline{h})/C(\underline{o}) \tag{2.16}$$

Thus, the autocorrelation can be viewed as the degree of linear dependence between random variables in the field.

The estimator described above is referred to as BLUE for best linear unbiased estimator (Journel and Huijbregts, 1978). Although somewhat oversimplified, the previous example is completely analogous to the geostatistical estimation procedure known as kriging.

In geostatistics, another second-order moment is sometimes useful. It is the semivariogram. If it exists, it is defined by

$$\gamma(\underline{x},\underline{x}+\underline{h}) = (1/2)\mathrm{Var}[f(\underline{x}+\underline{h}) - f(\underline{x})] \tag{2.17}$$

Note that in general, neither the variance of $f(\underline{x}+\underline{h})$ nor that of $f(\underline{x})$ need exist in order for the semivariogram to exist. Thus, the condition for its existence is less restrictive than that of the covariance (equation 2.7). If the covariance exists, then the semivariogram may be written

$$\gamma(\underline{x},\underline{x}+\underline{h}) = [\sigma^2(\underline{x}) + \sigma^2(\underline{x}+\underline{h})]/2 - C(\underline{x},\underline{x}+\underline{h}) \tag{2.18}$$

The semivariogram of a first-order stationary random field may be written

$$\gamma(\underline{x},\underline{x}+\underline{h}) = (1/2)E\{[f(\underline{x}+\underline{h}) - f(\underline{x})]^2\} \tag{2.19}$$

If in addition to being first-order stationary, a random field has a

finite semivariogram which is dependent only upon the lag vector, the field is said to be intrinsic. Then the semivariogram is

$$\gamma(\underline{h}) = (1/2)E\{[f(\underline{x}+\underline{h}) - f(\underline{x})]^2\} \tag{2.20}$$

These two assumptions, taken together, constitute what is known as the intrinsic hypothesis. Finally, if the random field is not only intrinsic but second-order stationary, the semivariogram may be written

$$\gamma(\underline{h}) = C(\underline{o}) - C(\underline{h}) \tag{2.21}$$

2.3.2 Properties

The covariance function and the semivariogram possess several properties which are useful to note. For instance, both the covariance and the semivariogram are even functions of the separation vector:

$$C(-\underline{h}) = C(\underline{h}) \tag{2.22}$$

$$\gamma(-\underline{h}) = \gamma(\underline{h}) \tag{2.23}$$

In addition, the absolute magnitude of the covariance is bounded above by the variance, through Schwarz's inequality (Journel and Huijbregts, 1978):

$$|C(\underline{h})| \leq C(\underline{o}) \tag{2.24}$$

Though the semivariogram does not generally possess an upper bound, since it is a variance it possesses the property of nonnegative definiteness:

$$\gamma(\underline{h}) \geq 0 \tag{2.25}$$

At the origin of the lag space, the covariance is simply a variance and therefore is nonnegative definite:

$$C(\underline{o}) \geq 0 \tag{2.26}$$

However, it is easy to see that the semivariogram vanishes at the origin:

$$\gamma(\underline{o}) = 0 \tag{2.27}$$

The behavior of the covariance and semivariogram of a homogeneous field at infinite separation are given by, respectively (Christakos, 1984),

$$\lim_{|h| \to \infty} \frac{C(\underline{h})}{|\underline{h}|^{\frac{1-n}{2}}} = 0 \tag{2.28}$$

$$\lim_{|h| \to \infty} \frac{\gamma(\underline{h})}{|\underline{h}|^2} = 0 \tag{2.29}$$

where $\underline{h}$ is the n-dimensional spatial separation vector.

Perhaps the most important requirement of the covariance function is that it must be nonnegative definite. To see why this restriction is imposed, consider the random function $f(\underline{x})$ and the weighting function $g(\underline{x})$ (generally complex), both defined on a real n-dimensional parameter space, R^n. Consider the linear combination

$$Y = \int_{R^n} g(\underline{x}) f(\underline{x}) \, d\underline{x} \tag{2.30}$$

Clearly Y is a random variable and as such must have a nonnegative variance (equation 2.26)

$$\text{Var } Y \geq 0 \tag{2.31}$$

This implies that the covariance function must satisfy, for any function $g(\underline{x})$,

$$\int_{R^n} \int_{R^n} g(\underline{x})g^*(\underline{x}')C(\underline{x},\underline{x}')\, d\underline{x}\, d\underline{x}' \geq 0 \tag{2.32}$$

where an asterisk (*) denotes complex conjugate. The weighting function $g(\underline{x})$ may even be taken to be a series of Dirac distributions,

$$g(\underline{x}) = \sum_{i=1}^{N} g_i \delta(\underline{x}-\underline{x}_i) \tag{2.33}$$

where the g_i are complex constants (i=1,2,...,N).
Then the integral in equation (2.30) is replaced by the sum,

$$Y = \sum_{i=1}^{N} g_i f(\underline{x}_i) \tag{2.34}$$

while the nonnegative definite requirement is written

$$\sum_i \sum_j g_i g_j^* C(\underline{x}_i,\underline{x}_j) \geq 0 \tag{2.35}$$

Utilizing Stieltjes integrals, these results can be summarized more compactly:

$$Y = \int_{R^n} f(\underline{x})\, dG(\underline{x}) \tag{2.36}$$

$$\int_{R^n}\int_{R^n} C(\underline{x},\underline{x}')\, dG(\underline{x})\, dG^*(\underline{x}') \geq 0 \tag{2.37}$$

Note that when $G(\underline{x})$ is differentiable, $dG(\underline{x})$ is replaced by $g(\underline{x})d\underline{x}$ and the Stieltjes integral is replaced by the ordinary Riemann integral.

In a similar manner, it is easily shown that the negative semivariogram is conditionally nonnegative definite. Using equation (2.18), equation (2.37) becomes

$$\frac{1}{2}\int_{R^n} dG^*(\underline{x}') \int_{R^n} \sigma^2(\underline{x})\, dG(\underline{x}) + \frac{1}{2}\int_{R^n} dG(\underline{x}') \int_{R^n} \sigma^2(\underline{x})\, dG^*(\underline{x})$$

$$-\int_{R^n}\int_{R^n} \gamma(\underline{x},\underline{x}')\, dG(\underline{x})\, dG^*(\underline{x}') \geq 0 \tag{2.38}$$

Since the variance $\sigma^2(\underline{x})$ need not exist under the intrinsic hypothesis, it is sometimes considered useful to impose the conditions,

$$\int_{R^n} dG^*(\underline{x}) = \int_{R^n} dG(\underline{x}) = 0 \tag{2.39}$$

Then the nonnegative definite variance requirement (equation 2.31) becomes

$$-\int_{R^n}\int_{R^n} \gamma(\underline{x},\underline{x}')\, dG(\underline{x})\, dG^*(\underline{x}') \geq 0 \tag{2.40}$$

whenever (2.39) is satisfied.

If $G(\underline{x})$ is differentiable, Y is given by equation (2.30) and the requirements can be stated this way:

$$-\int_{R^n}\int_{R^n} g(\underline{x})g^*(\underline{x}')\gamma(\underline{x},\underline{x}')\,d\underline{x}\,d\underline{x}' \geq 0 \qquad (2.41)$$

whenever

$$\int_{R^n} g^*(\underline{x})\,d\underline{x} = \int_{R^n} g(\underline{x})\,d\underline{x} = 0 \qquad (2.42)$$

A case of interest is that corresponding to equation (2.34). Then (2.40) can be written

$$-\sum_i \sum_j g_i g_j^* \gamma(\underline{x}_i,\underline{x}_j) \geq 0 \qquad (2.43)$$

when the g_i satisfy the condition,

$$\sum_i g_i = \sum_i g_i^* = 0 \qquad (2.44)$$

Any Y which satisfies both (2.43) and (2.44) is called an authorized linear combination (Journel and Huijbregts, 1978).

2.3.3 Anisotropy

A stationary random field is isotropic if the spatial covariance function is dependent only on the modulus of the separation vector:

$$C(\underline{h}) = C(|\underline{h}|) \qquad (2.45)$$

The constant surfaces of the function are spheres given by

$$|\underline{h}| = \text{constant} \qquad (2.46)$$

Generally, the covariance is dependent on the orientation of the separation vector, as well as its magnitude. This type of stochastic process is statistically anisotropic.

A stochastic process may exhibit a specific type of anisotropy known as ellipsoidal (Vanmarcke, 1983) or geometric (Journel and Huijbregts, 1978). In this case the covariance function takes the form

$$C(\underline{h}) = F[(h_1/b_1)^2 + (h_2/b_2)^2 + (h_3/b_3)^2] \tag{2.47}$$

where the parameters b_1, b_2 and b_3 are real positive constants. The argument of the function F is a real quadratic form, so equation (2.47) can be restated

$$C(\underline{h}) = F[\underline{h}^T \underline{B}\ \underline{h}] \tag{2.48}$$

where

$$\underline{B} = [B_{ij}] = [\delta_{ij}/b_i^2] \tag{2.49}$$

For separation vectors oriented parallel to the coordinate axes, the covariance is dependent only on the separation distance. For instance, equation (2.47) gives

$$C(h_1,0,0) = F[(h_1/b_1)^2] = F[(|h_1|/b_1)^2] \tag{2.50}$$

Equation (2.49) gives the form of $\underline{B}$ when the separation vector $\underline{h}$ is measured relative to the principal coordinate system. From this point on then, $\underline{h}$ will be used to represent the displacement vector relative to the principal coordinate system.

Naturally we expect, and indeed require, that the covariance remains invariant under a linear coordinate transformation:

$$C'(\underline{h}') = C(\underline{h}) \tag{2.51}$$

The prime indicates that the quantity is expressed relative to the newly transformed (working) coordinate system. For example, if a coordinate system is formed by a nonsingular linear transformation of the principal coordinate axes (e.g., any combination of rotations and linear magnifications/contractions), the new coordinates are related to the principal coordinates through the expression

$$\underline{h}' = \underline{A}\,\underline{h} \tag{2.52}$$

where $\underline{A}$ is the 3x3 nonsingular matrix of the transformation. Then the covariance is written

$$C'(\underline{h}') = F[(\underline{h}')^T \underline{B}'\underline{h}'] \tag{2.53}$$

The constant surfaces of a geometric covariance function are specified by

$$\underline{h}^T\,\underline{B}\,\underline{h} = \text{constant (principal coordinate system)} \tag{2.54}$$

or

$$(\underline{h}')^T\,\underline{B}'\,\underline{h}' = \text{constant (linearly transformed systems)} \tag{2.55}$$

Since these are real, three-dimensional quadratic forms, the constant surfaces are quadric surfaces. In fact, owing to the nonnegative

definite nature of the tensor $\underline{B}$, the surfaces are ellipsoids whose major and minor axes coincide with the principal coordinate axes.

Because they are perhaps the simplest type of anisotropic covariance functions to work with, only ellipsoidal models are used in this study. Specific examples include the exponential, Gaussian and spherical models. Each is discussed briefly at the end of this section.

It is useful to characterize the covariance function of a random field through the use of certain parameters or correlation measures (Vanmarcke, 1983). One group of such measures is the integral scales (Lumley and Panofsky, 1964). The integral scales, if they exist, are defined by

$$\lambda(\underline{u}) = \frac{1}{C(\underline{o})} \lim_{L \to +\infty} \int_0^L C(r\underline{u})\, dr \qquad \underline{u} = \underline{h}/|\underline{h}|,\ \underline{h} \neq \underline{0}. \tag{2.56}$$

The integral scale is a measure of the degree of persistence of spatial correlation in a given direction. It has the dimensions of length. If the field is statistically isotropic, the scale is independent of direction

$$\lambda(\underline{u}) = \lambda,\ \lambda \text{ constant} \tag{2.57}$$

The principal integral scales are those corresponding to the orthogonal basis vectors of the principal coordinate system

$$\lambda_1 = \lambda(\underline{e}_1) = \lambda(1,0,0)$$
$$\lambda_2 = \lambda(\underline{e}_2) = \lambda(0,1,0) \qquad (2.58)$$
$$\lambda_3 = \lambda(\underline{e}_3) = \lambda(0,0,1)$$

For the ellipsoidal covariance functions examined in this study, the square of the inverse of the integral scale is a tensor. In the following examples, some well-known ellipsoidal models are introduced and expressions for their integral scales are given.

Consider first the exponential covariance

$$C(\underline{h}) = C(\underline{o}) \exp[-(\underline{h}^T \underline{B}\ \underline{h})^{1/2}] \qquad (2.59)$$

Straightforward integrations yield

$$\underline{B} = \underline{\lambda}^{-2} \qquad (2.60)$$

where $\underline{\lambda}^{-2}$ is the integral scale tensor given by

$$\underline{\lambda}^{-2} = [\delta_{ij}/\lambda_i^2] \qquad (2.61)$$

The general integral scales are

$$\lambda(\underline{u}) = \int_0^{+\infty} \exp[-(\underline{u}^T \underline{\lambda}^{-2} \underline{u})^{1/2} r]\, dr$$
$$= (\underline{u}^T \underline{\lambda}^{-2} \underline{u})^{-1/2} \qquad (2.62)$$

Christakos (1984) determined that the exponential model is suitable in one, two or three dimensions, and found it to be the covariance of a continuous, non-differentiable stochastic process. Priestley (1981)

shows it to be the covariance of a first-order autoregressive process. This function approaches zero asymptotically, as shown in Figure 2.1.

The Gaussian covariance function is also a permissible model (Christakos, 1984)

$$C(\underline{h}) = C(\underline{o}) \exp[-\underline{h}^T \underline{B}\ \underline{h}] \tag{2.63}$$

Simple integration shows that

$$\underline{B} = (\pi/4)\ \underline{\lambda}^{-2} \tag{2.64}$$

The general integral scales are given by

$$\begin{aligned} \lambda(\underline{u}) &= \int_0^{+\infty} \exp[-(\pi/4)\ \underline{u}^T \underline{\lambda}^{-2} \underline{u}\ r^2]\ dr \\ &= (\underline{u}^T \underline{\lambda}^{-2} \underline{u})^{-1/2} \end{aligned} \tag{2.65}$$

The Gaussian model is unique in that it is continuous and possesses derivatives of any order at the origin. Therefore, it corresponds to a random function which exhibits a high degree of regularity (Christakos, 1984). For this reason, its usefulness for describing the spatial pattern of natural hydrologic processes has been questioned (Bras and Rodriguez-Iturbe, 1976). Like the exponential model, the Gaussian covariance approaches zero asymptotically (see Figure 2.2).

The final example involves the so-called spherical covariance, sometimes used in geostatistics

$$C(\underline{h}) = \begin{cases} C(\underline{o})[1 - \frac{3}{2}(\underline{h}^T \underline{A}^{-2} \underline{h})^{1/2} + \frac{1}{2}(\underline{h}^T \underline{A}^{-2} \underline{h})^{3/2}, & \underline{h}^T \underline{A}^{-2} \underline{h} < 1 \\ 0, & \underline{h}^T \underline{A}^{-2} \underline{h} \geq 1 \end{cases} \tag{2.66}$$

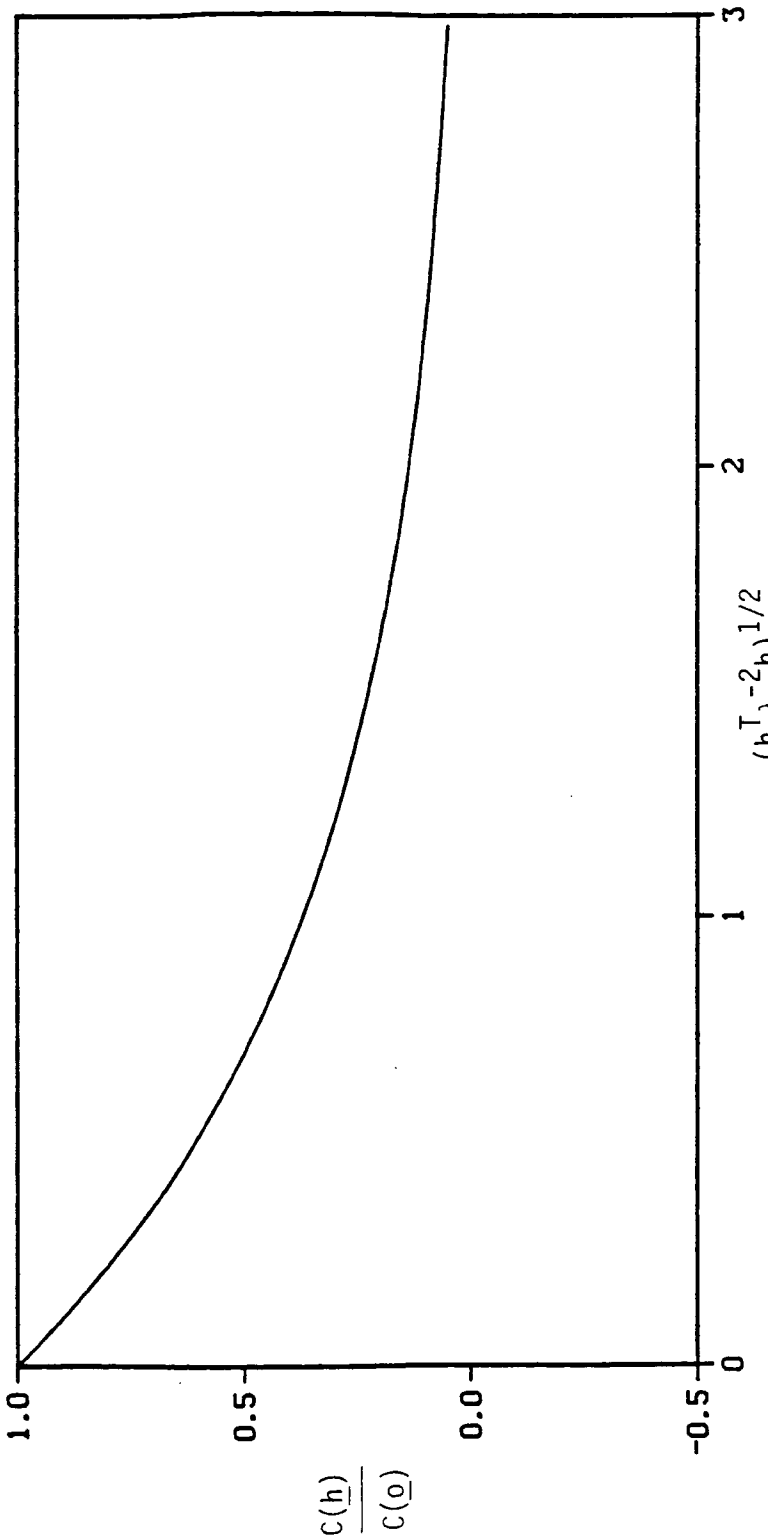

Figure 2.1. Autocorrelation Versus Dimensionless Distance, Exponential Model.

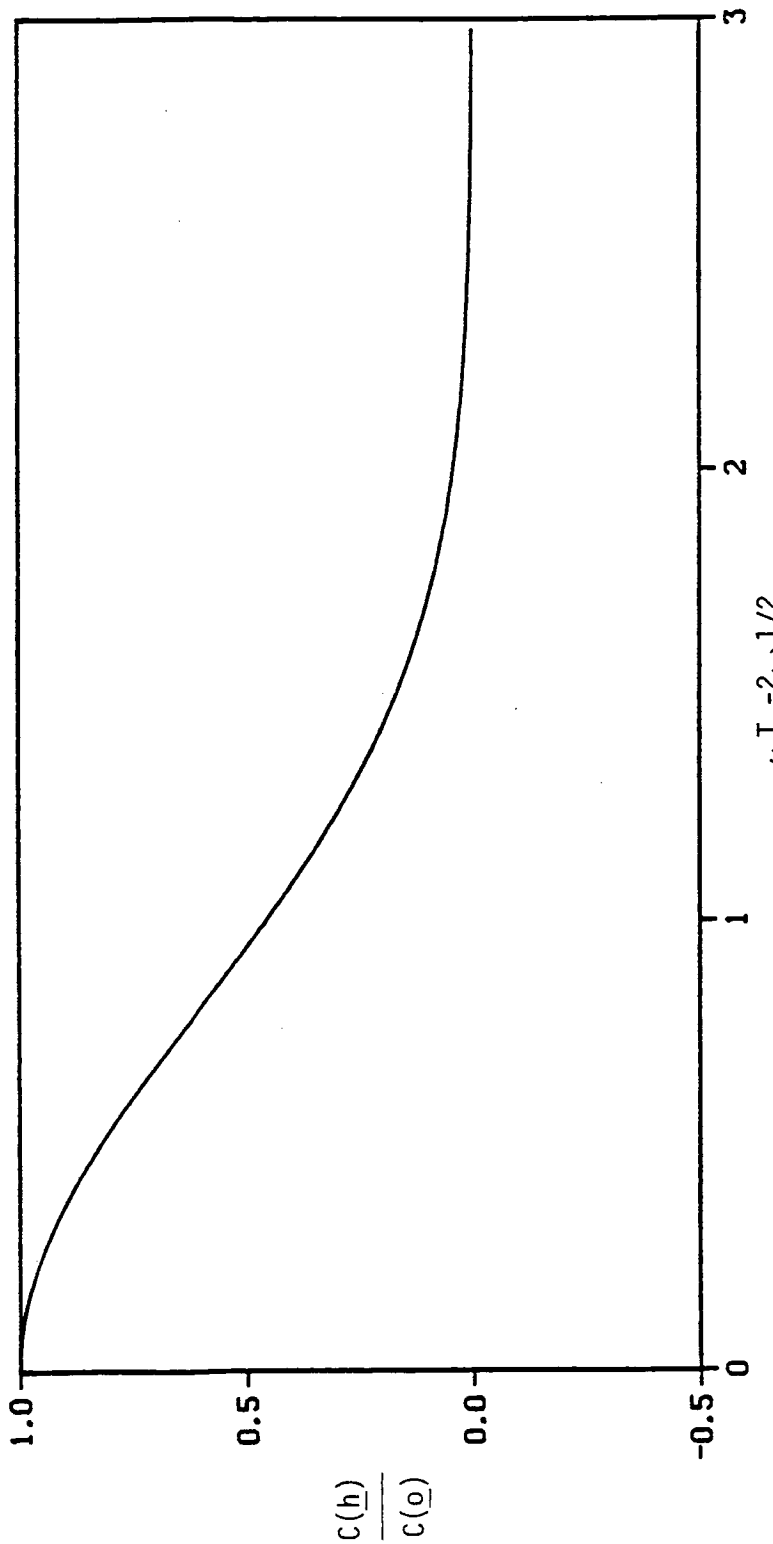

Figure 2.2. Autocorrelation Versus Dimensionless Distance, Gaussian Model.

where $\underline{A}^2$ is a tensor whose elements are the squares of the ranges in the principal directions. In a given direction, the range is the separation distance corresponding to zero covariance. Again, integration yields

$$\underline{A} = [a_i] = (8/3)[\lambda_i] = (8/3)\underline{\lambda} \tag{2.67}$$

where the a_i (i=1,2,3) are the ranges in the principal directions.

The general integral scales are

$$\lambda(\underline{u}) = \int_0^{(8/3)(\underline{u}^T\underline{\lambda}^{-2}\underline{u})^{-1/2}} [1-(9/16)(\underline{u}^T\underline{\lambda}^{-2}\underline{u})^{1/2}r + (27/1024)(\underline{u}^T\underline{\lambda}^{-2}\underline{u})^{3/2}r^3]\, dr = (\underline{u}^T\underline{\lambda}^{-2}\underline{u})^{-1/2} \tag{2.68}$$

The spherical covariance corresponds to a continuous, non-differentiable random field. Christakos (1984) showed that the spherical model is appropriate for three-dimensional fields. A graph of the spherical covariance function is given in Figure 2.3.

Each of the aforementioned covariance models can be expressed thusly:

$$C(\underline{h}) = C(r\ \underline{u}) = F[r^2/\lambda^2(\underline{u})] \tag{2.69}$$

In the special case where the field is isotropic, this is

$$C(\underline{h}) = F[r^2/\lambda^2] \tag{2.70}$$

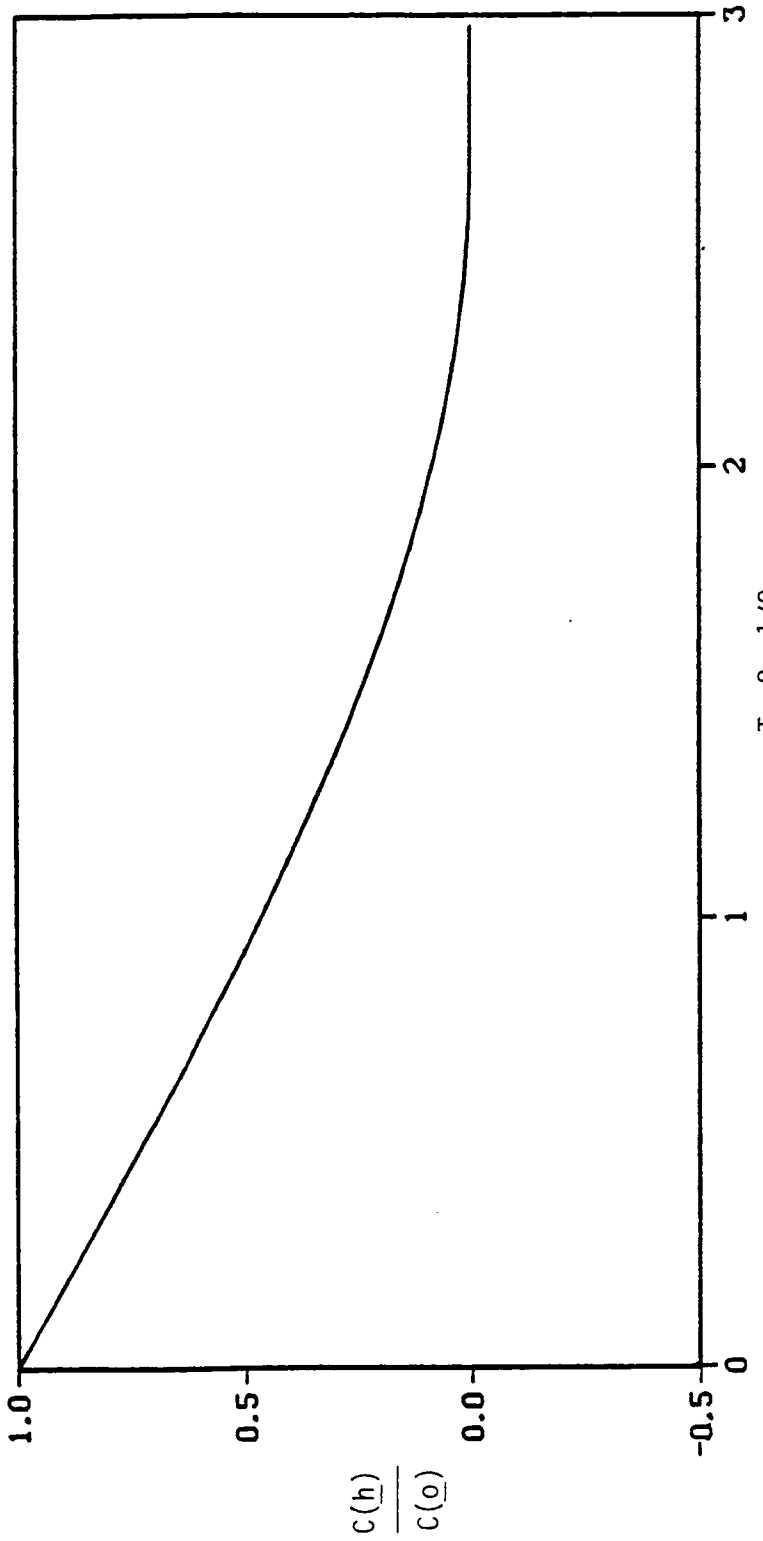

Figure 2.3. Autocorrelation Versus Dimensionless Distance, Spherical Model.

At this point, a legitimate question arises: "How is an covariance model, appropriate for a given set of data, chosen?" In the following sections this question is addressed.

2.4 Statistical Inference

The sample semivariogram (also called experimental semivariogram) is the computational tool most often used by geostatisticians for inference of the second-order properties of a random field. It is defined by

$$\gamma^*(\underline{h}) = [1/2N(\underline{h})] \sum_{i=1}^{N(\underline{h})} [f(\underline{x}_i+\underline{h}_i) - f(\underline{x}_i)]^2 \qquad (2.71)$$

where the $f(\underline{x}_i)$ are data obtained by sampling one particular realization of an intrinsic random field $f(\underline{x})$. For a fixed lag $\underline{h}$, $N(\underline{h})$ is the number of data pairs $[f(\underline{x}_i + \underline{h}_i, f(\underline{x}_i)]$ used for the computation of $\gamma^*(\underline{h})$. These data pairs must satisfy the following inequalities:

$$\left| |\underline{h}_i| - |\underline{h}| \right| \leq \Delta(\underline{h}) \qquad (2.72)$$

$$\frac{|\underline{h}_i \cdot \underline{h}|}{|\underline{h}||\underline{h}_i|} \geq \cos \eta, \; 0 \leq \eta \leq \pi/2, \; \underline{h}_i \neq \underline{0}, \; \underline{h} \neq \underline{0} \qquad (2.73)$$

where $\Delta(\underline{h})$ denotes the distance tolerance as a function of the lag $\underline{h}$. Similarly η represents the angle tolerance or window, as it is often called. The selection of distance and angle tolerances is discussed further in Section 2.4.2.

The reasons for using the experimental semivariogram rather than a covariance estimator, are two-fold. First, the conditions for

existence of the semivariogram $\gamma(\underline{h})$ are less restrictive than those of the covariance $C(\underline{h})$ (intrinsic hypothesis versus weak stationarity). Second, given that a field is weakly stationary, direct estimation of the covariance usually requires simultaneous estimation of the mean $\overline{f}$. As such there is an increased risk of bias (see p. 195 of Journel and Huijbregts, 1978). The sample semivariogram however, does not require estimation of the mean and is therefore not subject to this type of bias. Once the semivariogram is estimated, the corresponding covariance function can be obtained through the use of equation (2.21).

2.4.1 Estimation Error

In estimating the theoretical semivariogram (equation 2.20) from the experimental semivariogram, error from various sources may be introduced. Quantitatively, the error is treated as a random variable with a mean and a variance. For example, the error of estimation of the theoretical semivariogram is

$$\varepsilon_*(\underline{h}) = \gamma^*(\underline{h}) - \gamma(\underline{h}) \tag{2.74}$$

Ideally, the estimator $\gamma^*(\underline{h})$ is chosen in such a way as to be unbiased,

$$E\,[\varepsilon_*(\underline{h})] = 0 \tag{2.75}$$

and to yield a minimum estimation variance. Then the estimator is said to be optimal.

For simplification, let us ignore for the moment the effects of grouping the data pairs by distance and angle classes. Note that this

corresponds to either of two special cases. In one case, the field is assumed to be isotropic, and the experimental semivariogram is only calculated for those lag vectors whose modulus is exactly equal to the distances between data locations. For the other case, the distance and angle tolerances are set equal to zero and no restrictions are made on either the data configuration or the field. In either case, if the field $f(\underline{x})$ is intrinsic, then the non-bias requirement is fulfilled and the variance of estimation of the theoretical semivariogram is given by

$$E\{[\varepsilon_*(\underline{h})]^2\} = E\{[\gamma^*(\underline{h}) - \gamma(\underline{h})]^2\} \tag{2.76}$$

Journel and Huijbregts (1978) define a local semivariogram

$$\gamma_{(v)}(\underline{h}) = \frac{1}{2V'(\underline{h})} \int_{V'(\underline{h})} [f(\underline{x}+\underline{h}) - f(\underline{x})]^2 \, d\underline{x} \tag{2.77}$$

where $V(\underline{h})$ consists of all $\underline{x}$, $\underline{x}+\underline{h}$ which are in the "local" domain of interest, V. Thus, the calculation of the local semivariogram generally requires complete knowledge of a particular realization of the random function $f(\underline{x})$, over the domain V.

For theoretical purposes, it is useful to think of the local semivariogram not only as a spatial average over a single realization of the field, but as an estimator of the theoretical semivariogram. Then the estimation error is called a fluctuation (Journel and Huijbregts, 1978)

$$\varepsilon_{(v)}(\underline{h}) = \gamma_{(v)}(\underline{h}) - \gamma(\underline{h}) \tag{2.78}$$

Again, if the field is intrinsic, the estimator is unbiased,

$$E[\varepsilon_{(v)}(\underline{h})] = 0 \tag{2.79}$$

and the "fluctuation variance," as Journel and Huijbregts (1978) call it, is given by

$$E\{[\varepsilon_{(v)}(\underline{h})]^2\} = E\{[\gamma_{(v)}(\underline{h}) - \gamma(\underline{h})]^2\} \tag{2.80}$$

Finally, if a random field is intrinsic and the measuring process is free of systematic error, then the experimental semivariogram behaves without bias as an estimator of the local semivariogram.

$$E[\varepsilon_{*(v)}(\underline{h})] = 0 \tag{2.81}$$

where the error of estimation is the difference

$$\varepsilon_{*(v)}(\underline{h}) = \gamma^*(\underline{h}) - \gamma_{(v)}(\underline{h}) \tag{2.82}$$

and the variance of estimation of the local semivariogram (Journel and Huijbregts, 1978) is:

$$E\{[\varepsilon_{*(v)}(\underline{h})]^2\} = E\{[\gamma^*(\underline{h}) - \gamma_{(v)}(\underline{h})]^2\} \tag{2.83}$$

Now consider the problem of estimating the underlying (theoretical) semivariogram $\gamma(\underline{h})$ of an intrinsic random field $f(\underline{x})$, from an experimental semivariogram $\gamma^*(\underline{h})$. The estimation error and its variance are given by equations (2.74) and (2.76), respectively. Note that the estimation error can be expressed in terms of the experimental, local and theoretical semivariograms this way:

$$\gamma^*(\underline{h}) - \gamma(\underline{h}) = [\gamma^*(\underline{h}) - \gamma_{(v)}(\underline{h})] + [\gamma_{(v)}(\underline{h}) - \gamma(\underline{h})] \quad (2.84)$$

or

$$\varepsilon_*(\underline{h}) = \varepsilon_{*(v)}(\underline{h}) + \varepsilon_{(v)}(h)$$

Its variance is

$$E\{[\varepsilon_*(\underline{h})]^2\} = E\{[\varepsilon_{*(v)}(\underline{h})]^2\} + 2E\{\varepsilon_{*(v)}(\underline{h})\ \varepsilon_{(v)}(\underline{h})\} + E\{[\varepsilon_{(v)}(\underline{h})]^2\} \quad (2.85)$$

The form of equation (2.84) suggests that the semivariogram estimation problem can be viewed as the combination of two separate estimation problems. The first problem is the estimation of the local semivariogram from the experimental semivariogram. It concerns directly only one realization of the stochastic process, that corresponding to the actual physical system. The second problem is the estimation of the theoretical semivariogram from the local semivariogram, and it concerns the entire ensemble.

Estimation of the local semivariogram can be complicated by any one or more of various possible characteristics of a data set. Important considerations include possible effects due to (1) measurement error, (2) support size - data abundance or scarcity, (3) nonstationarity and (4) regularization. The effect of measurement error is to be examined presently while the last three possibilities will be considered in subsequent sections.

To see what effect measurement error has on the calculated experimental semivariogram, consider the intrinsic random field $f(\underline{x})$

and the corresponding measured values of $f^*(\underline{x})$ of the variable f, at various locations $\underline{x}$. Because the measurement process is imperfect, there is an error $\varepsilon(\underline{x})$ associated with each measurement $f^*(\underline{x})$:

$$f^*(\underline{x}) = f(\underline{x}) + \varepsilon(\underline{x}) \tag{2.86}$$

The error is itself a random variable. The true semivariogram of the measured values, f*, is then

$$\gamma_{f^*}(\underline{x},\underline{x}+\underline{h}) = \gamma(\underline{h}) + 2\gamma_{\varepsilon f}(\underline{x},\underline{x}+\underline{h}) + \gamma_{\varepsilon}(\underline{x},\underline{x}+\underline{h}) \tag{2.87}$$

where

$$\gamma_{\varepsilon f}(\underline{x},\underline{x}+\underline{h}) = E\{[\varepsilon(\underline{x}+\underline{h}) - \varepsilon(\underline{x})][f(\underline{x}+\underline{h}) - f(\underline{x})]\}$$

A special case is worthy of consideration here. If the measurement process is free of bias, then

$$E\,[\varepsilon(\underline{x})] = 0 \tag{2.88}$$

If additionally, the measurement error (1) lacks spatial autocorrelation,

$$E\,[\varepsilon(\underline{x}+\underline{h})\ \varepsilon(\underline{x})] = 0 \tag{2.89}$$

(2) possesses a finite variance which is independent of the position,

$$E\{[\varepsilon(\underline{x})]^2\} = \sigma_{\varepsilon}^2 < +\infty \tag{2.90}$$

and (3) lacks spatial correlation with the field itself,

$$\gamma_{\varepsilon f}(\underline{x},\underline{x}+\underline{h}) = 0 \tag{2.91}$$

then the semivariogram of the error takes the form

$$\gamma_\varepsilon(\underline{h}) = \sigma_\varepsilon^2 \, U(\underline{h}) \tag{2.92}$$

where $U(\underline{h})$ is the unit step function

$$U(\underline{h}) = \begin{cases} 0, & \underline{h} = \underline{0} \\ 1, & \underline{h} \neq \underline{0} \end{cases} \tag{2.93}$$

Under these conditions, the error $\varepsilon(\underline{x})$ can be interpreted as white noise. The behavior of its semivariogram (equation 2.92), near the origin, is known in geostatistics as the pure nugget effect. The semivariogram of the random field $f^*(\underline{x})$ is then

$$\gamma_{f^*}(\underline{h}) = \gamma(\underline{h}) + \sigma_\varepsilon^2 \, U(\underline{h}) \tag{2.94}$$

It also has an apparent discontinuity at the origin, known simply as the nugget effect. A common practice is to replace the model (2.94) with

$$\gamma_{f^*}(\underline{h}) = \gamma(\underline{h}) + C_0 \tag{2.95}$$

Here C_0 represents the error variance σ_ε^2 and is called the nugget constant.

Although the presence of measurement error can produce an apparent nugget effect on the experimental semivariogram, it is not the only possible cause of this effect. A scale phenomenon can manifest itself in a similar manner. In particular, if the range is small compared to the distance coordinate of the first point on the sample semivariogram, an apparent nugget effect may result.

The local semivariogram is an unbiased estimator of the theoretical semivariogram, but the associated error variance (fluctuation variance) may be large. In fact, the fluctuation variance may be so great as to render the local semivariogram useless as an estimator. If this is the case, then statistical inference of the semivariogram or covariance is impossible and the entire stochastic conceptual approach is impractical. To avoid this difficulty, the ergodic hypothesis (Section 2.2.3) is exploited. Under the ergodic hypothesis, the local semivariogram converges to the theoretical semivariogram as the size of the local domain V increases. For an infinite n-dimensional field, R^n,

$$\lim_{V \to R^n} \gamma_{(v)}(\underline{h}) = \gamma(\underline{h}) \tag{2.96}$$

Equivalently, the fluctuation dies out:

$$\lim_{V \to R^n} \varepsilon_{(v)}(\underline{h}) = 0 \tag{2.97}$$

The rate of convergence typically depends on the lag $\underline{h}$ because for a given size of the local domain V, the actual volume $V'(\underline{h})$ over which the average (local semivariogram) is taken depends on $\underline{h}$. This follows immediately from equation (2.77).

2.4.2 Practical Considerations

In practice, field data often do not fall on a regular spatial grid. Therefore, experimental semivariogram computation requires that data pairs be sorted into groups, according to whether or not the relative orientation of each pair is within certain distance and angle

tolerances of the specified orientation, $\underline{h}$. Because land surveys and other measurement techniques are inexact, even data pairs from a so-called regular grid must be grouped this way. Inequalities (2.72) and (2.73) are the mathematical expressions of this grouping procedure.

For a fixed separation $\underline{h}$, all of those data pairs whose coordinates satisfy inequalities (2.72) and (2.73) are said to belong to the same class or group. The distance class size is $2\Delta(\underline{h})$. An actual distance value is usually assigned to the class by taking the average of the distances corresponding to the constituent data pairs of that class,

$$\text{Mean Distance} = [1/N(\underline{h})] \sum_{i=1}^{N(\underline{h})} |\underline{h}_i| \qquad (2.98)$$

The mean distance is taken to be representative of the group and is used for plotting the experimental semivariogram.

Distance tolerances can be chosen in various ways. First, a general scheme is selected. For example, one possibility is to group the data according to relative distance deviations:

$$\Delta(\underline{h}) = \Delta|\underline{h}|, \ \Delta \text{ a constant} \qquad (2.99)$$

Under this scheme Δ is chosen to be a "small" constant, say 0.1 or 0.2, and the distance class size increases linearly with separation distance $|\underline{h}|$. A simpler approach, used in this study, is to choose a constant distance tolerance:

$$\Delta(\underline{h}) = \Delta, \ \Delta \text{ a constant} \qquad (2.100)$$

Then the distance class size is uniform. Next, actual values of the tolerance are selected, usually by trial and error.

It is clear from the previous discussion and from equations (2.71), (2.72) and (2.73) that computation of the experimental semivariogram involves an averaging of the squared data differences over distance and angle classes. The consequences of this averaging are mixed. On one hand, averaging results in the loss of specific information regarding differences in spatial variability within a given distance or angle class of the semivariogram. The sacrifice is not without its reward, however. By grouping the data pairs, the number of pairs available for calculation of any single point on the semivariogram increases. Generally as the number of data pairs increases, the variance of estimation (equation (2.83)) decreases. More importantly, the semivariogram generally becomes better behaved in the sense that its points become less scattered and its overall form less oscillatory. Therefore, the selection of distance and angle tolerances involves a compromise between (1) resolution and (2) reliability and interpretability. This apparent antagonism between resolvability and reliability is analogous to a similar situation occurring in spectral estimation, which has been named "Grenander's uncertainty principle" (Priestley, 1981).

As a rule of thumb, Journel and Huijbregts (1978) recommend that the distance and angle tolerances should be chosen so that each point of the experimental semivariogram uses at least 30 to 50 data pairs for its computation. The purpose of this restriction is to limit

the local estimation variance. Similarly, if all of the data from the field come from a sub-volume of maximum extent L, then only those distance classes for which the mean distance is less than about L/2 should be used for semivariogram estimation. For greater distances, the fluctuation variance may be too great for reliable estimation (Journel and Huijbregts, 1978). However, rather than discard data which fail to satisfy these somewhat arbitrarily chosen criteria, they can be plotted with the remaining data while keeping in mind their lower reliability. Then to distinguish between data of higher and lower reliability, the following operational procedures are considered standard practice. First, for each point of the experimental semivariogram, the number of data pairs utilized in the computation is tabulated for reference. Second, those points for which the number of data pairs is less than some minimum (say 50) are plotted with a different symbol. For this study, a small circle o will be used to indicate that less than 50 data pairs were used in the calculation of that point while a dot • indicates that the class contains 50 or more data pairs.

2.4.3 Effect of a Drift

It is conceivable that the mean or expectation of a random field may be a function of the coordinates, rather than a constant. Then the field is said to exhibit a drift. The drift is given by the deterministic function of space,

$$\overline{f}(\underline{x}) = E[f(\underline{x})] \qquad (2.101)$$

This type of field is non-stationary, even to first order. Utilizing equations (2.5), (2.6) and (2.17), the theoretical semivariogram may be written:

$$\gamma(\underline{x},\underline{x}+\underline{h}) = (1/2)E\{[f(\underline{x}+\underline{h}) - f(\underline{x})]^2\} - (1/2)[\overline{f}(\underline{x}+\underline{h}) - \overline{f}(\underline{x})]^2 \qquad (2.102)$$

To see what kind of effect the drift has on the estimate given by the experimental semivariogram (equation 2.71), we can take its expectation to find

$$E[\gamma^*(\underline{x},\underline{x}+\underline{h})] = (1/2)E\{[f(\underline{x}+\underline{h}) - f(\underline{x})]^2\} \qquad (2.103)$$

Rewriting the equation in terms of the theoretical semivariogram,

$$E[\gamma^*(\underline{x},\underline{x}+\underline{h})] = \gamma(\underline{x},\underline{x}+\underline{h}) + (1/2)[\overline{f}(\underline{x}+\underline{h}) - \overline{f}(\underline{x})]^2 \qquad (2.104)$$

Obviously then, in the presence of a drift the experimental semivariogram gives a biased estimate of the theoretical semivariogram.

The theoretical semivariogram (equation 2.102) can also be written in terms of the residuals $f'(\underline{x})$:

$$\gamma(\underline{x},\underline{x}+\underline{h}) = (1/2)E\{[f'(\underline{x}+\underline{h}) - f'(\underline{x})]^2\} \qquad (2.105)$$

The residual $f'(\underline{x})$ is a first-order stationary random field. If the residuals can be considered intrinsic or second-order stationary, then the quantity estimated by the experimental semivariogram is obtained by substituting equation (2.105) into equation (2.104):

$$E[\gamma^*(\underline{x},\underline{x}+\underline{h})] = \gamma(\underline{h}) + (1/2)[\overline{f}(\underline{x}+\underline{h}) - \overline{f}(\underline{x})]^2 \qquad (2.106)$$

Although the presence and/or form of a drift may be difficult to determine, equation (2.106) shows that non-stationarity may show up in various ways on the experimental semivariogram. For example, if the drift is such that the mean $f(\underline{x})$ changes linearly or faster in a given direction, then experimental semivariograms for that direction can be expected to show a persistent, quadratic or greater increase with distance. Because the drift may be direction dependent, experimental data might also be characterized by an apparent anisotropy such as that reported by Neuman and Jacobson (1984). This can occur even if the field of residuals is statistically isotropic.

2.4.4 Effect of Regularization

Let $f(\underline{x})$ be a three-dimensional random process, such as log permeability. Often, information about the statistical properties of $f(\underline{x})$ will be derived from field data such as those obtained in aquifer pump tests or packer tests. The results of these tests generally represent some type of spatial average of the measured quantity $f(\underline{x})$ rather than the quantity itself. For illustration, I will assume that the measurement process is linear so that the measured values $f_p(\underline{x})$ can be expressed as

$$f_p(\underline{x}) = \int_{R^3} f(\underline{x}+\underline{s})\ p(\underline{s})\ d\underline{s} \qquad (2.107)$$

where the weight function $p(\underline{s})$ is a characteristic of the measuring instrument. The function $f_p(\underline{x})$ is also a random function and is called

the regularization of $f(\underline{x})$ (Matheron, 1971). A simple example is volume averaging. In three dimensions, this is

$$f_V(\underline{x}) = (1/V) \int_V f(\underline{x}+\underline{s})\, d\underline{s} \tag{2.108}$$

where V is a reference volume associated with the measuring instrument.

Now consider the estimation of the mean of the first-order stationary random field $f(\underline{x})$. Let the estimator be given by

$$\hat{(\overline{f})} = \frac{1}{N} \sum_{i=1}^{N} f_p(\underline{x}_i) \tag{2.109}$$

To determine whether $\hat{(\overline{f})}$ is biased, we take its expectation

$$E\hat{(\overline{f})} = \int_{R^3} p(\underline{s})\, d\underline{s}\ \overline{f} \tag{2.110}$$

Expression (2.112) shows that the estimator is generally biased, unless the integral equals one

$$\int_{R^3} p(\underline{s})\, d\underline{s} = 1 \tag{2.111}$$

Simple volume averaging fulfills this requirement.

Because of the regularization, the second moments of the field $f(\underline{x})$ cannot be estimated directly from the sample semivariogram. Rather, the sample semivariogram estimates the semivariogram of the regularization, $\gamma_V(\underline{x},\underline{x}+\underline{h})$.

Consider the case of simple volume averaging of the stochastic process $f(\underline{x})$. If $f(\underline{x})$ is first-order stationary,

$$C_V(\underline{x},\underline{x}+\underline{h}) = E\{[f_V(\underline{x}) - \overline{f}][f_V(\underline{x}+\underline{h}) - \overline{f}]\} \qquad (2.112)$$

This can also be expressed

$$C_V(\underline{x},\underline{x}+\underline{h}) = (1/V^2) \int_V \int_V \{E[f(\underline{x}+\underline{s})f(\underline{x}+\underline{h}+\underline{s}')] - \overline{f}^2\}\, d\underline{s}\, d\underline{s}' \qquad (2.113)$$

Letting $\underline{t} = \underline{h}+\underline{s}'$,

$$C_V(\underline{x},\underline{x}+\underline{h}) = (1/V^2) \int_V \int_{V'} \{E[f(\underline{x}+\underline{s})f(\underline{x}+\underline{t})] - \overline{f}^2\}\, d\underline{s}\, d\underline{t} \qquad (2.114)$$

where V' is the translation of the volume V, by the vector $\underline{h}$. If $f(\underline{x})$ is second-order stationary,

$$C_V(\underline{h}) = (1/V^2) \int_V \int_{V'} C(\underline{t}-\underline{s})\, d\underline{s}\, d\underline{t} \qquad (2.115)$$

This is sometimes abbreviated to C(V,V').

The semivariogram of the regularized process is determined through a similar procedure. Again, if $f(\underline{x})$ is first-order stationary,

$$\gamma_V(\underline{x},\underline{x}+\underline{h}) = (1/2)E\{[f_V(\underline{x}) - f_V(\underline{x}+\underline{h})]^2\} \qquad (2.116)$$

If $f(\underline{x})$ is second-order stationary,

$$\gamma_V(\underline{h}) = (1/V^2) \int_V \int_V C(\underline{t}-\underline{s})\, d\underline{s}\, d\underline{t} - C_V(\underline{h}) \qquad (2.117)$$

This is sometimes written (Journel and Huijbregts, 1978):

$$\gamma_V(\underline{h}) = C_V(\underline{o}) - C_V(\underline{h})$$

or (2.118)

$$\gamma_V(\underline{h}) = \overline{C}(V,V) - \overline{C}(V,V')$$

Generally, the regularized process has a lower variance and a greater range or integral scale. Its spatial variation is more regular than the underlying process, thus the term "regularized."

CHAPTER 3

RELATIONSHIP BETWEEN STATISTICS OF LOCAL PERMEABILITY FIELD AND EFFECTIVE DIRECTIONAL PERMEABILITY

3.1 Introduction

In this chapter I derive, in detail, approximate analytical expressions relating the statistics of a log permeability field to the effective average permeability tensor. The derivation is an extension of that by Gelhar and Axness (1983a).

3.2 Derivation

3.2.1 Darcy's Law

The generalized form of Darcy's Law gives the relationship between the specific discharge vector, $\underline{q}$, the hydraulic head gradient, ∇H, and the permeability tensor, $\underline{K}$, of a saturated porous medium:

$$\underline{q} = -\underline{K}\nabla H \tag{3.1}$$

I shall assume that the medium is locally isotropic, as Gelhar and Axness (1983a) have done. Then, the appropriate form of Darcy's law is

$$\underline{q}(\underline{x}) = -K(\underline{x})\nabla H(\underline{x}) \tag{3.2}$$

where the specific discharge, the hydraulic head, and the permeability are understood to vary with the spatial coordinates, $\underline{x}$.

As discussed in Section 2.1, the spatial distributions of $\underline{q}$, K and H are unknown and are represented stochastically as random quantities (random fields). Each of the quantities is written as the sum of its mean and a perturbation or fluctuation term:

$$\begin{aligned} q_j(\underline{x}) &= \overline{q}_j(\underline{x}) + q'_j(\underline{x});\ E[q'_j(\underline{x})] = 0 \qquad (j=1,2,3) \\ H(\underline{x}) &= \overline{H}(\underline{x}) + H'(\underline{x})\ ;\ E[H'(\underline{x})] = 0 \\ f(\underline{x}) &= \overline{f}(\underline{x}) + f'(\underline{x})\ ;\ E[f'(\underline{x})] = 0 \end{aligned} \tag{3.3}$$

where

$$f(\underline{x}) = \ln K(\underline{x}) \tag{3.4}$$

Upon dropping $\underline{x}$ for brevity, Darcy's law in (3.2) can be written in indicial notation as

$$q_j = -\exp \overline{f} \exp f' \left[\frac{\partial \overline{H}}{\partial x_j} + \frac{\partial H'}{\partial x_j}\right] \tag{3.5}$$

Utilizing Taylor's series representation for exp f', (3.5) becomes

$$q_j = K_\ell \left[1 + f' + \frac{(f')^2}{2!} + \frac{(f')^3}{3!} + \cdots\right]\left[J_j - \frac{\partial H'}{\partial x_j}\right] \tag{3.6}$$

where

$$J_j = J_j(\underline{x}) = -\frac{\partial \overline{H}(\underline{x})}{\partial x_j} \tag{3.7}$$

$$K_\ell = K_\ell(\underline{x}) = \exp \overline{f}(\underline{x}) \tag{3.8}$$

Expression (3.6) is the same as equation (48) of Gelhar and Axness (1983a). Taking the expectation of (3.6) gives

$$\overline{q}_j = K_\ell[(1 + \frac{\sigma_f^2}{2} + \frac{\overline{(f')^3}}{6} + \overline{\cdots}) J_j$$

$$-(\overline{f' \frac{\partial H'}{\partial x_j}} + \frac{\overline{(f')^2 \frac{\partial H'}{\partial x_j}}}{2} + \overline{\cdots})] \qquad (3.9)$$

At this stage, Gelhar and Axness (1983a) drop all terms of (3.9) involving expectations of third- and higher-order products of perturbations. The result is the following approximation for the averaged form of Darcy's law:

$$\overline{q_j} \cong K_\ell[(1 + \frac{\sigma_f^2}{2})J_j - \overline{f' \frac{\partial H'}{\partial x_j}}]$$

or (3.10)

$$\underline{\overline{q}} \cong K_\ell[(1 + \frac{\sigma_f^2}{2})\underline{J} - \overline{f' \nabla H'}]$$

This is a second-order approximation which, to be valid, requires that (1) the perturbation f' have a finite variance, σ_f^2, or equivalently that $f'(\underline{x})$ be a second-order stationary process, and (2) that the perturbation be in some sense "small." This second condition will be discussed further in Section 3.3.1.

Equation (3.10) is not yet in a useful form. Ideally, we would like to express the last term, $f'\nabla H'$ in terms of the statistics of f and/or H. This is the goal of the next three sections.

3.2.2 Steady Flow

To derive the perturbed steady-state flow equation, one starts with the the conservation of mass principle. For incompressible flow in the absence of sources and sinks, this principle states that

$$\nabla \cdot \underline{q} = 0 \tag{3.11}$$

Substituting Darcy's law (3.2) into (3.11) gives

$$\nabla \cdot (K\nabla H) = 0$$

or

$$\frac{\nabla K}{K} \cdot \nabla H + \nabla^2 H = 0, \quad K \neq 0 \tag{3.12}$$

Equivalently,

$$\nabla f \cdot \nabla H + \nabla^2 H = 0 \tag{3.13}$$

where $f = \ln K$. This relationship (3.13) is known as the log-linearized form of the steady-state flow equation.

Expressing each of the random quantities $f(\underline{x})$ and $H(\underline{x})$ as the sum of a mean and a perturbation, as in (3.3), leads to the perturbed steady-state flow equation:

$$\nabla \overline{f} \cdot \nabla \overline{H} + \nabla f' \cdot \nabla \overline{H} + \nabla \overline{f} \cdot \nabla H' + \nabla f' \cdot \nabla H' + \nabla^2 \overline{H} + \nabla^2 H' = 0 \tag{3.14}$$

Taking the expectation of (3.14) results in the ensemble-averaged steady-state flow equation:

$$\nabla \overline{f} \cdot \nabla \overline{H} + \overline{\nabla f' \cdot \nabla H'} + \nabla^2 \overline{H} = 0 \tag{3.15}$$

Substitution of (3.15) into (3.14) yields

$$\nabla f' \cdot \nabla \overline{H} + \nabla \overline{f} \cdot \nabla H' + \nabla f' \cdot \nabla H' - \overline{\nabla f' \cdot \nabla H'} + \nabla^2 H' = 0 \qquad (3.16)$$

Unfortunately, (3.16) does not lend itself readily to spectral analysis. To surmount this difficulty, without additional information, requires making some assumptions. The approach taken here is that used by Glezen and Lerche (1985) to which they refer as "mean field renormalization." It relies on the assumption

$$\nabla f' \cdot \nabla H' - \overline{\nabla f' \cdot \nabla H'} \cong 0 \qquad (3.17)$$

Using this, (3.16) can be approximated as

$$\nabla f' \cdot \nabla \overline{H} + \nabla \overline{f} \cdot \nabla H' + \nabla^2 H' = 0 \qquad (3.18)$$

This approximation is first-order (linear) in the perturbed quantities and contains no constant terms, unlike the original form of (3.16). Hence, it is suitable for spectral analysis of the kind presented below.

3.2.3 Spectral Analysis of Steady-State Flow

Recall from Section 2.2.2 that the log permeability $f(\underline{x})$ or its perturbation $f'(\underline{x})$ is represented as a second-order stationary process in order to facilitate moment estimation. The stationarity assumption is required for another purpose--spectral representation. Because spectral representation is an extremely valuable tool for the present analysis, I will now follow the course taken by Gelhar and Axness (1983a) and extend the stationarity requirement to the hydraulic head

perturbation field, $H'(\underline{x})$. Then by the Spectral Representation theorem, the perturbed processes can be expressed as:

$$f'(\underline{x}) = \int_{\underline{k}} \exp(i\underline{k}\cdot\underline{x})\, dZ_f(\underline{k}) \tag{3.19}$$

$$H'(\underline{x}) = \int_{\underline{k}} \exp(i\underline{k}\cdot\underline{x})\, dZ_H(\underline{k}) \tag{3.20}$$

where

$$\int_{\underline{k}} g(\underline{k})\, dZ(\underline{k}) = \lim_{a,b,c \to \infty} \int_{-a}^{a}\int_{-b}^{b}\int_{-c}^{c} g(\underline{k})\, dZ(k_1,k_2,k_3) \tag{3.21}$$

$\underline{k}$ is a real three-dimensional wave number vector (analogous to angular frequency in one dimension), $i = \sqrt{-1}$ and $Z(\underline{k})$ is a complex, three-dimensional orthogonal process. Details regarding the Spectral Representation Theorem and the techniques of spectral analysis are discussed by Lumley and Panofsky (1964) and Priestley (1981).

Assuming that the expectation of the log permeability field is constant ($\nabla\overline{f} = \underline{0}$), the approximate perturbed flow equation (3.18) can be written as

$$\sum_{n=1}^{3} \left[- \frac{\partial f'}{\partial x_n} J_n + \frac{\partial^2 H'}{\partial x_n^2} \right] = 0 \tag{3.22}$$

Utilizing (3.19) and (3.20), the flow equation can be expressed as

$$\sum_{n=1}^{3} \left[iJ_n \int_{\underline{k}} k_n \exp(i\underline{k}\cdot\underline{x})\, dZ_f(\underline{k}) + \int_{\underline{k}} k_n^2 \exp(i\underline{k}\cdot\underline{x})\, dZ_H(\underline{k}) \right] = 0 \tag{3.23}$$

Since the Fourier-Stieltjes integrals in (3.23) are over the same wave number domain, the integrands can be grouped to read

$$\int_{\underline{k}} \exp(i\underline{k}\cdot\underline{x})\{i\underline{J}\cdot\underline{k}\ dZ_f(\underline{k}) + |\underline{k}|^2\ dZ_H(\underline{k})\} = 0 \tag{3.24}$$

Due to the uniqueness of the Fourier-Stieltjes representations (3.19) and (3.20), this can be expressed as

$$\underline{J}\cdot\underline{k}\ dZ_f(\underline{k}) = i|\underline{k}|^2\ dZ_H(\underline{k}) \tag{3.25}$$

Solving for the amplitude $dZ_H(\underline{k})$ yields

$$dZ_H(\underline{k}) = -i\ \frac{\underline{J}\cdot\underline{k}}{|\underline{k}|^2}\ dZ_f(\underline{k}) \tag{3.26}$$

3.2.4 Evaluation of $\overline{f'\nabla H'}$

The term $\partial H'/\partial x_j$ is real and is thus identical to its complex conjugate (denoted by asterisk),

$$\frac{\partial H'}{\partial x_j} = \left(\frac{\partial H'}{\partial x_j}\right)^* \tag{3.27}$$

Making use of the spectral representation (3.20), (3.27) becomes

$$\frac{\partial H'}{\partial x_j} = \left[i \int_{\underline{k}} k_j \exp(i\underline{k}\cdot\underline{x})\ dZ_H(\underline{k})\right]^* \tag{3.28}$$

Replacing the amplitude $dZ_H(\underline{k})$ in (3.28) with its corresponding expression from (3.26) and taking the complex conjugate gives

$$\frac{\partial H'}{\partial x_j} = \int_{\underline{k}} \frac{\underline{J}\cdot\underline{k}\ k_j}{|\underline{k}|^2} \exp(-i\underline{k}\cdot\underline{x})\ dZ_f^*(\underline{k}) \tag{3.29}$$

Using (3.19) and (3.29) results in

$$\overline{f'(\underline{x}+\underline{h})\ \frac{\partial H'(\underline{x})}{\partial x_j}} = E\{\int_{\underline{k}'} \exp[i\underline{k}'\cdot(\underline{x}+\underline{h})]\ dZ_f(\underline{k}') \int_{\underline{k}} \frac{\underline{J}\cdot\underline{k}\ k_j}{|\underline{k}|^2} \exp[-i\underline{k}\cdot\underline{x}]\ dZ_f^*(\underline{k})\} \tag{3.30}$$

From the Spectral Representation theorem,

$$E[dZ_f(\underline{k}')\ dZ_f^*(\underline{k})] = \begin{cases} S_{ff}(\underline{k})\ d\underline{k}, & \underline{k} = \underline{k}' \\ 0 \quad\quad\quad , & \underline{k} \neq \underline{k}' \end{cases} \tag{3.31}$$

where $S_{ff}(\underline{k})$ is the spectral density (power spectrum) of the process $f'(\underline{x})$ given by

$$S_{ff}(\underline{k}) = \frac{1}{(2\pi)^3} \int_{\underline{h}} \exp(-i\underline{k}\cdot\underline{h})\ C_{ff}(\underline{h})\ d\underline{h} \tag{3.32}$$

$C_{ff}(\underline{h})$ being the spatial covariance function of $f'(\underline{x})$. Thus, equation (3.30) can be expressed as

$$f'(\underline{x}+\underline{h})\ \frac{\partial H'(\underline{x})}{\partial x_j} = \int_{\underline{k}} \exp(i\underline{k}\cdot\underline{h})\ \frac{\underline{J}\cdot\underline{k}\ k_j}{|\underline{k}|^2}\ S_{ff}(\underline{k})\ d\underline{k} \tag{3.33}$$

or

$$\overline{f'(\underline{x}+\underline{h})\nabla H'(\underline{x})} = \int_{\underline{k}} \exp(i\underline{k}\cdot\underline{h})\ \underline{k}\ \underline{k}^T\ \frac{S_{ff}(\underline{k})}{|\underline{k}|^2}\ d\underline{k}\ \underline{J} \tag{3.34}$$

For use in the averaged form of Darcy's law, we need (3.33) for zero separation:

$$\overline{f' \frac{\partial H'}{\partial x_j}} = J_j \int_{\underline{k}} \frac{k_j^2}{|\underline{k}|^2} S_{ff}(\underline{k})\, d\underline{k} \tag{3.35}$$

or

$$\overline{f' \nabla H'} = \underline{F}\, \underline{J} \tag{3.36}$$

where $\underline{F}$ is the diagonal matrix given by

$$F_{jj} = \int_{\underline{k}} \frac{k_j^2}{|\underline{k}|^2} S_{ff}(\underline{k})\, d\underline{k} \tag{3.37}$$

3.2.5 Effective Permeability Tensor

Combining (3.10) and (3.36), the expression for average specific discharge is found to be

$$\overline{\underline{q}} \cong K_g[(1 + \sigma_f^2/2)\underline{I} - \underline{F}]\underline{J} = \overline{\underline{K}}\, \underline{J} \tag{3.38}$$

where $\underline{I}$ is the identity matrix, $\underline{J} = \underline{J}(\underline{x})$ is the negative mean hydraulic gradient and $\overline{\underline{K}}$ is an effective permeability tensor.

That $\overline{\underline{K}}$ is tensorial can be proven as follows. First rewrite equation (3.37) to read

$$\underline{F} = \int_{\underline{k}} \underline{k}\, \underline{k}^T \frac{S_{ff}(\underline{k})}{|\underline{k}|^2}\, d\underline{k} \tag{3.39}$$

Now consider the linear transformation in the spatial domain

$$\underline{x}' = \underline{A}\, \underline{x} \tag{3.40}$$

where $\underline{A}$ is a nonsingular matrix which transforms the coordinate vector $\underline{x}$ in the original system to $\underline{x}'$ in the new system. Then $\underline{F}$ can be expressed in terms of the transformed quantities (see also Appendix C):

$$\underline{F} = \int_{\underline{k}'} \underline{A}^T \underline{k}' (\underline{k}')^T \underline{A} \frac{S_{ff}'(\underline{k}')}{(\underline{k}')^T \underline{A}\, \underline{A}^T \underline{k}'} \, dk' \tag{3.41}$$

If the transformation consists of a rotation of the coordinate axes, then $\underline{A}$ is orthogonal,

$$\underline{A}^T = \underline{A}^{-1} \tag{3.42}$$

and (3.41) is expressed as

$$\underline{F} = \underline{A}^T \underline{F}' \underline{A} \tag{3.43}$$

where

$$\underline{F}' = \int_{\underline{k}'} \underline{k}' (\underline{k}')^T \frac{S_{ff}'(\underline{k}')}{|\underline{k}'|^2} \, d\underline{k}' \tag{3.44}$$

Thus $\underline{F}$ is a second-rank affine tensor. It follows that $\overline{\underline{K}}$, being a linear combination of $\underline{F}$ and $\underline{I}$, is likewise a second-rank tensor.

3.3 Special Cases

3.3.1 Large Variance in Log Permeability

The reader will recall that near the end of Section 3.2.1 there was some discussion about the validity of the second-order approximation used to derive the average Darcy's law (3.10). I will

now examine the question of how large is "too large" for the log permeability variance, σ_f^2, in order for the approximation to be valid. First consider the approximate analytical result for $\overline{K_{ii}}$, which is

$$\overline{K_{ii}^p} = K_\ell[1 + \sigma_f^2/2 - F_{ii}] \tag{3.45}$$

where F_{ii} is given by the integral (3.37). Because $S_{ff}(\underline{k}) \geq 0$ (Priestley, 1981; Lumley and Panofsky, 1964), it follows from (E.3) that the F_{ii} terms are bounded above and below,

$$0 \leq F_{ii} \leq \sigma_f^2 \tag{3.46}$$

so that whenever the variance is greater than or equal to 2, the potential exists for the resulting expression (3.45) to be negative (Gelhar and Axness, 1983a). A negative permeability is physically impossible and therefore equation (3.45) is not a suitable approximation under this condition ($\sigma_f^2 \geq 2$). In response to this inconsistency, Gelhar and Axness (1983a) suggest that the result (3.45) be generalized by considering that

$$1 + x \cong 1 + x + x^2/2! + x^3/3! + \ldots = e^x \tag{3.47}$$

where $x = \sigma_f^2/2 - F_{ii}$. Then (3.45) can be written as if the quantity in brackets is the first two terms of a truncated Taylor's series:

$$\overline{K_{ii}^p} = \exp[\overline{f} + \sigma_f^2/2 - F_{ii}], \quad \sigma_f^2 > 1 \tag{3.48}$$

The justification given by Gelhar and Axness (1983a) for (3.48) is that it gives exact results for the special cases of flow parallel or perpendicular to the layers of a perfectly stratified medium, when K is lognormally distributed. Unfortunately they give no justification for its general application, although an obvious advantage is its positiveness.

An approximate analytical expression for the effective scalar permeability is obtained by forming the geometric mean of the principal permeabilities given in (3.48):

$$\left[\prod_{i=1}^{3} \overline{K_{ii}^{p}}\right]^{1/3} = \exp[\overline{f} + \sigma_f^2/6] \tag{3.49}$$

It is interesting to note that the large variance expression (3.48) implies that the effective permeability matrix $\underline{\overline{K}}$ is generally non-tensorial, since $\underline{\overline{K}}$ is non-linear in $\underline{I}$ and $\underline{F}$. Instead, the logarithm of $\underline{\overline{K}}$ is tensorial.

Further insight into the conditions under which the approximations (3.45) and (3.48) are valid, can be gained by Monte Carlo simulations. Until exhaustive three-dimensional simulation studies are performed or until an alternative analysis is conducted, the accuracy of the approximations remains untested.

3.3.2 Geometric Anisotropy

As mentioned earlier (Chapter 2), ellipsoidal covariance models are useful because they provide a relatively simple means of characterizing statistical anisotropy. Their suitability, however, should be

determined on a case-by-case basis. Assuming that the log permeability field is geometrically anisotropic, the F_{ii} integral (3.37) can be generalized. Begin with equation (3.37). Then consider the nonsingular linear coordinate transformation

$$\underline{x}' = \underline{\lambda}^{-1}\underline{x} \tag{3.50}$$

in which $\underline{x}$, the coordinate vector in the statistically anisotropic system, is transformed by $\underline{\lambda}^{-1}$, the inverse diagonal matrix of principal integral scales (2.59), to the vector $\underline{x}'$ in the isotropic coordinate system. Then (3.37) is written

$$F_{ii} = \frac{1}{\lambda_i^2} \int_{\underline{k}'} \frac{(k_i')^2}{|\underline{\lambda}^{-1}\underline{k}'|^2} S_{ff}'(\underline{k}')\, d\underline{k}' \tag{3.51}$$

(see Appendix C, and let $\underline{A} = \underline{\lambda}^{-1}$).

Transforming the coordinates of isotropic wave number space $\underline{k}'$ into spherical coordinates gives

$$\underline{k}' = \rho\underline{y} \tag{3.52}$$

where

$$\underline{y} = \underline{y}(\theta,\phi) = \begin{bmatrix} \cos\theta & \sin\phi \\ \sin\theta & \sin\phi \\ & \cos\phi \end{bmatrix} \tag{3.53}$$

and

$$\rho = |\underline{k}'| \tag{3.54}$$

Because $S'_{ff}(\underline{k}')$ is relative to the isotropic lag space $\underline{h}'$, it follows that $S'_{ff}(\underline{k}') = S'_{ff}(\rho)$ and (3.51) becomes

$$F_{ii} = \frac{1}{\lambda_i^2} \int_0^{\pi} \int_0^{2\pi} \int_0^{+\infty} \frac{y_i^2}{|\underline{\lambda}^{-1}\underline{y}|^2} S'_{ff}(\rho)\rho^2 \sin\phi \, d\rho \, d\theta \, d\phi \qquad (3.55)$$

This integral is partially separable:

$$F_{ii} = \frac{1}{\lambda_i^2} \int_0^{\pi} \int_0^{2\pi} \frac{y_i^2}{|\underline{\lambda}^{-1}\underline{y}|^2} \sin\phi \, d\theta \, d\phi \int_0^{+\infty} \rho^2 S'_{ff}(\rho) \, d\rho \qquad (3.56)$$

It is easy to show that (see Appendix D)

$$\int_0^{+\infty} \rho^2 S'_{ff}(\rho) \, d\rho = \frac{\sigma_f^2}{4\pi} \qquad (3.57)$$

so that F_{ii} can be expressed independently of the spectral density:

$$F_{ii} = \frac{2\sigma_f^2}{\pi\lambda_i^2} \int_0^{\pi/2} \int_0^{\pi/2} \frac{y_i^2}{|\underline{\lambda}^{-1}\underline{y}|^2} \sin\phi \, d\theta \, d\phi \qquad (3.58)$$

The implication of (3.58) is that $\underline{F}$ is dependent only on the variance (σ_f^2) and the ratios of the integral scales (λ_i/λ_j; i,j=1,2,3) of the log permeability spatial covariance function. Therefore the results of numerical computation of the g_{ii} (= F_{ii}/σ_f^2) integrals for the case of an exponential covariance function, as reported by Gelhar and Axness (1983a), are applicable to any ellipsoidal field.

3.4 Limitations of the Theory

The derivations of this chapter rest on various assumptions which need to be examined critically. These include the assumption of stationarity, which was considered in Chapter 2, as well as the following conditions which are specific to the derivations of Section 3.2: (1) The medium is locally isotropic; (2) the variance in log permeability is "small;" (3) mean field renormalization is valid; (4) the log permeability field is without drift. Condition (2) was considered in Section 3.3.1. Conditions (1), (3) and (4) remain to be investigated in this section.

3.4.1 The Assumption of Local Isotropy

Throughout this chapter it has been assumed that permeability is a scalar, $K(\underline{x})$. A more realistic analysis might consider direction dependence in permeability. For instance, if permeability is believed to be tensorial, then the appropriate form of Darcy's law is (3.1), which is also written

$$q_j = -\sum_{j=1}^{3} K_{ij} \frac{\partial H}{\partial x_j} \tag{3.59}$$

where $K_{ij} = K_{ji}(\underline{x})$ are the spatially dependent components of the permeability tensor. This form is general enough to represent a medium in which not only the degree of hydraulic anisotropy, but also the orientation of the principal axes of the permeability ellipsoid, vary in space. Stochastically, this type of medium is represented by a random tensor field.

The corresponding steady-state flow equation is

$$\sum_{j=1}^{3} \sum_{\ell=1}^{3} \left[\frac{\partial K_{j\ell}}{\partial x_j} \frac{\partial H}{\partial x_\ell} + K_{j\ell} \frac{\partial^2 H}{\partial x_j \partial x_\ell} \right] = 0 \qquad (3.60)$$

This equation has 18 terms and the corresponding perturbed form contains 72 terms. Compare the 18 terms of equation (3.14). In addition to its cumbersome form, equation (3.60) cannot be log-linearized as equation (3.12) was. It is not obvious how one might simplify or manipulate (3.60) in order to derive information which is useful to evaluate the averaged version of (3.59). Thus the loss of generality accompanying the local isotropy assumption is evidently balanced by its simplicity, and hence tractability of the results.

In addition to its mathematical simplicity, the local isotropy assumption is advantageous for two reasons. First, because only rarely are detailed, small-scale, directional permeability data available, it is compatible with current data collection practices. Second, the local isotropy assumption and the accompanying analysis of Darcy's law make a unique contribution to the stochastic theory; they provide a quantitative conceptualization of the way in which the superposition of local heterogeneities, by themselves, can produce effective anisotropy.

3.4.2 Mean Field Renormalization

Recall from Section 3.2.2 (Steady Flow) that mean field renormalization (MFR) was assumed to be valid. Symbolically this is expressed by equation (3.17), rewritten here:

$$\nabla f' \cdot \nabla H' - \overline{\nabla f' \cdot \nabla H'} \cong 0 \tag{3.61}$$

Henceforth, I will refer to assumption (3.61) as MFR. Note that MFR implies that the vector product of the fluctuation gradients, being approximately equal to its expectation, has a small variance:

$$\mathrm{Var}[\nabla f' \cdot \nabla H'] \cong 0 \tag{3.62}$$

That is, MFR appears to imply that the inner product is very nearly nonrandom, though it need not be constant.

I will now show that, for a drift-free log permeability field, mean field renormalization is equivalent to a much more restrictive assumption than equation (3.62) seems to imply. Taking advantage of (3.20), (3.26) and (3.31), the cross-covariance at separation $\underline{h}$ is written:

$$\overline{f'(\underline{x}+\underline{h})H'(\underline{x})} = i \int_{\underline{k}} \exp(i\underline{k}\cdot\underline{h})\underline{J}\cdot\underline{k} \, \frac{S_{ff}(\underline{k})}{|\underline{k}|^2} \, d\underline{k} \tag{3.63}$$

At zero separation this simplifies to

$$\overline{f'(\underline{x})H'(\underline{x})} = 0 \tag{3.64}$$

It may be noted that since the expectation gradient, $-\underline{J} = -\underline{J}(\underline{x})$, is generally a function of the coordinates, $\underline{x}$, so too is the cross-covariance (3.63). That is, the fluctuations f' and H' generally are not jointly stationary.

Equation (3.63) predicts that the log permeability and hydraulic head perturbations have a non-zero correlation at non-zero

lag, while (3.64) predicts no correlation at zero lag. Note that this is not to say that the fluctuations are generally uncorrelated.

Similar consideration yields, for the expectation of the inner product,

$$\overline{\nabla f'(\underline{x}+\underline{h})\cdot\nabla H'(\underline{x})} = i \int_{\underline{k}} \exp(i\underline{k}\cdot\underline{h})\underline{J}\cdot\underline{k}\; S_{ff}(\underline{k})\; d\underline{k} \qquad (3.65)$$

and

$$\overline{\nabla f'(\underline{x})\cdot\nabla H'(\underline{x})} = 0 \qquad (3.66)$$

Substituting (3.66) into equation (3.61) produces

$$\nabla f'(\underline{x})\cdot\nabla H'(\underline{x}) \cong 0 \qquad (3.67)$$

Therefore, the use of mean field renormalization (3.61) is equivalent to making the assumption (3.67).

Note that (3.66) can be expressed in terms of the non-perturbed quantities as:

$$\overline{\nabla f(\underline{x})\cdot\nabla H(\underline{x})} = 0 \qquad (3.68)$$

Using Darcy's law (3.2) and noting that

$$\nabla(K^{-1}) = -\frac{\nabla K}{K^2}\,, \qquad (3.69)$$

equation (3.68) can be expressed as

$$\overline{\underline{q}\cdot\nabla(K^{-1})} = 0 \qquad (3.70)$$

This implies that, on the average, the flow-lines in a heterogeneous

medium tend to be perpendicular to those paths along which the hydraulic restivity, K^{-1}, experiences its most rapid change. Alternatively, substituting (3.66) into the ensemble-averaged steady-state flow equation (3.15) results in the mean hydraulic head condition

$$\nabla^2 \overline{H} \cong 0 \tag{3.71}$$

Condition (3.71) shows that the validity of mean field renormalization rests, in part, on very specific flow conditions. Notice that (3.71) is necessary but not sufficient to satisfy (3.67).

Bakr and others (1978) formulated the assumption (3.67) slightly differently, but their results are similar to those presented here. They assumed that the head fluctuation gradient is always negligible compared to the expected hydraulic gradient,

$$|\nabla H'| << |\nabla \overline{H}| \tag{3.72}$$

and that the log permeability field is without drift, so that the appropriate form of the ensemble-averaged steady-state flow equation is (3.71). They only considered fields in which the expectation of the hydraulic head varies linearly with the spatial coordinates, so that condition (3.71) is satisfied. Later Gelhar and Axness (1983a) relied on similar assumptions (equation (3.67) and $\nabla \overline{f} = \underline{0}$) to derive approximate analytical expressions for the ensemble averaged form of Darcy's law. Those derivations are given in the earlier part of this chapter.

To be consistent with the notation used to represent the approximations (3.61) and (3.64), the inequality (3.72) is rewritten

here,

$$|\nabla H'| \cong 0 \tag{3.73}$$

The reader will note that the orthogonality assumption (3.67) can be expressed as,

$$|\nabla f'||\nabla H'| \cos \alpha \cong 0, \; 0 \leq \alpha \leq \pi \tag{3.74}$$

where α is the angle between the gradient vectors. Therefore a slowly fluctuating head field is one example for which the orthogonality requirement is satisfied. Similarly, if the log permeability field is slowly fluctuating,

$$|\nabla f'| \cong 0 \tag{3.75}$$

then condition (3.67) is fulfilled.

Because Bakr and others (1978) and Gelhar and Axness (1983a) apparently made the orthogonality assumption (3.67) for mathematical convenience rather than based on physical evidence, their results have been criticized (see Cushman, 1983, and Gelhar and Axness, 1983b). Unfortunately, the exchange by the above authors serves mainly to demonstrate that little is known about how this assumption affects the results (3.37) and (3.38). Therefore, these latter equations should be used with caution.

3.4.3 Drift in Log Permeability

The main results of this chapter (equations (3.38), (3.45) and (3.48)) are based on the assumption that the ensemble average log

permeability field is without drift ($\nabla\overline{f}=0$). This is equivalent to making the assumption that the log permeability, as well as its fluctuation, is second-order stationary. This assumption can be tested, at least to some degree, by examining the experimental semivariograms of f (see Section 2.4.3).

CHAPTER 4

APPLICATION TO DATA FROM FRACTURED GRANITES NEAR ORACLE, ARIZONA

4.1 Introduction

In the two previous chapters, a general stochastic theory of spatial variability, and a particular analysis of the relationship between the spatial variability of permeability and the effective permeability tensor were presented. I will now apply this theory toward the solution of a real problem, that of estimating the spatial covariance function of log permeability at the Oracle site, using the results of the single-hole and cross-hole hydraulic tests described in Chapter 1.

4.2 Semivariogram Analysis of Small-Scale Permeability Data

Experimental semivariograms were calculated for the single-hole packer test data described in Chapter 1. The variable of interest is the base ten logarithm of the measured permeability,

$$f^*(\underline{x}) = \log_{10} K^*(\underline{x}) \tag{4.1}$$

The reason for using the logarithm of the permeability rather than the permeability itself is that later I will use the approximate analytical expressions derived in Chapter 3, which are in terms of the statistics of log permeability.

4.2.1 Effect of the Boreholes' Configuration

All of the boreholes at the Oracle field site are nearly vertical. As a result, there are many more data pairs with approximately vertical orientations than with any other orientation. The extent to which this is true depends on the separation distance, as shown in Figures 4.1 and 4.2.

In Figure 4.1, the curve labeled "Average Semivariogram" specifies the number of data pairs used in the computation of the average semivariogram, for each 3-meter distance class. It shows the relationship between the number of available data pairs and separation distance. The curve labeled "Vertical Semivariogram" specifies the number of data pairs used in the computation of the vertical (15-degree window) semivariogram, for each 3-meter distance class. It shows the relationship between the number of data pairs with a vertical relative orientation (within 15 degrees) and separation distance. The form of these curves is determined by, and therefore can be considered characteristic of, three things: (1) The spatial arrangement of the boreholes at the Oracle site. (2) The sampling density, with respect to the single-hole tests. (3) The distance class size.

The points on the graph in Figure 4.2 were obtained as follows. For each 3-meter distance class the number of data pairs used in the calculation of the vertical (15-degree angle tolerance) sample semivariogram was divided by the total number of available data pairs in that class and multiplied by 100. In effect, Figure 4.2 describes the degree of influence of the vertically oriented data on the average

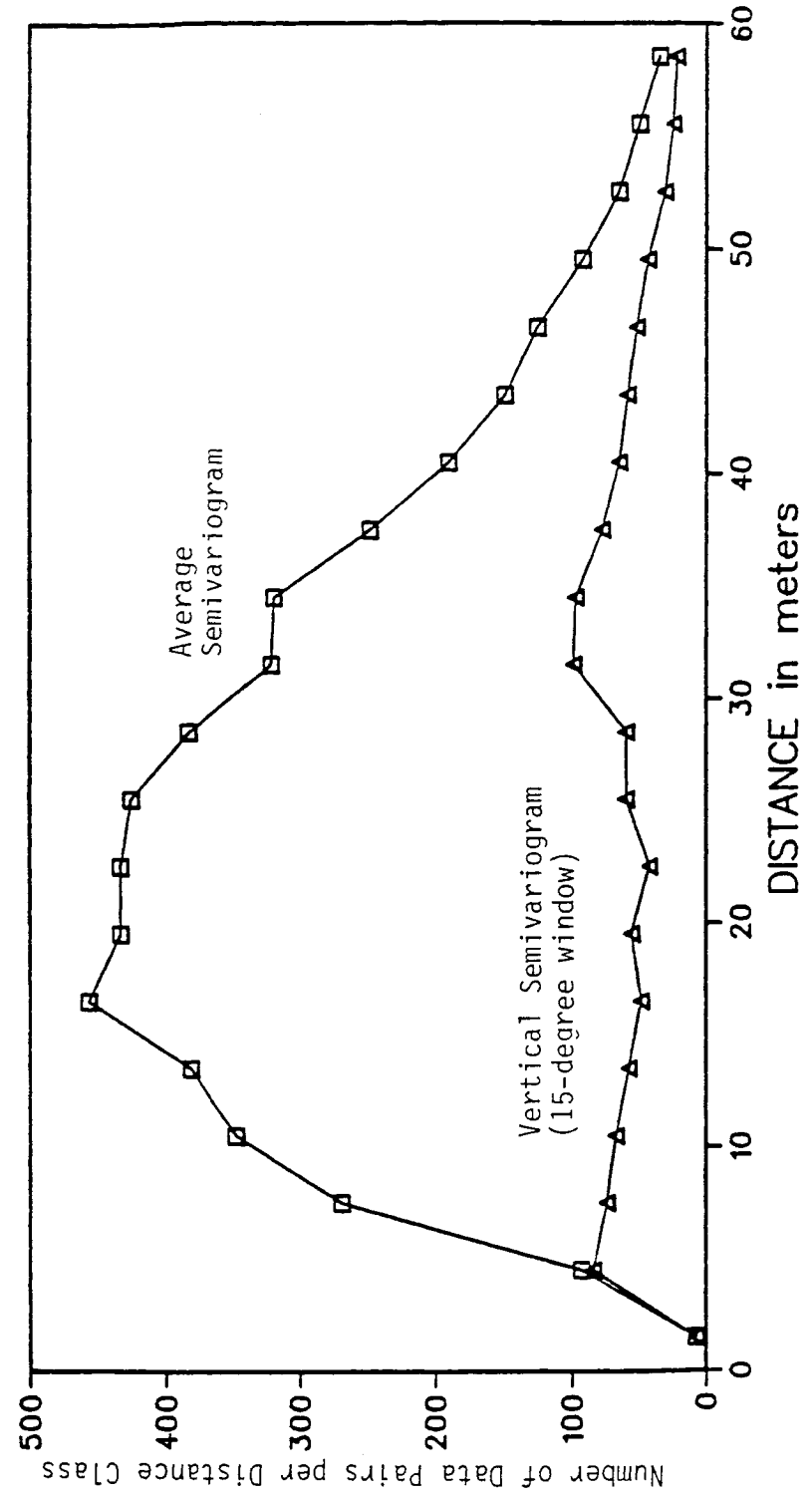

Figure 4.1. Number of Data Pairs per Distance Class, Sample Semivariograms.

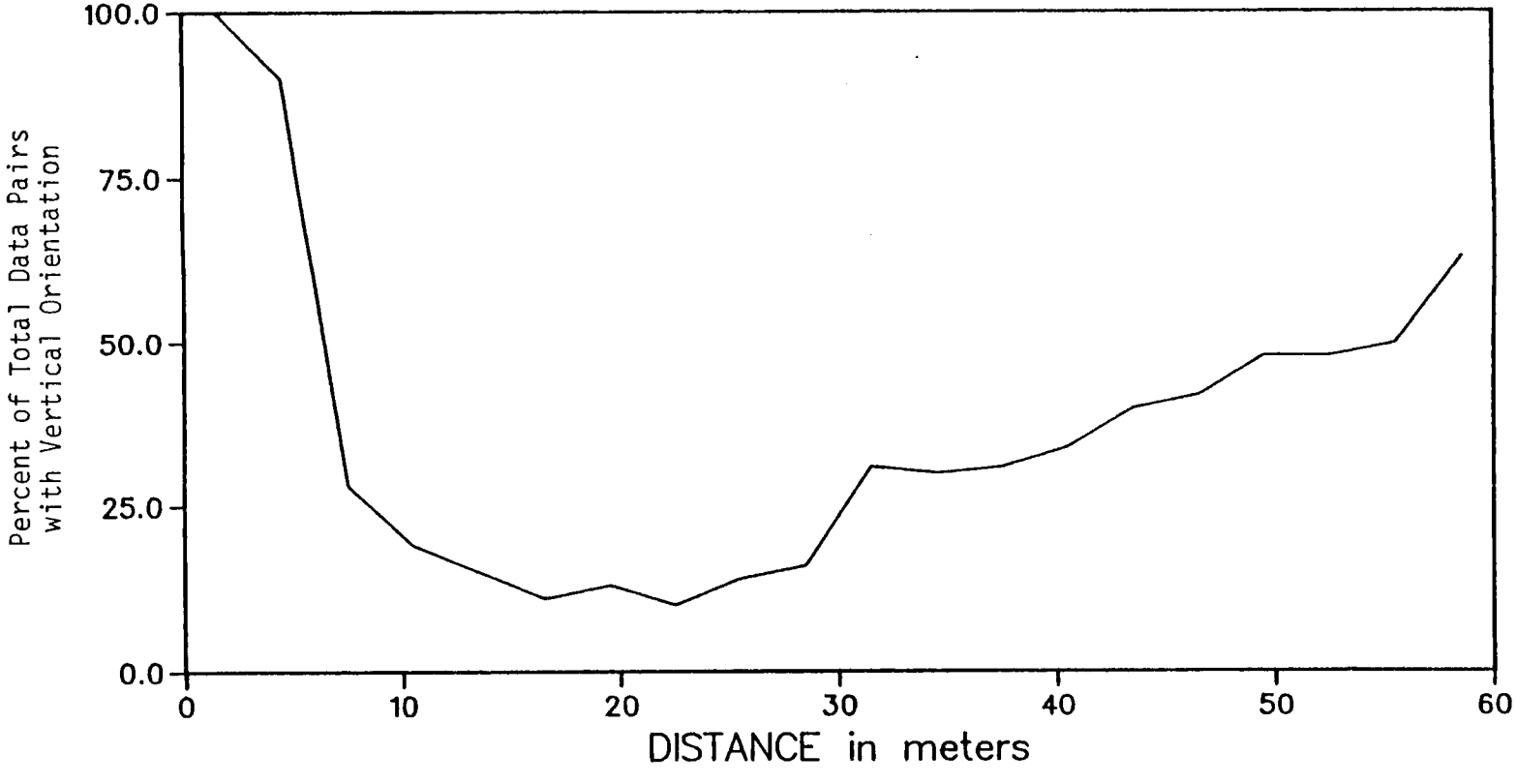

Figure 4.2. Percentage of Data Pairs with Vertical Orientation (within a 15-degree tolerance) Versus Separation Distance.

sample semivariogram, as a function of separation distance. Note the abrupt decrease at about 6 meters. This corresponds to the minimum horizontal distance between any two boreholes.

Clearly, if the log permeability field is statistically anisotropic, the average sample semivariogram is expected to be biased toward the vertical semivariogram, though the degree of the bias varies from one distance class to another, and is smallest in the midrange of these classes. To get an idea of the importance of this bias, consider the following ideal case. Suppose that data were available for each h-meter distance class, such that the endpoints of the relative orientation vectors of the data pairs were uniformly distributed over a sphere of radius h meters. The surface area of the sphere is $4\pi h^2$ meters^2. Now consider an experimental semivariogram in any direction, with an angle tolerance η as defined in equation (2.73), calculated from this hypothetical data set. The endpoints of the relative orientation vectors fall on two opposite portions of the sphere having a total surface area equal to $4\pi h^2(1-\cos \eta)$ meters^2. It follows that the contribution to the average sample semivariogram of these data pairs is $1-\cos \eta$. Ideally, data pairs available for calculation of a vertical semivariogram with a 15-degree window should thus not contribute more than about 3 percent of the total number of data pairs used in the average semivariogram calculation. Figure 4.2 shows that at the Oracle site, a disproportionate amount of the data is vertically oriented in each distance class.

Consequently, relative orientations of data pairs from the Oracle site are sparsely distributed over non-vertical directions. For instance, data pairs having a relative orientation within 15 degrees of vertical constitute (1201/5115) x 100% = 23% of the total number of available data pairs. This is an average over all 20 3-meter distance classes. However, these orientations constitute only (1 - cos 15°) x 100% = 3.4% of the total possible relative orientations. Therefore the relative density of the data in this direction class can be assigned the value [(1201/5115)]/(1-cos 15°) = 6.9, while the remaining data (exclusive of vertical $\pm$15 degrees) can be assigned the average data/direction relative density [(5115-1201)/5115]/cos 15° = 0.79, which is about one-ninth the former.

The single-hole packer test data are separated by vertical distances not exceeding 66 meters. According to the rule of thumb common in geostatistical analysis, experimental semivariogram points corresponding to more than half of this distance (about 33 meters) should be regarded with caution.

4.2.2 Sample Semivariograms of Non-corrected Data

The average semivariogram of the non-corrected data is shown in Figure 4.3. It was calculated from 5115 data pairs, grouped into twenty 3-meter distance classes. Its most salient feature is its distinct sill (approximately 1.5), which is approached rapidly within the first 10 meters of lag distance. The first point on the semivariogram (open circle) has been calculated from only 8 data pairs (see Figure 4.1) and can thus be ignored.

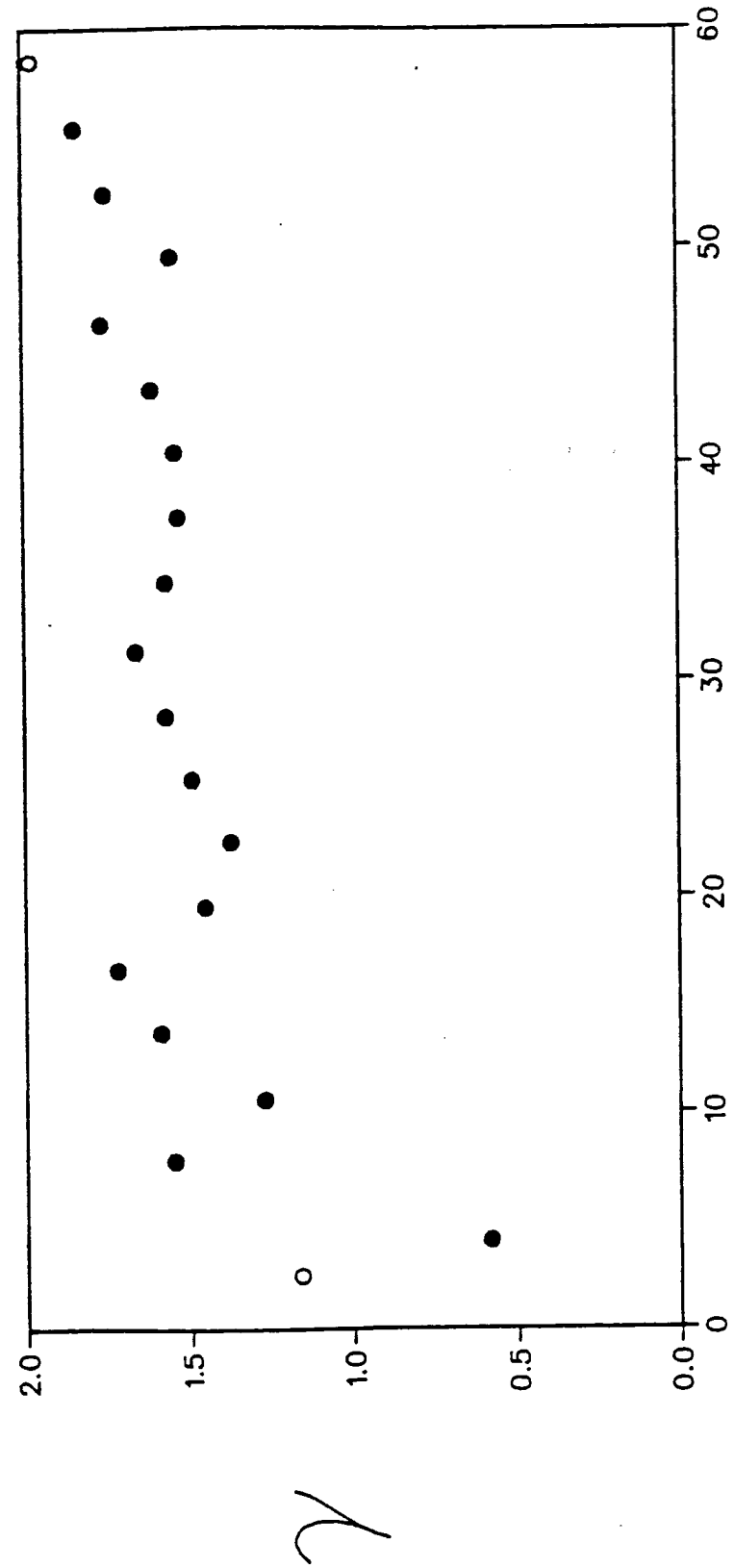

Figure 4.3. Average Sample Semivariogram of Non-Corrected Base Ten Log Permeabilities. (Closed circles denote points calculated from 50 or more data pairs; open circles denote points calculated from less than 50 pairs.)

Because it utilizes a 90-degree angle tolerance, the average sample semivariogram does not discriminate between data pairs with different relative orientations. By itself it lends no information about statistical anisotropy. Furthermore, as previously shown, the average sample semivariogram of the Oracle data is irregularly biased toward the vertical semivariogram. Therefore its use is limited primarily to the determination of a sill value. Having been calculated from a large number of data pairs, it serves this purpose adequately. Note that the sill is approximately equal to the sample variance, 1.53.

Conceivably, statistical anisotropy could be detected by comparing sample semivariograms for different directions. To be directly comparable, however, the semivariograms must be calculated using similar distance and angle tolerances. For maximum resolution of the directional effect, the angle tolerance must be small. Unfortunately, at the Oracle site the data allow computing only one reliable unidirectional sample semivariogram with a 15-degree window, in the vertical direction. This semivariogram was calculated from 1201 noncorrected log permeability data pairs, and is shown in Figure 4.4.

To demonstrate the effect of the angle tolerance on the experimental semivariogram, compare the vertical semivariogram shown in Figure 4.5. This semivariogram was computed from 2306 data pairs, using a 30-degree angle tolerance. Note that by increasing the angle tolerance from 15 to 30 degrees, the sample semivariogram's range is decreased from approximately 35 meters to less than 20 meters. This rather substantial change in form accompanying a relatively moderate

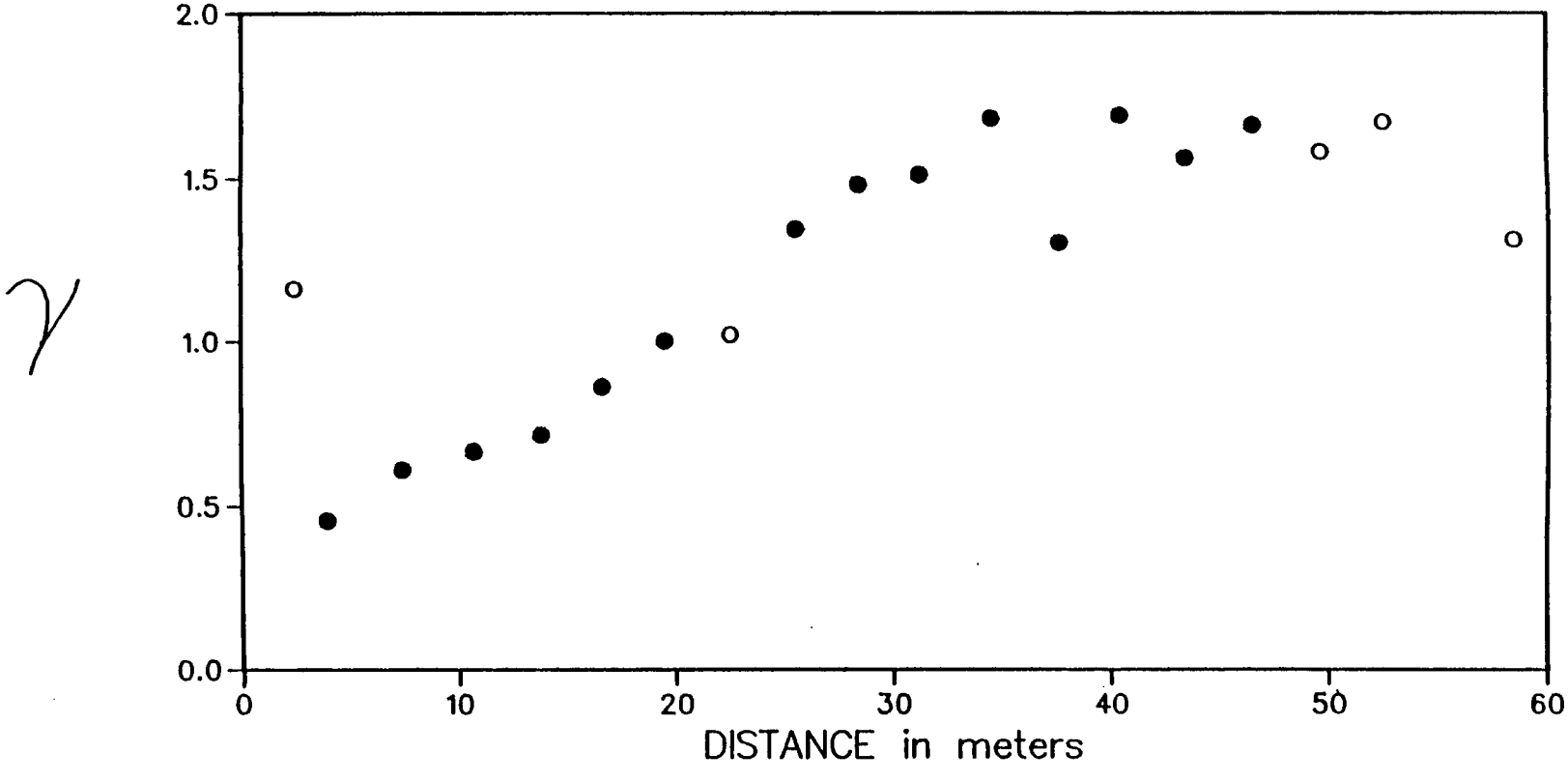

Figure 4.4. Vertical Sample Semivariogram of Non-Corrected Base Ten Log Permeabilities, 15-Degree Window. (Closed circles denote points calculated from 50 or more data pairs; open circles denote points calculated from less than 50 pairs.)

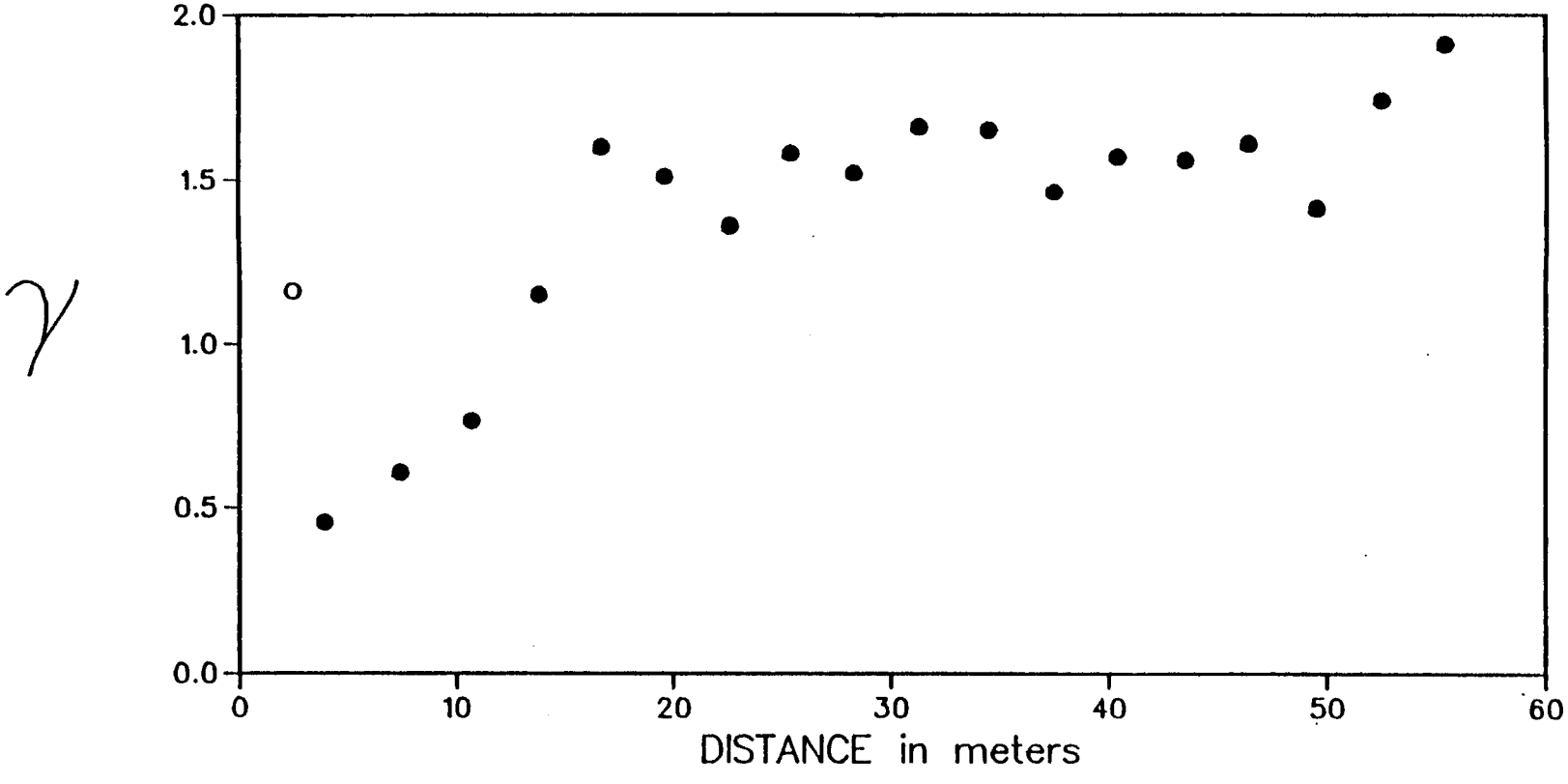

Figure 4.5. Vertical Sample Semivariogram of Non-Corrected Base Ten Log Permeabilities, 30-Degree Window. (Closed circles denote points calculated from 50 or more data pairs; open circles denote points calculated from less than 50 pairs.)

change in angle tolerance suggests the presence of a strong directional effect. Both sample semivariograms are for the vertical direction, but the one utilizing a 15-degree window was chosen for analysis because it required averaging much fewer data from non-vertical directions, thus decreasing the risk of introducing directional bias. This argument can be carried to excess. If the angle tolerance is chosen too small, insufficient data are available for the semivariogram's computation, as is the case for the semivariogram shown in Figure 4.6. This too is a vertical sample semivariogram of the non-corrected base ten log permeabilities, but it was calculated from 858 data pairs, using an angle tolerance of 10 degrees. Two things make this semivariogram less suitable for analysis than that calculated using a 15-degree window. First, there is much more scatter in the points, making the interpretation difficult. Second, only 7 of the points were calculated from 50 or more data pairs, as compared to 14 points on the semivariogram with a 15-degree window.

For comparison with the vertical sample semivariogram (15-degree window) of Figure 4.4, an experimental semivariogram was calculated from the remaining 3914 data pairs (excluding the pairs used for the vertical semivariogram). The resulting non-vertical semivariogram is shown in Figure 4.7. The vertical, non-vertical, and average semivariograms are seen to have similar sill values. However, whereas the range of the non-vertical semivariogram is less than about 15 meters, that of the vertical is seen to be approximately 35 meters. This difference suggests that the range, in at least some non-vertical

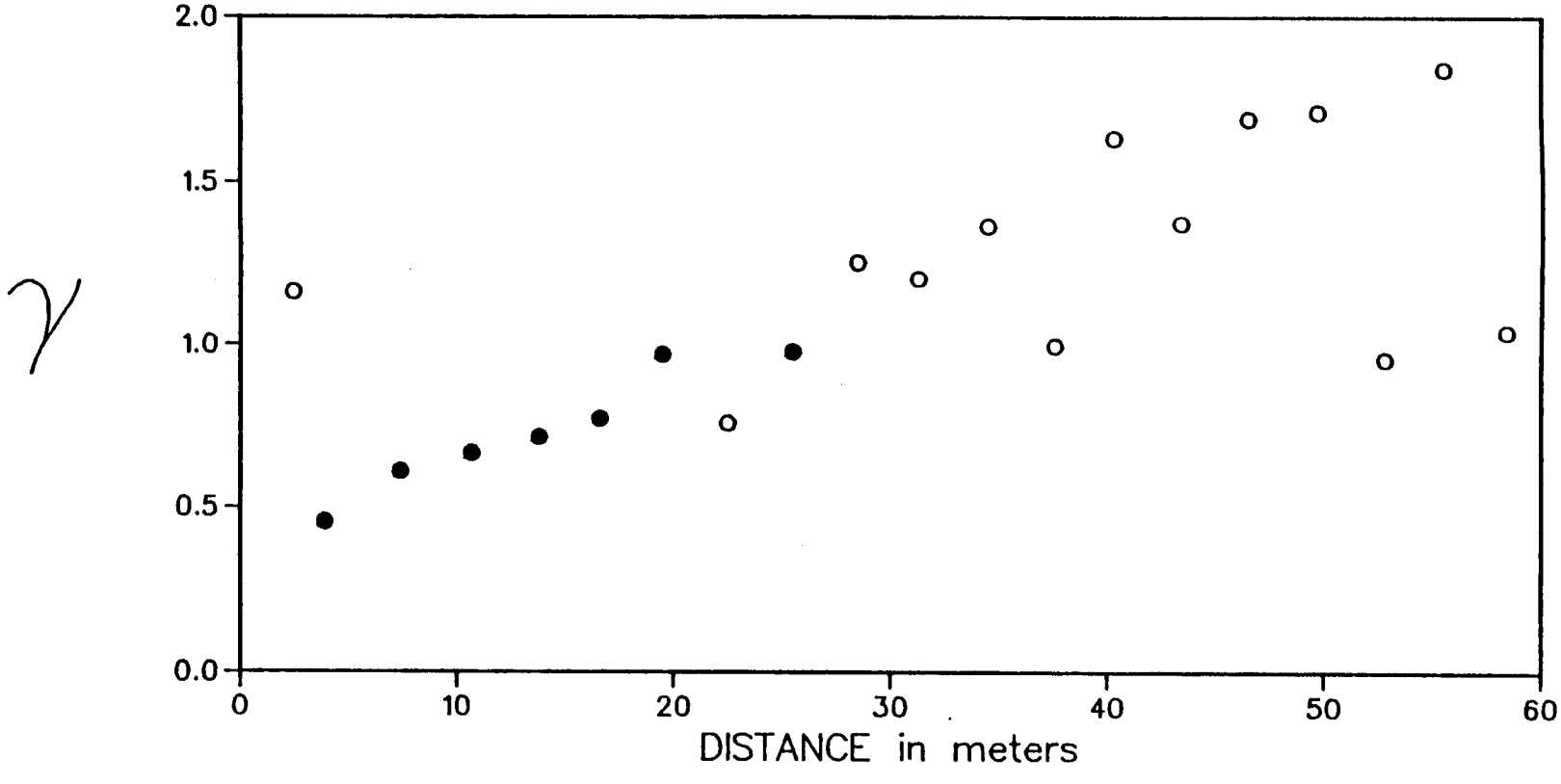

Figure 4.6. Vertical Sample Semivariogram of Non-Corrected Base Ten Log Permeabilities, 10-Degree Window. (Closed circles denote points calculated from 50 or more data pairs; open circles denote points calculated from less than 50 pairs.)

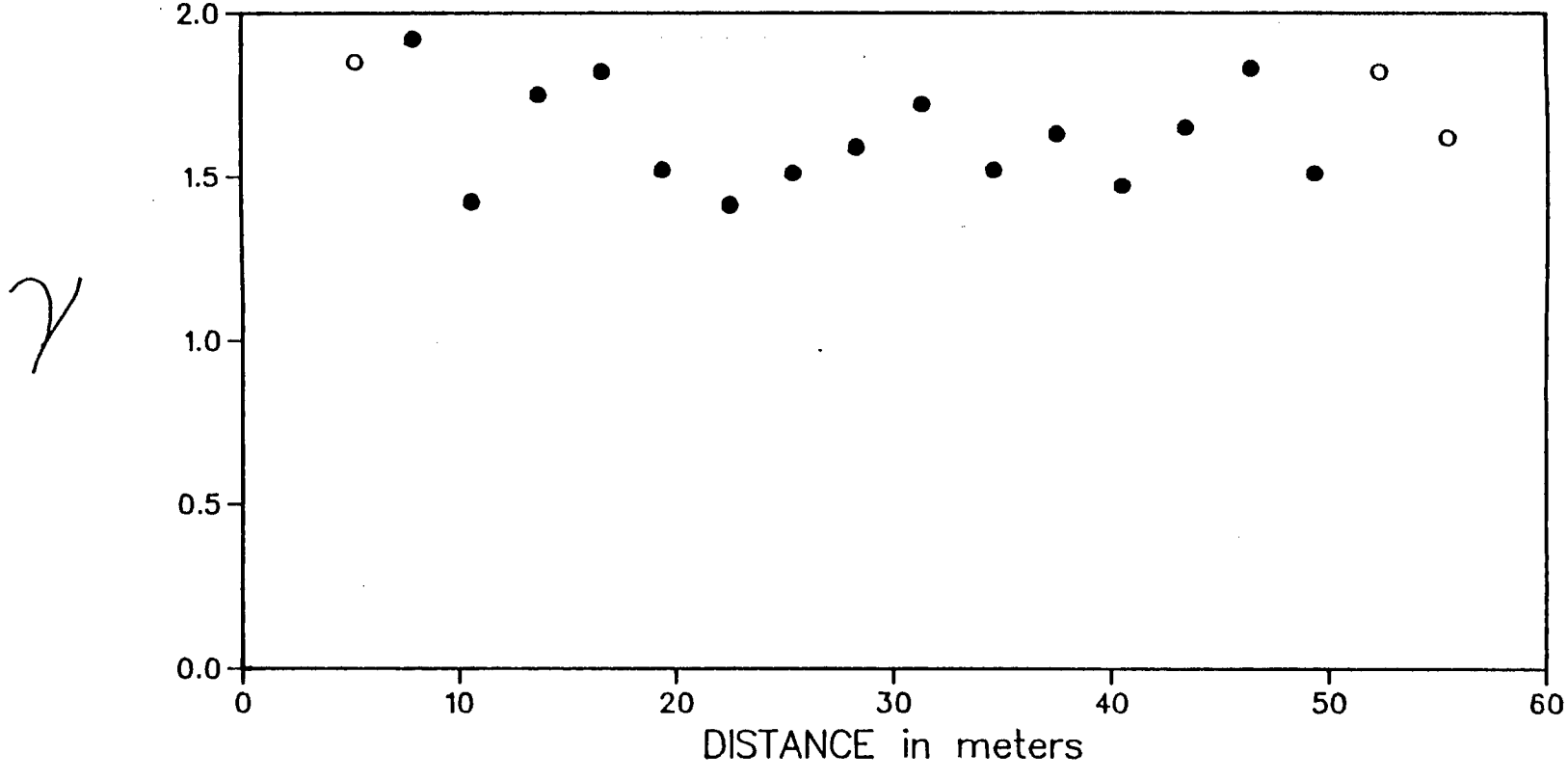

Figure 4.7. Non-Vertical Sample Semivariogram of Non-Corrected Base Ten Log Permeabilities. (Closed circles denote points calculated from 50 or more data pairs; open circles denote points calculated from less than 50 pairs.)

directions, is considerably less than 35 meters. In other words, the field is anisotropic.

The anisotropy suggested by the experimental semivariograms might be apparent, stemming from a drift in the measured log permeabilities, or real. The presence of a well-defined sill eliminates the first possibility, implying that the permeability field is statistically anisotropic. This is further supported (through the theory presented in Chapter 3) by independent results of the cross-hole tests (Table 1.2).

4.2.3 Deregularization and Model Fitting

Inferring the true log permeability semivariogram from the sample semivariogram must take into consideration data errors and the scale of measurement of the data (i.e., the data support). Specifically, the effects of measurement error (Section 2.4.1) and regularization (Section 2.4.4) must be removed from the sample semivariogram. Because neither of these effects is well understood, some simplifying assumptions must be made in order to obtain approximate results. These assumptions were discussed in Chapter 2 and will only be summarized here.

The first set of assumptions is made in an attempt to account for the effects of measurement error. Here the errors are taken to be an integrated white noise process whose effect on the experimental semivariogram is a discontinuity at the origin, or a nugget effect. Quantitatively, this part of the semivariogram model is described by the specification of a nugget constant, C_0 (equation 2.95).

A second set of assumptions is made in order to account for the finite scale of the permeability measurements. They are as follows: First, the single-hole measurements represent a regularization of log permeability, equivalent to volume averaging (equation 2.108). Second, the averaging volume is a cylinder whose axis or center line coincides with that of the test section of the borehole, and whose radius is negligible in comparison to its length. Therefore, neglecting measurement errors, each measurement represents an average of log permeability along a line segment of length ℓ = 3.8 meters, the length of the test zone. Since all of the boreholes at the site are nearly vertical, the regularization is assumed to take place along a vertically oriented segment:

$$f_\ell(\underline{x}) = \frac{1}{\ell} \int_{x_3-\ell/2}^{x_3+\ell/2} f(\underline{y})\, dy_3 \qquad (4.2)$$

where f_ℓ is the regularized log permeability.

Combining the hypothesized effects of measurement error and regularization, gives for the measured log permeabilities, $f^*(\underline{x})$:

$$f^*(\underline{x}) = f_\ell(\underline{x}) + \varepsilon(\underline{x}) \qquad (4.3)$$

Therefore, the sample semivariogram estimates the semivariogram of the regularized <u>measured</u> log permeabilities rather than the underlying punctual semivariogram:

$$E[\gamma^*(\underline{h})]\ C_o + \gamma_\ell(\underline{h}) \qquad (4.4)$$

Here $\gamma^*(\underline{h})$ represents the sample semivariogram, C_0 is the nugget constant, and $\gamma(\underline{h})$ is the semivariogram of regularized log permeability, $f_\ell(\underline{x})$.

To obtain the underlying vertical semivariogram, the procedure outlined in Section 2.4.4 was employed. Two three-dimensional covariance models were chosen without specifying their parameters, based on mathematical considerations such as those discussed by Christakos (1984) and empirical indications such as the shape of the experimental semivariograms. These models were integrated to obtain analytical expressions for the semivariograms of the regularized variable. Substitution of these expressions into equation (4.4) gave hypothetical expressions for the semivariogram of measured permeability. Upon fitting these expressions to the sample semivariogram in Figure 4.4 by trial and error, the parameters were determined.

The functional forms used here are the three-dimensional, geometrically anisotropic exponential and spherical models, given by equations (2.59) and (2.66), respectively. Analytical expressions for the corresponding vertical semivariogram models, regularized according to (4.2), are listed in Appendices F and G, respectively. During the trial-and-error fitting procedure, the experimental points were weighted subjectively based on the number of data pairs used for their computation (Figure 4.1). For example, the first point on the vertical semivariogram in Figure 4.4 has been calculated from only eight data pairs and was thus given very little weight in comparison to the second point, which was calculated from 89 data pairs.

The results of this curve-fitting exercise are shown in Figures 4.8 and 4.9 for the exponential and spherical semivariograms, respectively. The corresponding parameter estimates are summarized in Table 4.1. The listed nugget, variance and sill parameter estimates are for the base ten logarithm of permeability, but in parentheses following each is the estimate corresponding to the semivariogram of the natural logarithm of permeability. The conversion factor is

$$(\ln 10)^2 = (2.303)^2 = 5.302$$

Each model involves three independent parameters: the integral scale, variance and nugget. All other parameters can be obtained from these.

Figures 4.8 and 4.9 show that the general shape of the experimental semivariogram (its long, approximately linear rising limb and nearly level sill) is better reproduced by the spherical model than by the exponential model.

4.2.4 Leakage-Corrected Data

The analyses discussed in Sections 4.2.2 and 4.2.3 were also applied to the leakage-corrected permeability data presented in Chapter 1. The resulting experimental semivariograms are shown in Figures 4.10, 4.11 and 4.12. Comparison with Figures 4.3, 4.4 and 4.7 indicates that the main effect of the leakage adjustment is to lower the experimental sill value from about 1.5 to about 1.4. The magnitude of the vertical semivariogram decreases only at lag distances in excess of about 20 meters, while the magnitude of the non-vertical semivariogram decreases at shorter separations. The leakage modification has also resulted in a smoothing of the sample semivariograms.

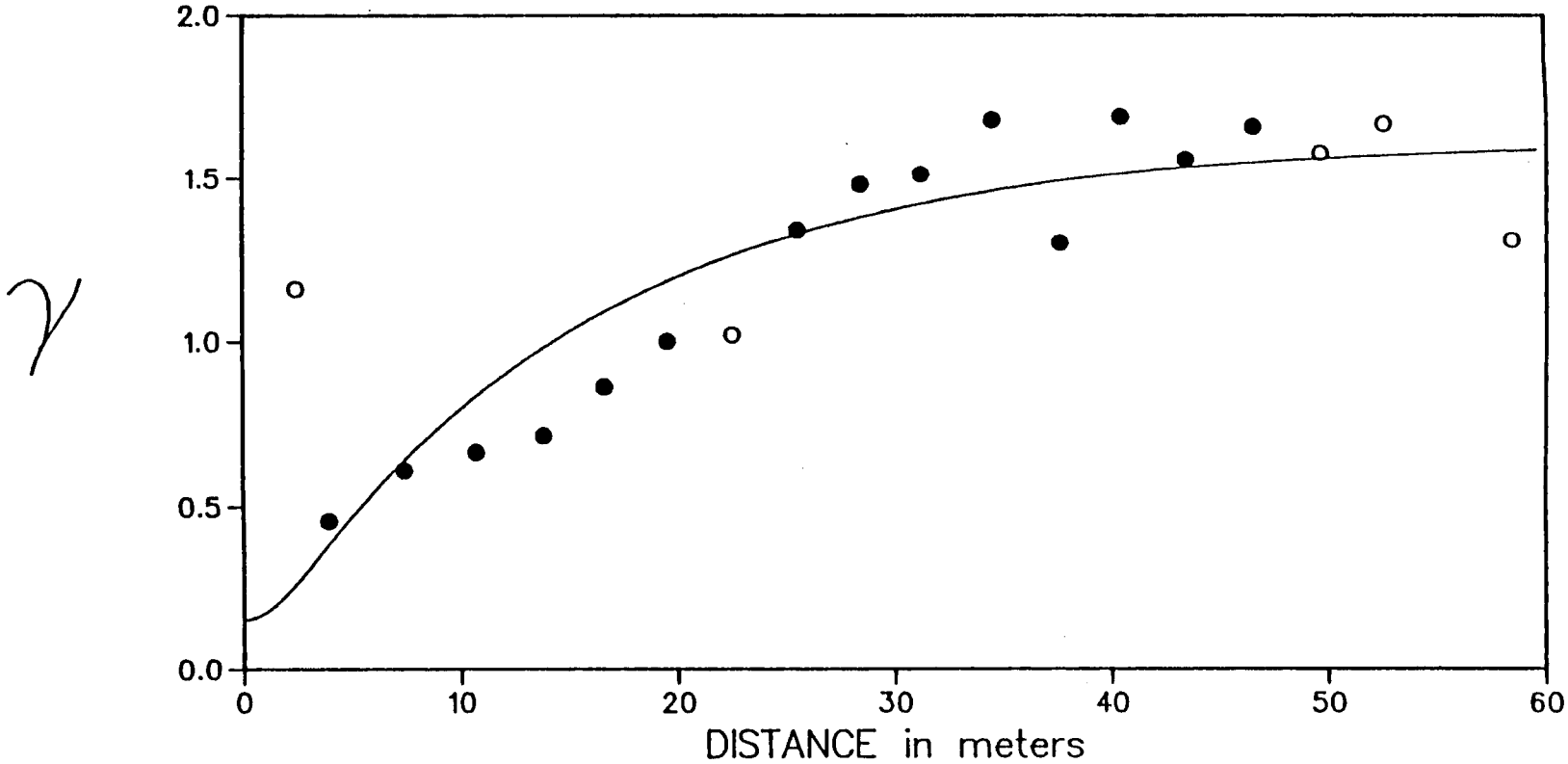

Figure 4.8. Regularized Exponential Semivariogram Fitted to Vertical Sample Semivariogram of Non-Corrected Base Ten Log Permeabilities. (Closed circles denote points calculated from 50 or more data pairs; open circles denote points calculated from less than 50 pairs.)

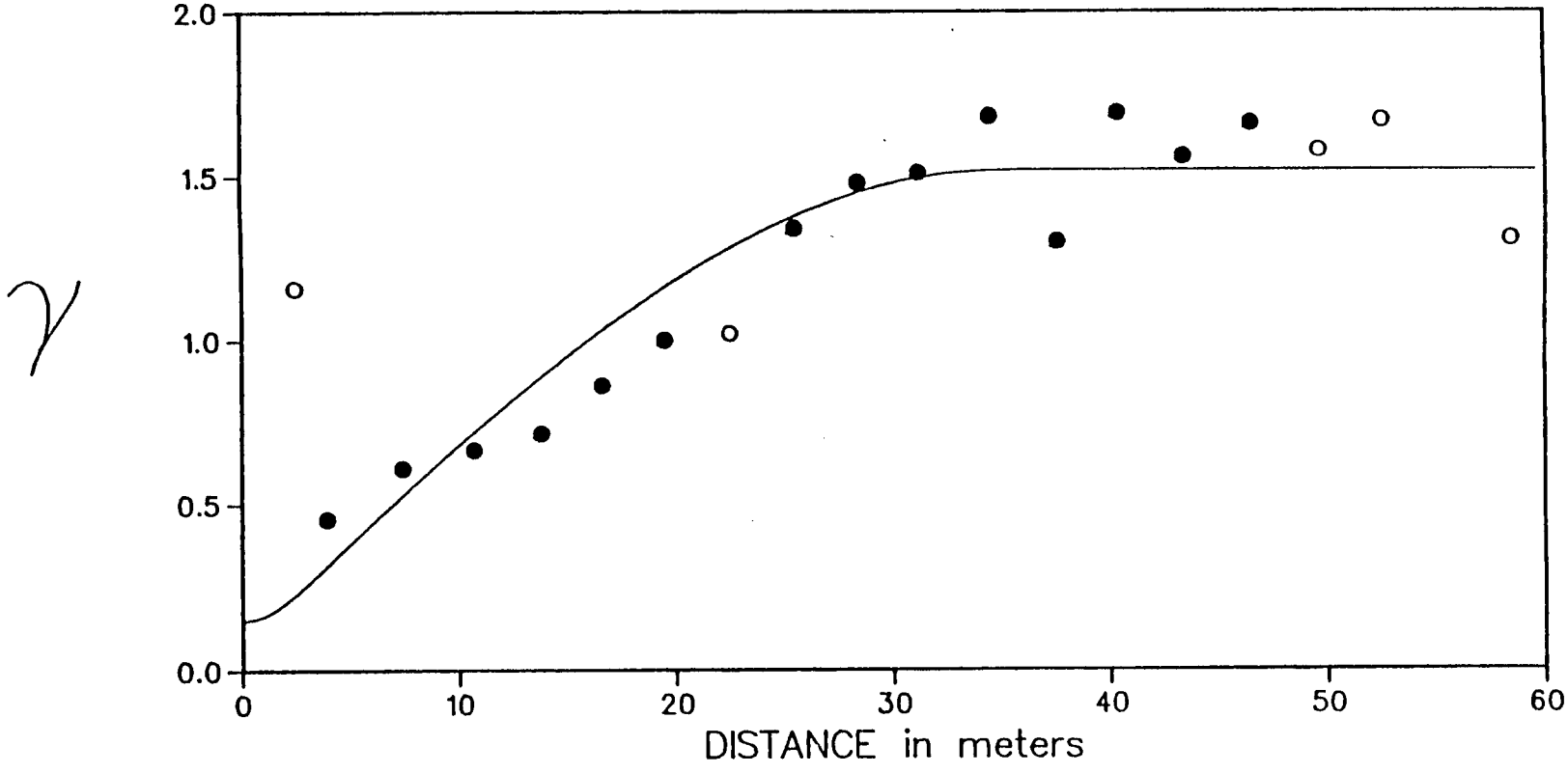

Figure 4.9. Regularized Spherical Semivariogram Fitted to Vertical Sample Semivariogram of Non-Corrected Base Ten Log Permeabilities. (Closed circles denote points calculated from 50 or more data pairs; open circles denote points calculated from less than 50 pairs.)

Table 4.1. Parameter Estimates Obtained by Fitting Regularized Exponential and Spherical Models to Vertical Sample Semivariogram of Non-Corrected Base Ten Log Permeabilities. (Equivalent parameters in natural log permeability in parentheses following).

Parameter	Symbol	Parameter Estimates	
		Exponential Model	Spherical Model
Integral Scale (meters)	$\lambda'(0,0,1)$	15.0	13.0
Range (meters)	a	--	34.7
Sill of Underlying Semivariogram	$C(\underline{o})$	1.60 (8.48)	1.45 (7.69)
Nugget Constant	C_o	0.15 (0.80)	0.15 (0.80)
Regularized Sill	$C_\ell(\underline{o})$	1.47 (7.81)	1.37 (7.27)
Experimental Sill	$C_\ell(\underline{o})+C_o$	1.62 (8.61)	1.52 (8.06)

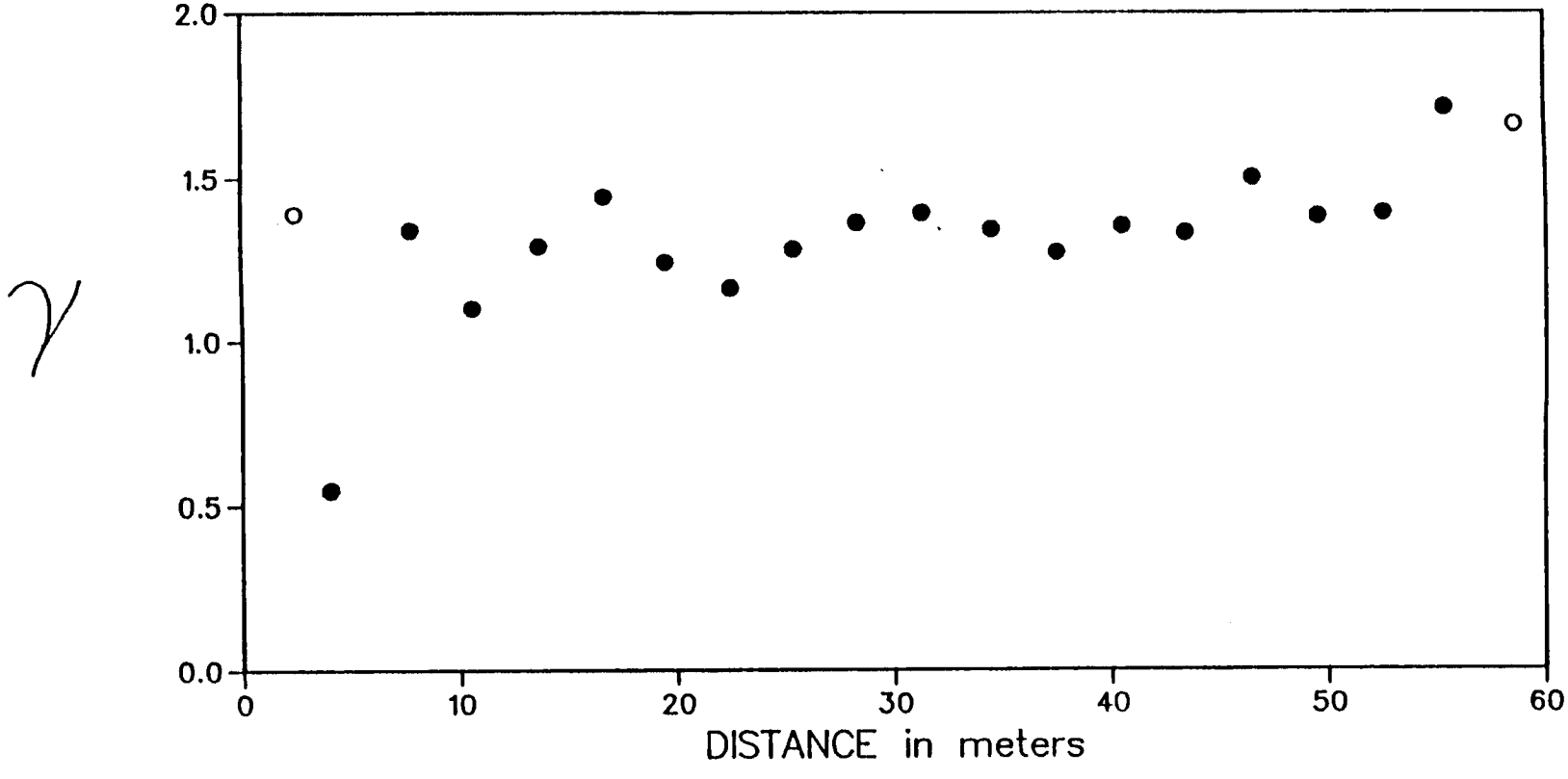

Figure 4.10. Average Sample Semivariogram of Leakage-Corrected Base Ten Log Permeabilities. (Closed circles denote points calculated from 50 or more data pairs; open circles denote points calculated from less than 50 pairs.)

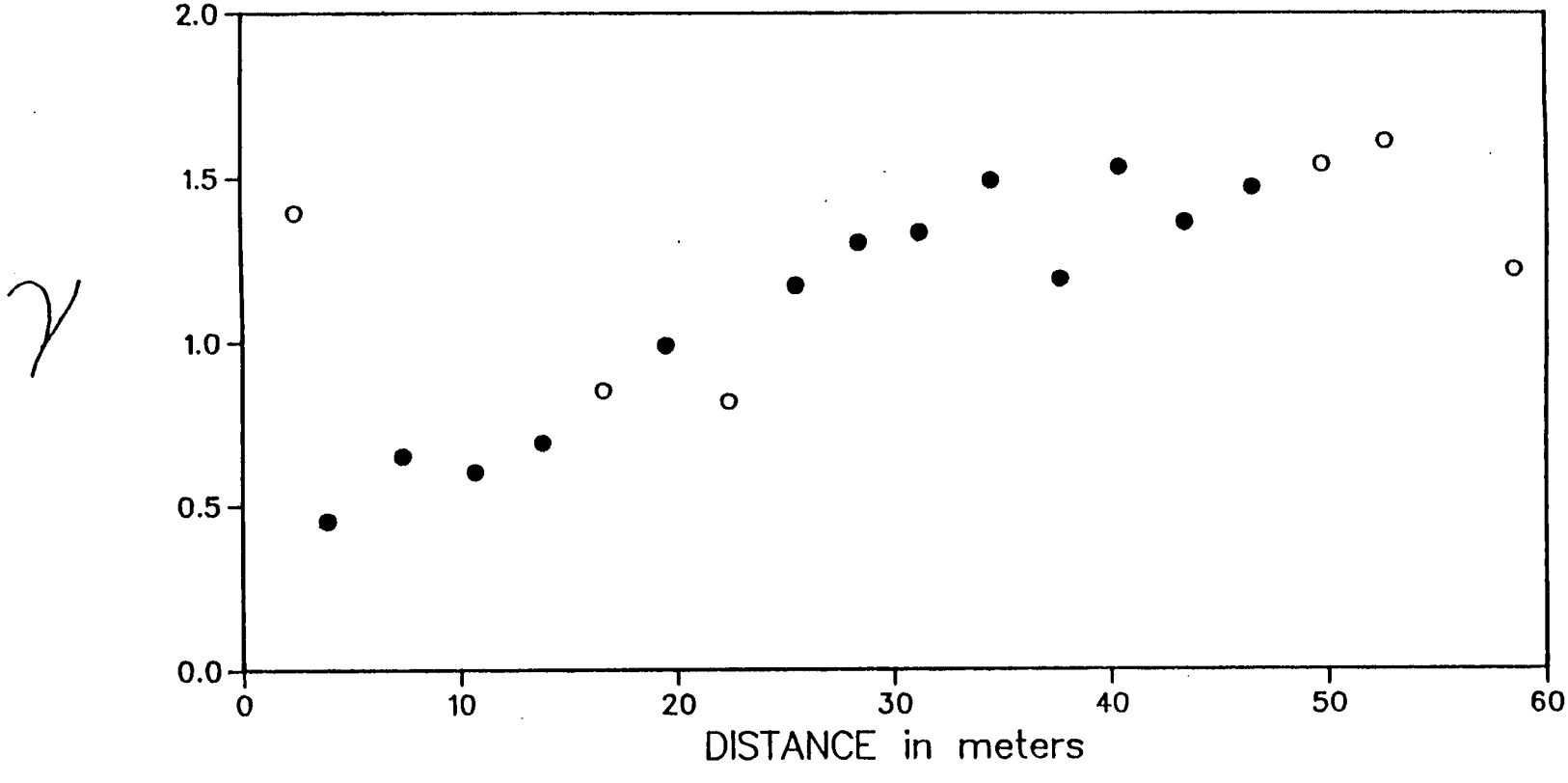

Figure 4.11. Vertical Sample Semivariogram of Leakage-Corrected Base Ten Log Permeabilities, 15-Degree Window. (Closed circles denote points calculated from 50 or more data pairs; open circles denote points calculated from less than 50 pairs.)

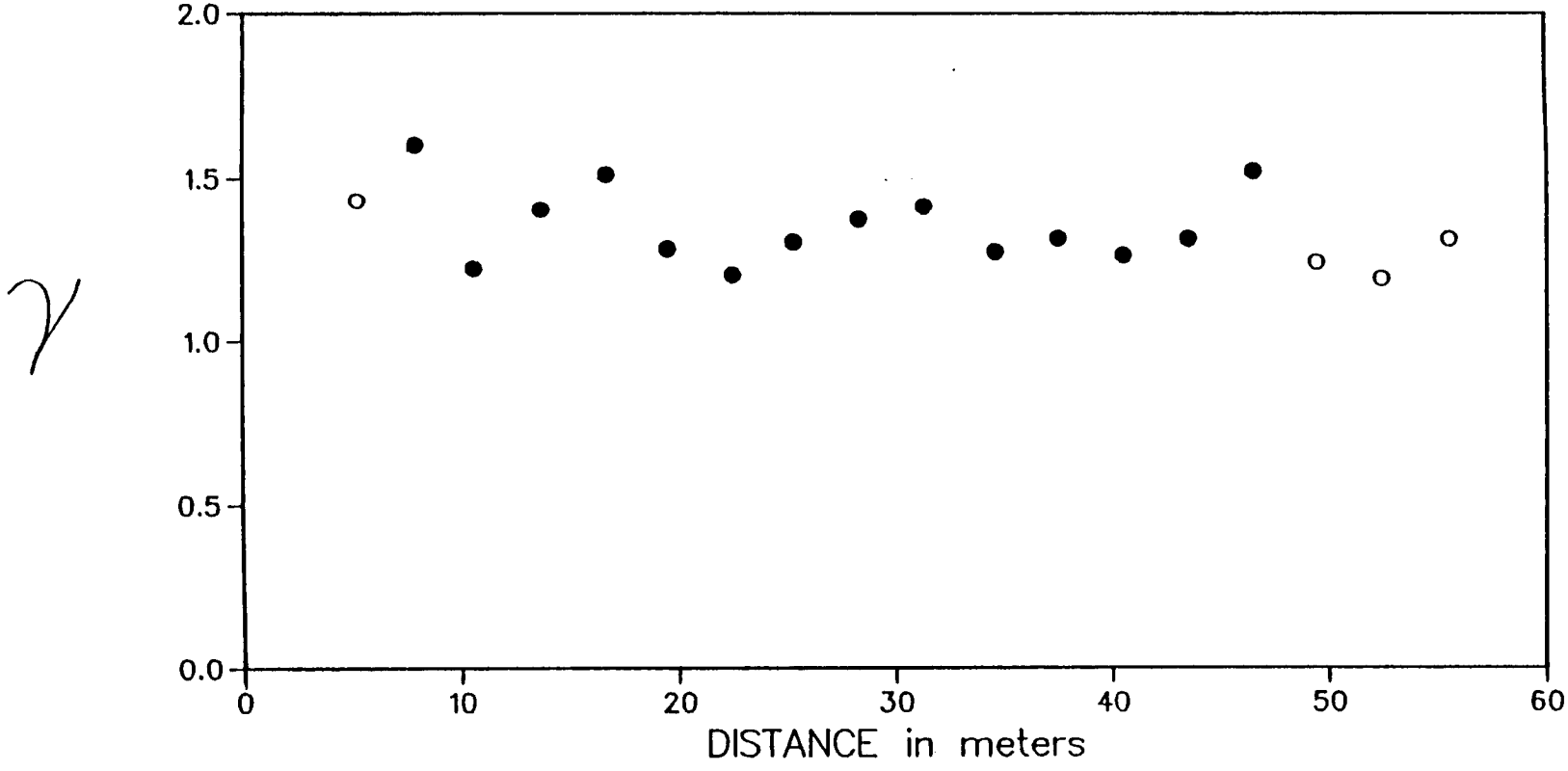

Figure 4.12. Non-Vertical Sample Semivariogram of Leakage-Corrected Base Ten Log Permeabilities. (Closed circles denote points calculated from 50 or more data pairs; open circles denote points calculated from less than 50 pairs.)

Regularized exponential and spherical semivariogram models were fitted to the vertical sample semivariogram of the leakage-corrected log permeabilities. Figures 4.13 and 4.14 display the fitted curves, and the corresponding parameter estimates are compiled in Table 4.2. The spherical model fits the sample semivariogram slightly better than the exponential curve does, except for distances less than 10 meters.

4.2.5 Previous Work

Jones (1983) also calculated experimental semivariograms of log permeability. His results were reported in Jones (1983) and in Jones and others (1985). The difference between his results and those presented here is explained by three facts. First, Jones used a different set of log permeability data than those used here to calculate his semivariograms. As was pointed out in Section 1.3.1, his permeability estimates are based on subjective leakage corrections. Second, Jones calculated semivariograms for lag distances of only up to 100 feet (about 33 meters), while the semivariograms shown here (Figures 4.3 through 4.14) are plotted for a lag distance of up to 60 meters (about 197 feet). This led him to adopt smaller sills. Third, Jones used a different angle tolerance than was used here (35 degrees versus 15 degrees) to compute the vertical sample semivariogram. This resulted in smaller range values than those reported here.

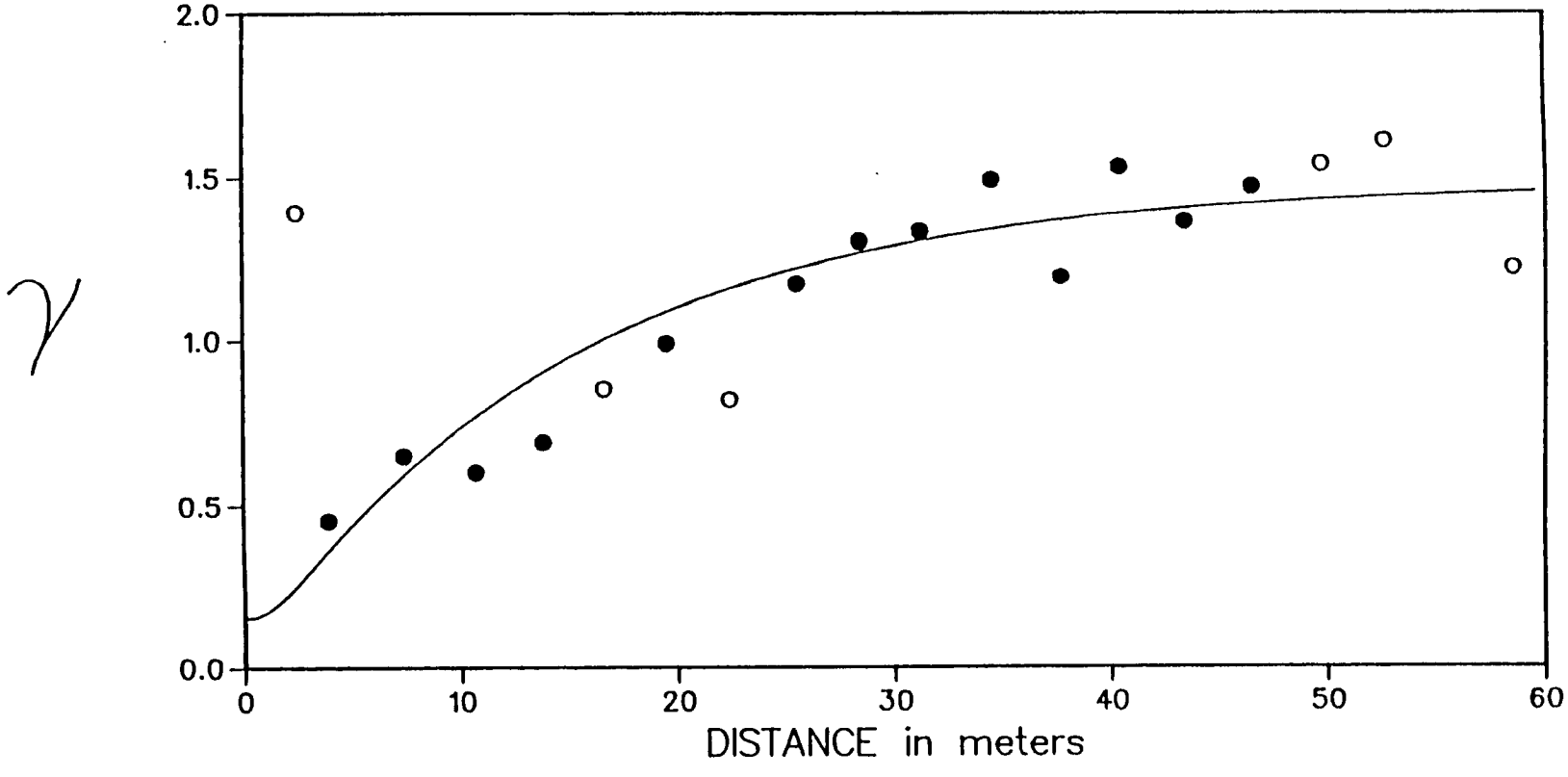

Figure 4.13. Regularized Exponential Semivariogram Fitted to Vertical Sample Semivariogram of Leakage-Corrected Base Ten Log Permeabilities. (Closed circles denote points calculated from 50 or more data pairs; open circles denote points calculated from less than 50 pairs.)

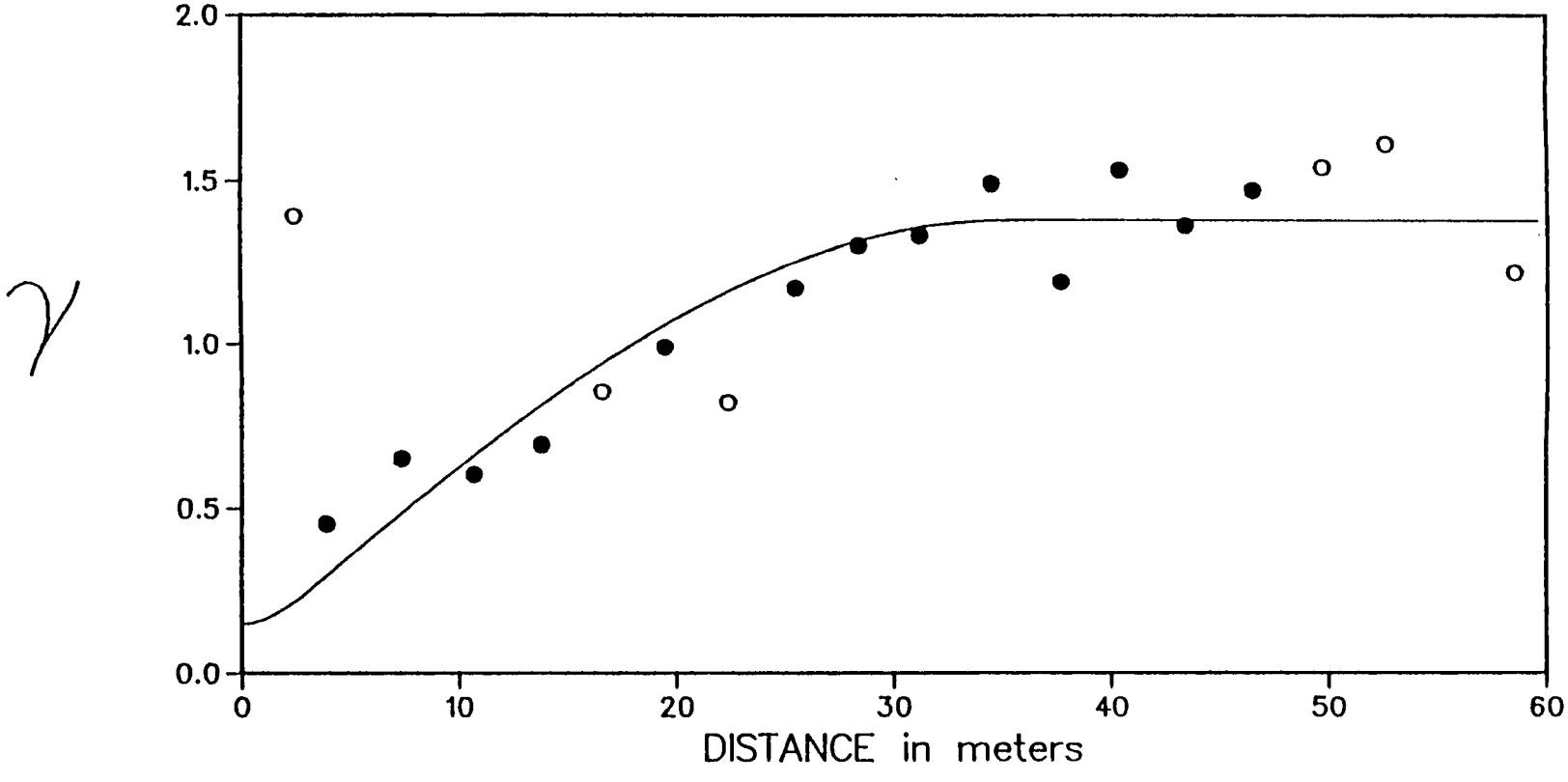

Figure 4.14. Regularized Spherical Semivariogram Fitted to Vertical Sample Semivariogram of Leakage-Corrected Base Ten Log Permeabilities. (Closed circles denote points calculated from 50 or more data pairs; open circles denote points calculated from less than 50 pairs.)

Table 4.2. Parameter Estimates Obtained by Fitting Regularized Exponential and Spherical Models to Vertical Sample Semivariogram of Leakage-Corrected Base Ten Log Permeabilities. (Equivalent parameters in natural log permeability in parentheses following)

Parameter	Parameter Estimates	
	Exponential Model	Spherical Model
Integral Scale (meters)	15.0	13.0
Range (meters)	--	34.7
Sill of Underlying Semivariogram	1.45 (7.69)	1.30 (6.89)
Nugget Constant	0.15 (0.80)	0.15 (0.80)
Regularized Sill	1.33 (7.08)	1.23 (6.52)
Experimental Sill	1.48 (7.87)	1.38 (7.31)

4.3 Determination of Statistical Anisotropy from Results of Cross-Hole Tests

4.3.1 Method

The above semivariogram analyses of the single-hole hydraulic test data indicate that the covariance function of the log permeability field is anisotropic, and provide estimates of the semivariogram function in the vertical direction. Using the approximate analytical expressions developed in Chapter 3, this information can now be integrated with that obtained independently from the cross-hole tests to estimate the directional dependence of the three-dimensional log permeability covariance function. The covariance function is assumed to be ellipsoidal, and I will estimate the ratios of its principal integral scales (anisotropy ratios), λ_2/λ_1 and λ_3/λ_1. Based on theory, the principal axes of the covariance are assumed to be parallel to the principal axes of the effective permeability tensor, as determined from the cross-hole tests.

The main analytical expressions to be used here are equations (3.48) and (3.57). Solving (3.48) for F_{ii} and dividing the resulting equation by σ_f^2 gives:

$$g_{ii} = (\overline{f} - \ln \overline{K_{ii}^p})/\sigma_f^2 + 1/2 \qquad (i=1,2,3) \tag{4.5}$$

where

$$g_{ii} = F_{ii}/\sigma_f^2 \qquad (i=1,2,3) \tag{4.6}$$

Similarly, dividing equation (3.57) by σ_f^2 produces the useful expression

$$g_{ii} = (2/\pi L_i^2) \int_0^{\pi/2} \int_0^{\pi/2} [y_i^2 \sin \phi / |\underline{L}^{-1}\underline{y}|^2] \, d\theta \, d\phi \qquad (4.7)$$

where the y_i terms are defined in (3.52) and $\underline{L} = (1/\lambda_1)\underline{\lambda}$.

Equations (4.5) and (4.7) suggest that one might be able to estimate the anisotropy ratios from the inferred statistics of log permeability and the estimated effective permeability tensor. The parameters entering into (4.5) and (4.7) are obtained as follows: (1) $\bar{f}$, the mean log permeability, is taken to be the sample mean of the log permeabilities measured in the single-hole tests (Table 1.1). (2) σ_f^2, the variance of log permeability is taken to be the sill of the punctual semivariogram underlying the fitted model (Tables 4.1, 4.2 and 4.3). (3) $\overline{K_{ii}^p}$ (i = 1,2,3), the principal values of the effective permeability tensor and the corresponding principal directions, are adopted from the cross-hole test interpretation by Hsieh and others (1985) summarized in Table 1.2.

The approach is as follows: (1) Calculate g_{ii} (i=1,2,3) from equation (4.5) using the estimates of $\bar{f}$, σ_f^2, and $\overline{K_{ii}^p}$. Call these g_{ii}^*. (2) Make an initial guess about the anisotropy ratios, $L_2 = \lambda_2/\lambda_1$ and $L_3 = \lambda_3/\lambda_1$. Call these $\hat{L}_2$ and $\hat{L}_3$. (3) Calculate g_{ii} (i=1,2,3) from equation (4.7) using the anisotropy ratio estimates $\hat{L}_2$ and $\hat{L}_3$. Call these $\hat{g}_{ii}$. (4) Calculate the value of an appropriate estimation criterion, Ω, which measures the difference between g_{ii}^* and $\hat{g}_{ii}$ (i=1,2,3). Most common is the least-squares criterion

$$\Omega(\hat{L}_2,\hat{L}_3) = \sum_{i=1}^{3} (\hat{g}_{ii} - g_{ii}^*)^2 \qquad (4.8)$$

I use the minimax approach in which the criterion to be minimized is

$$\Omega(\hat{L}_2,\hat{L}_3) = \max_i |\hat{g}_{ii} - g^*_{ii}| \tag{4.9}$$

(5) If the value of the estimation criterion is less than or equal to a predetermined tolerance, stop; otherwise, adjust the estimates and repeat steps (3) through (5).

As shown in Appendix E, the sum of the $\hat{g}_{ii}$ terms calculated by equation (4.7) is one, give or take numerical errors. The sum of the g^*_{ii} values calculated by equation (4.5) generally differ from one for two reasons: (a) These values are calculated from estimates of $\bar{f}$, $\sigma^2_{\bar{f}}$ and $\overline{K^p_{ii}}$ and (b) equation (4.5) is an approximation. Therefore, for the estimation procedure to be consistent, the g^*_{ii} terms must be adjusted so that their sum is one, before they are used for the estimation of anisotropy ratios. For the Oracle data, this was done by multiplying the three g^*_{ii} values by the reciprocal of their sum:

$$g^*_{ii}(\text{adjusted}) = \frac{g^*_{ii}(\text{initial})}{\sum_{i=1}^{3} g^*_{ii}(\text{initial})} \tag{4.10}$$

The quality of the initial guess about the anisotropy ratios influences the length of the iterative procedure. The guess should be based on knowledge of site geology, on the results of semivariogram analysis, and on knowledge of the relationship between g_{ii} and the ratios, L_2 and L_3.

Step (3) of this procedure requires that the $\hat{g}_{ii}$ terms be calculated from expression (4.7), using the estimates $\hat{L}_2$ and $\hat{L}_3$. Two of these terms can be calculated by numerical integration. Since the sum of g_{ii} terms is equal to one (Appendix E), the third term is easily calculated from the other two. The region of integration is a square in the θ-ϕ plane having sides equal to $\pi/2$. For this study, the square was subdivided into a 50 by 50 grid for numerical integration by means of the midpoint or rectangular rule (Davis and Rabinowitz, 1967).

Step (5) requires that a tolerance be chosen. A tolerance of 0.004 was selected. Therefore the estimation objective can be stated thusly: Choose the anisotropy ratio estimates $\hat{L}_2$ and $\hat{L}_3$ such that $\Omega \leq 0.004$.

4.3.2 Results

The anisotropy ratio estimates are grouped into sets, based on whether they correspond to corrected or non-corrected single-hole data, and to an exponential or spherical semivariogram model. They are further separated according to whether the relevant effective permeability estimates are from the ordinary or weighted least-squares analysis by Hsieh and others (1985).

For example, Table 4.3 shows the anisotropy ratio estimates corresponding to the non-corrected permeability data and a spherical semivariogram model. These numbers are typical of the entire collection of estimates, the remainder of which is listed in Appendix H. The principal directions are indexed from i = 1 to 3 in the order they appear in Table 1.2. The estimates range from $L_2 = 0.73$ and $L_3 = 1.4$

Table 4.3. Estimated Anisotropy Ratios for Non-Corrected Log Permeabilities, Spherical Semivariogram

		Ordinary Least-Squares	Weighted Least-Squares
Initial	g^*_{11}	0.32	0.32
	g^*_{22}	0.50	0.47
	g^*_{33}	0.19	0.21
	Total	1.01	1.00
Adjusted	g^*_{11}	0.32	0.32
	g^*_{22}	0.50	0.47
	g^*_{33}	0.19	0.21
	Total	1.01	1.00
	$\hat{L}_2$	0.67	0.72
	$\hat{L}_3$	1.5	1.4
	Ω	0.004	0.002

(Table H.1) (smallest degree of anisotropy) to $L_2 = 0.62$ and $L_3 = 1.8$ (Table H.3) (largest degree of anisotropy).

The sums of the initial (un-adjusted) g_{ii} estimates range from 0.84 (Table H.3) to 1.06 (Table H.1). Those requiring the least adjustment correspond to the non-corrected permeability data and a spherical semivariogram (Table 4.3). For the ordinary least-squares effective permeability estimates, the adjustment was so minor that the adjusted values were indistinguishable from the initial values, within two significant figures. For the weighted least-squares estimates, no adjustment was necessary.

When the sum of the initial g_{ii} estimates is approximately one, several interpretations are possible: (1) Assuming the approximation given by (4.5) is suitable, a sum close to one may indicate that the estimates for $\overline{f}$, σ_f^2 and $\overline{K_{ii}^p}$ are reasonably good; (2) assuming that the estimates for $\overline{f}$, σ_f^2 and $\overline{K_{ii}^p}$ are reasonable, a sum equal to unity may suggest that expression (4.5) is a good approximation; (3) if neither the estimates nor the approximation are very good, the two errors may compensate for each other.

To determine the sensitivity of the estimation procedure to the anisotropy ratio parameters L_2 and L_3, the estimation criterion was contoured over a portion of the L_3-L_2 plane for the case: $g_{ii}^* = 0.32$, $g_{22}^* = 0.47$, $g_{33}^* = 0.21$. The remaining sets of g_{ii}^* values (Table 4.3 and Appendix H) are similar, so the results shown in Figure 4.15 are a good representation of the corresponding contours.

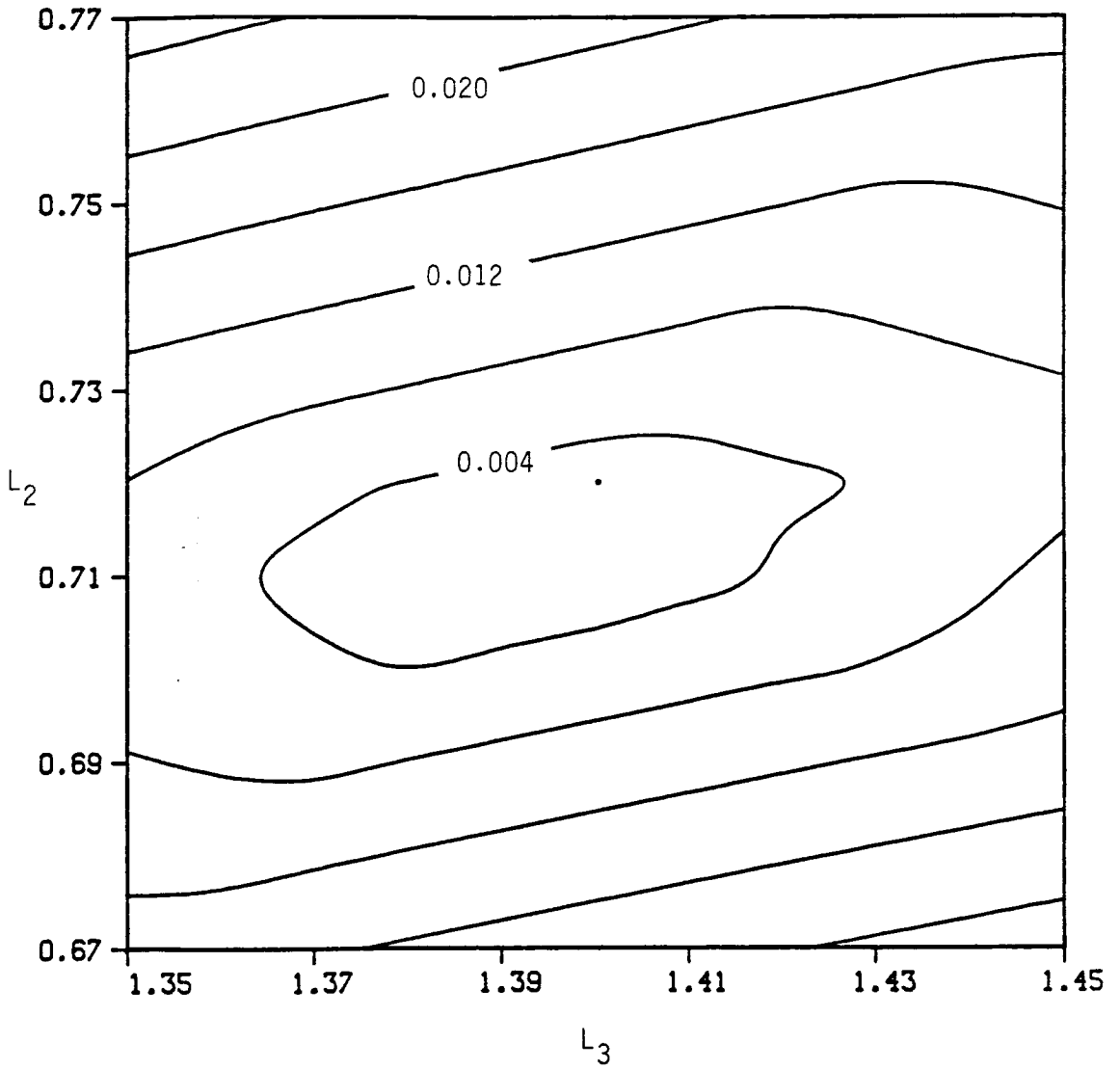

Figure 4.15. Contours of the Estimation Criterion in the L_3-L_2 Plane, for the Example Given in the Text. (Dot shows estimate.)

Note that the ordinate and abscissa in Figure 4.15 have the same relative scale. The contours roughly describe ellipses with major semiaxes subparallel to the L_3 axis, indicating that the estimation criterion is somewhat less sensitive to the L_3 parameter than to the L_2 parameter, for these g^*_{ii} values. The Ω = 0.004 contour, which corresponds to the selected tolerance, encloses a region in which L_3 varies from about 1.365 to 1.425 and L_2 varies from about 0.700 to 0.725. This indicates that with the present tolerance of 0.004, the minimum of Ω can be determined to within approximately $\pm$0.06 in L_3 (2 significant figures) and to within $\pm$0.025 in L_2 (not quite 2 significant figures).

For each set of g^*_{ii} values, between 5 and 8 iterations involving adjustment of the $\hat{L}_2$ and $\hat{L}_3$ values were required in order to obtain an estimation criterion less than or equal to 0.004.

4.4 Determination of Integral Scales

At this point, I have estimates of the stochastic anisotropy ratios for the log permeabilities at the Oracle site, but I still don't know the actual values of the principal integral scales, λ_1, λ_2 and λ_3. I have, however, estimates of the vertical integral scale (note that the vertical is <u>not</u> a principal direction) from the fitted semivariograms in the same direction. Since both the exponential and spherical semivariograms are ellipsoidal, they are completely determined by their sill and principal integral scales, λ_1, λ_2 and λ_3. Thus, it should be possible to determine these principal integral scales from the information available to us.

To show this, let $\underline{L}$ denote the diagonal matrix of anisotropy ratios,

$$\underline{L} = [L_i] = [\delta_{ij}\lambda_i/\lambda_1] \tag{4.11}$$

and observe that the matrix of integral scales, $\underline{\lambda}$, can be written as

$$\underline{\lambda} = \underline{L}\,\frac{\lambda_1}{\lambda'(\underline{u}')}\,\lambda'(\underline{u}') \tag{4.12}$$

where $\lambda'(\underline{u}')$ is a known integral scale for some direction, $\underline{u}'$. For the ellipsoidal exponential and spherical covariance functions, $\underline{\lambda}$ is given by the expression

$$\underline{\lambda} = \underline{L}[(\underline{u}')^T(\underline{A}^{-1})^T\underline{L}^{-2}\underline{A}^{-1}\underline{u}']^{1/2}\,\lambda'(\underline{u}') \tag{4.13}$$

where $\underline{A}$ is the matrix which transforms the coordinates of the principal system to those of the working system

$$\underline{x}' = \underline{A}\,\underline{x} \tag{4.14}$$

Equation (4.13) follows directly from equations (4.12), (2.62) and (2.68).

As shown in Appendix J, the entries of $\underline{A}$ are given by the direction cosines of the positive principal axes relative to the working system. For the two sets of estimated principal directions, corresponding to ordinary and weighted least-squares, these coordinates are given in Table 4.4. In both cases, the transformation is a rotation.

Table 4.4. Estimated Principal Directions Relative to Working Coordinate System.

	Estimated Principal Direction (from Hsieh and others, 1985)			Positive Principal Axis Direction		
	i	Bearing	Plunge	θ_i	ϕ_i	Coordinates of Unit Basis Vector
Ordinary Least-Squares	1	248°	32°	22°	58°	$\underline{e}_1' = (0.7863, 0.3177, 0.5299)$
	2	340°	4°	110°	94°	$\underline{e}_2' = (-0.3412, 0.9374, -0.06976)$
	3	77°	58°	193°	32°	$\underline{e}_3' = (-0.5163, -0.1192, 0.8480)$
Weighted Least-Squares	1	247°	51°	23°	39°	$\underline{e}_1' = (0.5793, 0.2459, 0.7771)$
	2	342°	4°	108°	94°	$\underline{e}_2' = (-0.3083, 0.9487, -0.06976)$
	3	75°	39°	195°	51°	$\underline{e}_3' = (-0.7507, -0.2011, 0.6293)$

For illustration let us examine the cases where regularized spherical semivariograms were fitted to the vertical sample semivariograms of non-corrected and leakage-corrected log permeabilities. These cases were chosen for two reasons. First, the spherical models appear to give better fits than the exponential curves to the sample semivariograms. Second, of all the sets of anisotropy ratio estimates compiled in the previous section, these two cover nearly the entire range from the least to the greatest degree of computed statistical anisotropy.

For example, consider the case where a regularized spherical semivariogram was fitted to the vertical sample semivariogram of non-corrected log permeabilities, and the effective permeability tensor was estimated by weighted least-squares. In this case, the elements of L are estimated by the anisotropy ratios in the right-hand column of Table 4.3:

$$\underline{L} = \begin{bmatrix} 1.0 & 0 & 0 \\ 0 & 0.72 & 0 \\ 0 & 0 & 1.4 \end{bmatrix}$$

The known integral scale is that in the vertical direction, whose estimate is listed in the right-hand column of Table 4.1:

$$\lambda'(\underline{u}') = \lambda'(0,0,1) = 13.0 \text{ m}$$

The elements of the rotation matrix, $\underline{A}$, are obtained from the coordinates of the basis vectors in the lower part of Table 4.4:

$$\underline{A} = \begin{bmatrix} 0.5793 & -0.3083 & -0.7507 \\ 0.2459 & 0.9487 & -0.2011 \\ 0.7771 & -0.06976 & -0.6293 \end{bmatrix}$$

Substituting these values into (4.13) yields the following principal integral scales (ranges):

$$\lambda_1 = 12 \text{ m} \qquad (a_1 = 31 \text{ m})$$
$$\lambda_2 = 8.5 \text{ m} \qquad (a_2 = 23 \text{ m})$$
$$\lambda_3 = 16 \text{ m} \qquad (a_3 = 44 \text{ m})$$

When the effective permeability tensor is estimated by ordinary least squares the estimates are:

$$\lambda_1 = 10 \text{ m} \qquad (a_1 = 27 \text{ m})$$
$$\lambda_2 = 6.8 \text{ m} \qquad (a_2 = 18 \text{ m})$$
$$\lambda_3 = 15 \text{ m} \qquad (a_3 = 41 \text{ m})$$

The greatest degree of statistical anisotropy predicted was from the leakage-corrected log permeabilities, fitted with a regularized spherical semivariogram (Figure 4.14 and Tables 4.2 and H.3). Using the ordinary least-squares effective permeability estimates, the resulting estimates of the principal integral scales (ranges) are:

$$\lambda_1 = 9.3 \text{ m} \qquad (a_1 = 25 \text{ m})$$
$$\lambda_2 = 5.8 \text{ m} \qquad (a_2 = 15 \text{ m})$$
$$\lambda_3 = 17 \text{ m} \qquad (a_3 = 45 \text{ m})$$

The maximum and minimum range estimates differ by about a factor of 3 here. For the corresponding weighted least-squares effective permeability estimates the scale estimates are given by:

$$\lambda_1 = 11 \text{ m} \qquad (a_1 = 30 \text{ m})$$
$$\lambda_2 = 7.4 \text{ m} \qquad (a_2 = 20 \text{ m})$$
$$\lambda_3 = 18 \text{ m} \qquad (a_3 = 49 \text{ m})$$

The average sample semivariogram is computed by arithmetically averaging the squared differences corresponding to data pairs with various relative orientations. Therefore, for any given distance its expectation is equal to some linear combination of semivariograms whose integral scales are between the minimum and maximum principal integral scales. Of course, the specific form of the linear combination depends on the data configuration. This information from the average sample semivariogram can be used as a partial check of the integral scale estimates. If the estimates are valid, we might expect that the range of the average sample semivariogram, or of any other sample semivariogram for that matter, should neither be less than the estimated minimum principal range nor greater than the estimated maximum principal range. Strictly though, this is only true of the expectation of the sample semivariogram. Actual experimental semivariograms are themselves stochastic processes, subject to fluctuations about their expected values. Therefore, as a check this should be performed cautiously. Generally, conclusions can be drawn with greater confidence from the average sample semiovariogram than from other sample semivariograms, because

the average form is computed from more data pairs and thus has a lower associated fluctuation variance.

Comparison of the range estimates given above and the average sample semivariograms (Figures 4.3 and 4.10) indicates that the two are not in close agreement. The average semivariograms, of both the non-corrected and the leakage-corrected log permeabilities, have apparent ranges of about 10 to 15 meters. This is less than any of the estimates of the minimum principal range. However, the determination of the ranges of the average sample semivariograms is made difficult by two facts. First, as discussed above, the average sample semivariograms are subject to random fluctuations about their expected values. Second, as shown in Figure 4.1, the early part of the average sample semivariograms is calculated from considerably fewer data pairs than the later part. Obviously, the early part is critical to determination of the range. In spite of these two facts, it cannot be said that the range estimates are consistent with the average sample semivariograms.

4.5 Effective Scalar Permeabilities

Using equation (3.49) and the estimates of the mean and variance of log permeability given in Tables 1.1, 4.1 and 4.2, the effective scalar permeability of the Oracle granite was estimated. These estimates are compiled in Table 4.5. The effective scalar permeability was also estimated by taking the geometric mean of the effective principal permeabilities obtained from the cross-hole tests (Table 1.2). These results are listed in Table 4.6. Note that although the two sets of estimates given in Tables 4.5 and 4.6 were

Table 4.5. Effective Scalar Permeabilities, Based on Estimated Log Permeability Statistics. (Permeability in m/s)

	Covariance Model	
	Exponential	Spherical
Non-Corrected Log Permeabilities	6.9×10^{-8}	6.1×10^{-8}
Leakage-Corrected Log Permeabilities	5.0×10^{-8}	4.3×10^{-8}

Table 4.6. Effective Scalar Permeabilities, Based on Effective Principal Permeability Estimates from Cross-Hole Tests. (Permeability in m/s)

	Permeability
Ordinary Least-Squares	5.8×10^{-8}
Weighted Least-Squares	6.2×10^{-8}

obtained independently, they are within an order of magnitude of one another.

CHAPTER 5

CONCLUSIONS AND RECOMMENDATIONS

5.1 Conclusions

The following conclusions are drawn from this thesis:

1. The continuous injection single-hole packer test data from the Oracle site can be interpreted in at least two ways. The interpretation depends on whether late-time borehole pressure changes above and below the packed-off test zone are treated as manifestations of prolate ellipsoidal flow, or as an indication of leakage past the packers when flow is essentially radial. The two interpretations call for somewhat different methods of analysis and lead to some differences in the log permeability estimates. It is difficult, if not impossible, to decide which interpretation is more appropriate for any given test. For this reason, both interpretations are used in this thesis. The sample means of the two log permeability data sets obtained from the two interpretations are nearly identical.

2. Analyses of experimental semivariograms of the two log permeability data sets suggest that each set may be considered to represent a randomly perturbed volume-averaged sample from a statistically anisotropic, second-order stationary random field. The vertical semivariogram of the non-regularized base ten log permeability field is best approximated by a spherical model with a range of 30 to 40 meters

and a sill (variance) of 1.30 to 1.45. The available single-hole data are, by themselves, insufficient to define semivariograms in directions other than the vertical.

3. A theoretical relationship between parameters describing the spatial variability of scalar log permeabilities on the local scale, and the large-scale effective permeability tensor of the rock mass, was developed by Gelhar and Axness (1983a). By treating the two single-hole test log permeability data sets from the Oracle site as scalars, and adopting the effective permeability tensor values obtained for the site from cross-hole tests by Hsieh and others (1985), one can estimate the principal directions of the anisotropic semivariogram for each of the two log permeability data sets, as well as the ratios between the principal integral scales (or range values), by means of the above relationship. When these results are combined with the available vertical semivariograms, the absolute values of the principal integral scales (or ranges) can also be estimated. In this manner, the three-dimensional directional properties of the semivariograms are fully characterized.

The suitability of this approach to the fractured Oracle granite hinges on the validity of three important assumptions underlying the theory: (a) the local permeability is a scalar, (b) the variance of the local natural log permeabilities is small, and (c) the stochastic anisotropy of the local log permeabilities is of an ellipsoidal nature.

Since the rock is fractured, the assumption that the local permeability is a scalar must be questioned. Indeed, Neuman and others (1985) and Hsieh and others (1985) point out that the single-hole packer test data represent largely the horizontal component of the rock permeability because flow during these tests is predominantly horizontal (since the boreholes are vertical). Nevertheless, when the equivalent scalar permeability of the rock mass is computed analytically from the local data by means of equation (3.49), the result is very close to that obtained independently by taking the geometric mean of the principal permeabilities from the cross-hole tests. This suggests that the theory may work despite the fact that the local permeabilities are not scalars.

The variance of the local natural log permeabilities is close to 7 or 8, while the perturbation theory of Gelhar and Axness (1983) on which I rely has been derived by assuming that this variance is much less than 1.0. Again, the fact that the equivalent scalar permeability values obtained from the single-hole and cross-hole tests agree suggests that the theory may work despite the relatively large magnitude of the variance. This is in agreement with other data which recently led Gelhar (1985) to conclude that "... the perturbation approach has proven to be quite robust for steady state saturated flow problems ..."

As far as the ellipsoidal nature of the semivariograms is concerned, the data are insufficient to either verify or refute this hypothesis.

4. When the stochastic anisotropy is of the geometric form (that is, characterized by an ellipsoidal spatial covariance function or semivariogram), the theoretical relationship between the statistical parameters of the local log permeabilities and the effective permeability tensor, derived by Gelhar and Axness (1983a), simplifies. In this case the effective principal permeabilities are dependent only upon the mean, variance and integral scales of the local log permeabilities, but not on the specific type of covariance function (e.g., exponential, spherical, etc.).

5. My results show that in the granitic rock mass at the Oracle site, the principal directions of structural anisotropy (same as those of the effective permeability tensor) and the corresponding principal integral scales and ranges are

i	θ_i	ϕ_i	λ_i	a_i
1	23°	30°	12 m	31 m
2	108°	94°	8.5 m	23 m
3	195°	51°	16 m	44 m

The ratios between these principal values are

$$\lambda_2/\lambda_1 = 0.72$$
$$\lambda_3/\lambda_1 = 1.4$$

For comparison, the ratios between the principal permeabilities and the cube roots of these ratios are

$$\overline{K^p_{22}}/\overline{K^p_{11}} = 0.32 \qquad (\overline{K^p_{22}}/\overline{K^p_{11}})^{1/3} = 0.68$$
$$\overline{K^p_{33}}/\overline{K^p_{11}} = 2.3 \qquad (\overline{K^p_{33}}/\overline{K^p_{11}})^{1/3} = 1.3$$

If the vertical range is assumed to fall between 30 and 40 meters, then the principal ranges vary from $a_1 = 27$ m, $a_2 = 20$ m, and $a_3 = 38$ m, to $a_1 = 36$ m, $a_2 = 26$ m, and $a_3 = 51$ m.

6. An analysis of the estimation criterion shows that it is relatively sensitive to the parameters λ_2/λ_1 and λ_3/λ_1, that represent the ratios between the principal integral scales. I thus conclude that these ratios can be estimated reliably.

5.2 Suggestions for Future Research

The results of this study show that more work needs to be done to validate the results of this thesis at the Oracle site, and to validate the methodology at other sites. I recommend that a computer simulation study be conducted before any further drilling or hydraulic testing is done at the Oracle site, because the results of such a study have the potential to be very valuable in designing further tests. The study should be aimed at determining the validity of mean field renormalization and the accuracy of the approximate analytical expressions (3.45) and (3.48), derived by Gelhar and Axness (1983a), under a variety of conditions. These conditions should include large variances and large stochastic anisotropy ratios. This type of investigation might help explain the result obtained here and those obtained by Hufschmied (1985).

If further work is to be done in this area at the Oracle site, an effort should be made to match the total volumes of rock investigated using the single-hole and cross-hole test methods. At present there is a slight discrepancy, due to the fact that cross-hole tests were only conducted in intervals connecting boreholes H2, H3, and H6. The discrepancy might be corrected by conducting more cross-hole tests in intervals connecting the other boreholes. However, although this change will render the stochastic analysis more consistent, it does not address one of the main problems with the present study -- the scarcity of single-hole data pairs with non-vertical relative orientations. It is this scarcity which makes it so difficult to verify the non-vertical integral scale estimates. In fact, the reader will recall that it was this scarcity of data for estimation of non-vertical semivariograms that prompted this investigation. This information can also be used to determine to what degree the covariance function is ellipsoidal.

Other work that might prove useful includes field studies of regularization and measurement error. This might be done by repeating single-hole tests at the site, using shorter or longer packer assemblies, and comparing the statistics of the resulting data sets.

APPENDIX A

SUMMARY OF NON-CORRECTED SINGLE-HOLE PACKER TEST DATA

Table A.1. Non-Corrected Base Ten Log Permeabilities

X (m)	Y (m)	Z (m)	K (m/s)	Log10 K
M1				
28.90	.60	-39.82	.2E-06	-6.6990
28.70	.60	-44.38	.3E-06	-6.5229
28.40	.70	-48.32	.3E-05	-5.5229
28.20	.70	-51.68	.3E-05	-5.5229
27.80	.80	-55.62	.7E-06	-6.1549
27.60	.80	-59.57	.4E-05	-5.3979
27.30	.80	-62.60	.4E-05	-5.3979
27.00	.90	-66.85	.4E-06	-6.3979
26.60	.90	-71.12	.4E-07	-7.3979
26.50	.90	-73.26	.7E-07	-7.1549
26.10	.90	-78.86	.1E-05	-6.0000
25.80	.90	-82.37	.1E-05	-6.0000
25.50	1.00	-86.32	.4E-05	-5.3979
H2				
21.30	.20	-20.79	.2E-07	-7.6990
21.30	.20	-23.84	.6E-07	-7.2218
21.30	.30	-26.89	.1E-06	-7.0000
21.30	.40	-32.37	.3E-07	-7.5229
21.30	.50	-36.03	.3E-08	-8.5229
21.30	.60	-39.99	.8E-08	-8.0969
21.30	.70	-43.65	.9E-09	-9.0458
21.30	.70	-47.31	.7E-09	-9.1549
21.30	.80	-50.97	.3E-08	-8.5229
21.30	.90	-53.86	.6E-09	-9.2218
21.30	.90	-58.28	.2E-08	-8.6990
21.30	1.00	-61.94	.3E-08	-8.5229
21.30	1.10	-65.60	.4E-08	-8.3979
21.30	1.20	-69.25	.2E-08	-8.6990
21.30	1.30	-73.22	.3E-08	-8.5229
21.30	1.50	-77.79	.8E-07	-7.0969
21.30	1.60	-82.67	.6E-05	-5.2218
21.30	1.60	-85.10	.9E-09	-9.0458

Table A.1--Continued

X (m)	Y (m)	Z (m)	K (m/s)	Log10 K
H3				
14.90	.00	-19.93	.5E-06	-6.3010
14.80	.00	-22.24	.5E-06	-6.3010
14.60	.00	-27.55	.1E-06	-7.0000
14.60	.00	-30.29	.2E-06	-6.6990
14.50	.00	-35.47	.5E-06	-6.3010
14.30	.00	-39.89	.5E-05	-5.3010
14.10	.10	-45.84	.2E-05	-5.6990
14.00	.10	-50.71	.1E-06	-7.0000
13.90	.10	-54.68	.1E-06	-7.0000
13.70	.10	-58.64	.1E-06	-7.0000
13.60	.10	-62.30	.3E-07	-7.5229
13.40	.10	-66.26	.1E-07	-8.0000
13.20	.10	-70.22	.5E-07	-7.3010
13.00	.20	-76.62	.8E-06	-6.0969
12.60	.30	-85.16	.8E-07	-7.0969
H4				
.00	-.30	-23.16	.7E-07	-7.1549
-.10	-.30	-26.82	.8E-10	-10.0970
-.10	-.40	-30.48	.5E-09	-9.3010
-.15	-.45	-34.72	.6E-10	-10.2220
-.20	-.50	-39.01	.3E-09	-9.5229
-.20	-.50	-42.67	.3E-09	-9.5229
-.20	-.50	-47.55	.1E-07	-8.0000
-.20	-.50	-51.21	.2E-09	-9.6990
-.20	-.50	-53.34	.7E-08	-8.1549
-.30	-.50	-57.30	.6E-07	-7.2218
-.30	-.50	-60.96	.4E-07	-7.3979
-.40	-.50	-64.62	.2E-08	-8.6990
-.40	-.50	-68.28	.9E-07	-7.0458
-.50	-.50	-71.93	.4E-07	-7.3979
-.60	-.50	-75.59	.2E-08	-8.6990
-.70	-.50	-79.25	.8E-08	-8.0969
-.80	-.50	-82.91	.2E-07	-7.6990
H5				
30.48	15.24	-36.29	.7E-07	-7.1549
30.48	15.24	-44.03	.8E-07	-7.0969
30.48	15.24	-47.46	.1E-06	-7.0000
30.48	15.24	-50.89	.2E-08	-8.6990
30.48	15.24	-54.32	.6E-09	-9.2218

Table A.1--Continued

X (m)	Y (m)	Z (m)	K (m/s)	Log10 K
H5				
30.48	15.24	-57.75	.4E-08	-8.3979
30.48	15.24	-61.79	.1E-07	-8.0000
30.48	15.24	-65.22	.3E-08	-8.5229
30.48	15.24	-68.65	.6E-08	-8.2218
30.48	15.24	-72.07	.1E-07	-8.0000
H6				
22.86	7.62	-29.39	.6E-06	-6.2218
22.86	7.62	-32.51	.6E-09	-9.2218
22.86	7.62	-35.94	.3E-07	-7.5229
22.86	7.62	-39.37	.3E-07	-7.5229
22.86	7.62	-42.80	.3E-07	-7.5229
22.86	7.62	-46.23	.8E-07	-7.0969
22.86	7.62	-49.65	.4E-09	-9.3979
22.86	7.62	-53.08	.6E-09	-9.2218
22.86	7.62	-56.51	.4E-07	-7.3979
22.86	7.62	-59.94	.2E-07	-7.6990
22.86	7.62	-63.37	.4E-09	-9.3979
22.86	7.62	-66.80	.1E-07	-8.0000
22.86	7.62	-70.23	.1E-07	-8.0000
22.86	7.62	-73.66	.3E-07	-7.5229
H7				
15.24	7.62	-26.18	.9E-08	-8.0458
15.24	7.62	-29.31	.2E-08	-8.6990
15.24	7.62	-32.74	.1E-09	-10.0000
15.24	7.62	-36.17	.2E-09	-9.6990
15.24	7.62	-39.60	.2E-09	-9.6990
15.24	7.62	-43.33	.1E-08	-9.0000
15.24	7.62	-46.76	.2E-08	-8.6990
15.24	7.62	-48.97	.3E-08	-8.5229
15.24	7.62	-52.17	.4E-08	-8.3979
15.24	7.62	-54.91	.5E-09	-9.3010
15.24	7.62	-58.16	.2E-08	-8.6990
15.24	7.62	-61.74	.3E-08	-8.5229
15.24	7.62	-65.40	.8E-09	-9.0969
15.24	7.62	-69.16	.1E-08	-9.0000
15.24	7.62	-72.91	.5E-07	-7.3010

APPENDIX B

SUMMARY OF LEAKAGE-CORRECTED SINGLE-HOLE PACKER TEST DATA

Table B.1. Leakage-Corrected Base Ten Log Permeabilities

X (m)	Y (m)	Z (m)	K (m/s)	Log10 K
M1				
28.90	.60	-39.82	.2E-06	-6.6990
28.70	.60	-44.38	.3E-06	-6.5229
28.40	.70	-48.32	.3E-05	-5.5229
28.20	.70	-51.68	.3E-05	-5.5229
27.80	.80	-55.62	.6E-06	-6.2218
27.60	.80	-59.57	.4E-05	-5.3979
27.00	.90	-66.85	.2E-07	-7.6990
26.60	.90	-71.12	.3E-07	-7.5229
26.50	.90	-73.26	.7E-07	-7.1549
26.10	.90	-78.86	.1E-05	-6.0000
25.80	.90	-82.37	.1E-05	-6.0000
25.50	1.00	-86.32	.1E-05	-6.0000
H2				
21.30	.20	-20.79	.2E-07	-7.6990
21.30	.20	-23.84	.5E-07	-7.3010
21.30	.30	-26.89	.1E-06	-7.0000
21.30	.40	-32.37	.3E-07	-7.5229
21.30	.50	-36.03	.3E-08	-8.5229
21.30	.60	-39.99	.8E-08	-8.0969
21.30	.70	-43.65	.9E-09	-9.0458
21.30	.70	-47.31	.7E-09	-9.1549
21.30	.80	-50.97	.3E-08	-8.5229
21.30	.90	-53.86	.6E-09	-9.2218
21.30	.90	-58.28	.2E-08	-8.6990
21.30	1.00	-61.94	.3E-08	-8.5229
21.30	1.10	-65.60	.4E-08	-8.3979
21.30	1.20	-69.25	.2E-08	-8.6990
21.30	1.30	-73.22	.3E-08	-8.5229
21.30	1.50	-77.79	.8E-07	-7.0969
21.30	1.60	-82.67	.6E-05	-5.2218
21.30	1.60	-85.10	.9E-09	-9.0458

Table B.1--Continued

X (m)	Y (m)	Z (m)	K (m/s)	Log10 K
H3				
14.90	.00	-19.93	.5E-06	-6.3010
14.60	.00	-27.55	.1E-07	-8.0000
14.60	.00	-30.29	.1E-06	-7.0000
14.50	.00	-35.47	.5E-06	-6.3010
14.30	.00	-39.89	.2E-05	-5.6990
14.10	.10	-45.84	.9E-07	-7.0458
14.00	.10	-50.71	.1E-06	-7.0000
13.90	.10	-54.68	.1E-06	-7.0000
13.70	.10	-58.64	.1E-06	-7.0000
13.60	.10	-62.30	.3E-07	-7.5229
13.40	.10	-66.26	.1E-07	-8.0000
13.20	.10	-70.22	.5E-07	-7.3010
13.00	.20	-76.62	.6E-06	-6.2218
12.60	.30	-85.16	.8E-07	-7.0969
H4				
.00	-.30	-23.16	.7E-07	-7.1549
-.10	-.30	-26.82	.8E-10	-10.0970
-.10	-.40	-30.48	.5E-09	-9.3010
-.20	-.50	-39.01	.3E-09	-9.5229
-.20	-.50	-42.67	.3E-09	-9.5229
-.20	-.50	-47.55	.1E-07	-8.0000
-.20	-.50	-51.21	.2E-09	-9.6990
-.20	-.50	-53.34	.7E-08	-8.1549
-.30	-.50	-57.30	.6E-07	-7.2218
-.30	-.50	-60.96	.4E-07	-7.3979
-.40	-.50	-64.62	.2E-08	-8.6990
-.40	-.50	-68.28	.9E-07	-7.0458
-.50	-.50	-71.93	.4E-07	-7.3979
-.60	-.50	-75.59	.2E-08	-8.6990
-.70	-.50	-79.25	.8E-08	-8.0969
-.80	-.50	-82.91	.2E-07	-7.6990
H5				
30.48	15.24	-36.29	.7E-07	-7.1549
30.48	15.24	-44.03	.4E-07	-7.3979
30.48	15.24	-47.46	.8E-07	-7.0969
30.48	15.24	-50.89	.2E-08	-8.6990
30.48	15.24	-54.32	.6E-09	-9.2218

Table B.1--Continued

X (m)	Y (m)	Z (m)	K (m/s)	Log10 K
H5				
30.48	15.24	-57.75	.4E-08	-8.3979
30.48	15.24	-61.79	.1E-07	-8.0000
30.48	15.24	-65.22	.3E-08	-8.5229
30.48	15.24	-68.65	.6E-08	-8.2218
30.48	15.24	-72.07	.1E-07	-8.0000
H6				
22.86	7.62	-29.39	.6E-06	-6.2218
22.86	7.62	-32.51	.6E-09	-9.2218
22.86	7.62	-35.94	.4E-07	-7.3797
22.86	7.62	-39.37	.4E-07	-7.3797
22.86	7.62	-42.80	.3E-07	-7.5229
22.86	7.62	-46.23	.8E-07	-7.0969
22.86	7.62	-49.65	.4E-09	-9.3979
22.86	7.62	-53.08	.6E-09	-9.2218
22.86	7.62	-56.51	.4E-07	-7.3979
22.86	7.62	-59.94	.2E-07	-7.6990
22.86	7.62	-63.37	.4E-09	-9.3979
22.86	7.62	-66.80	.1E-07	-8.0000
22.86	7.62	-70.23	.1E-07	-8.0000
22.86	7.62	-73.66	.3E-07	-7.5229
H7				
15.24	7.62	-26.18	.9E-08	-8.0458
15.24	7.62	-29.31	.2E-08	-8.6990
15.24	7.62	-32.74	.1E-09	-10.0000
15.24	7.62	-36.17	.2E-09	-9.6990
15.24	7.62	-39.60	.2E-09	-9.6990
15.24	7.62	-43.33	.1E-08	-9.0000
15.24	7.62	-46.76	.2E-08	-8.6990
15.24	7.62	-48.97	.3E-08	-8.5229
15.24	7.62	-52.17	.4E-08	-8.3979
15.24	7.62	-54.91	.5E-09	-9.3010
15.24	7.62	-58.16	.2E-08	-8.6990
15.24	7.62	-61.74	.3E-08	-8.5229
15.24	7.62	-65.40	.8E-09	-9.0969
15.24	7.62	-69.16	.1E-08	-9.0000
15.24	7.62	-72.91	.5E-07	-7.3010

APPENDIX C

EFFECT OF LINEAR COORDINATE TRANSFORMATION ON SPECTRUM

Consider the linear spatial coordinate transformation

$$\underline{x}' = \underline{A}\,\underline{x} \tag{C.1}$$

where $\underline{x}$ and $\underline{x}'$ are spatial coordinates and $\underline{A}$ is a nonsingular matrix. Any separation vector, $\underline{h}$, transforms similarly

$$\underline{h}' = \underline{A}\,\underline{h} \tag{C.2}$$

because it is linear in $\underline{x}$. Therefore,

$$\begin{aligned} \underline{k}\cdot\underline{h} = \underline{k}^T\underline{h} &= \underline{k}^T\underline{A}^{-1}\underline{h}' \\ &= [(\underline{A}^{-1})^T\underline{k}]^T\underline{h}' \\ &= \underline{k}'\cdot\underline{h}' \end{aligned} \tag{C.3}$$

provided the wave number coordinate transformation is defined as

$$\underline{k}' = (\underline{A}^{-1})^T\underline{k} \tag{C.4}$$

The volume differential transforms as follows,

$$d\underline{h} = |\underline{A}|^{-1}d\underline{h}' \tag{C.5}$$

where $|\underline{A}|$ denotes the absolute value of the determinant of $\underline{A}$ and is the Jacobian of the transformation. Therefore, the spectral density

$$S(\underline{k}) = \frac{1}{(2\pi)^3} \int_{\underline{h}} \exp(-i\underline{k}\cdot\underline{h})\, C(\underline{h})\, d\underline{h} \qquad (C.6)$$

can be written in terms of the transformed quantities as

$$S(\underline{k}) = \frac{1}{(2\pi)^3 |\underline{A}|} \int_{\underline{h}'} \exp(-i\underline{k}'\cdot\underline{h}')\, C'(\underline{h}')\, d\underline{h}' \qquad (C.7)$$

or

$$S(\underline{k}) = \frac{1}{|\underline{A}|} S'(\underline{k}')$$

APPENDIX D

PROOF OF EQUATION (3.57)

Because

$$C(\underline{h}) = \int_{\underline{k}} \exp(i\underline{k}\cdot\underline{h})\, S(\underline{k})\, d\underline{k} \tag{D.1}$$

it follows that

$$C(\underline{o}) = \int_{\underline{k}} S(\underline{k})\, d\underline{k} = \sigma^2 \tag{D.2}$$

where $C(\underline{h})$ is the spatial covariance corresponding to the three-dimensional spatial displacement vector, $\underline{h}$. Since this relationship holds in general, it holds for the particular case where the spectral density and the integral are written with respect to an isotropic wave number domain,

$$\sigma^2 = \int_{\underline{k}'} S'(\underline{k}')\, d\underline{k}' \tag{D.3}$$

Rewriting the integral in spherical coordinates:

$$\sigma^2 = 8 \lim_{L \to +\infty} \int_0^{\pi/2} \int_0^{\pi/2} \int_0^{L} \rho^2\, S'(\rho)\, d\rho\, d\theta \sin\phi\, d\phi \tag{D.4}$$

Thus,

$$\lim_{L \to +\infty} \int_0^{L} \rho^2\, S'(\rho)\, d\rho = \frac{\sigma^2}{4\pi} \tag{D.5}$$

APPENDIX E

PROOF THAT $\sum_i F_{ii} = \sigma_f^2$

Recall from Section (3.2.4) that in the absence of a drift in log conductivity, the F_{ii} integrals are

$$F_{ii} = \int_{\underline{k}} \frac{k_i^2}{|\underline{k}|^2} S_{ff}(\underline{k})\, d\underline{k} \qquad (E.1)$$

Obviously then,

$$\sum_{i=1}^{3} F_{ii} = \int_{\underline{k}} S_{ff}(\underline{k})\, d\underline{k} \qquad (E.2)$$

From equation (D.2) it follows that

$$\sum_{i=1}^{3} F_{ii} = \sigma_f^2 \qquad (E.3)$$

APPENDIX F

REGULARIZED EXPONENTIAL SEMIVARIOGRAM

For purely vertical separations, the three-dimensional, geometrically anisotropic exponential semivariogram is:

$$\gamma(0,0,h) = C(\underline{o})[1 - \exp(h/\lambda)] \tag{F.1}$$

The semivariogram of the regularized variable (4.2) is (Huijbregts, 1971):

$0 \leq h \leq \ell$:

$$\gamma_\ell(0,0,h) = C(\underline{o})(\lambda^2/\ell^2)\{2\exp(-\ell/\lambda) - 2 + 2h/\lambda + 2\exp(-h/\lambda) - \exp[-(h+\ell)/\lambda] - \exp[(h-\ell)/\lambda]\}$$

$\ell \leq h$:

$$\gamma_\ell(0,0,h) = C(\underline{o})(\lambda^2/\ell^2)\{2\exp(-\ell/\lambda) - 2 + 2\ell/\lambda + 2\exp(-h/\lambda) - \exp[-(h+\ell)/\lambda] - \exp[(\ell-h)/\lambda]\} \tag{F.2}$$

$h \to +\infty$:

$$\gamma_\ell(0,0,h) = C_\ell(\underline{o}) = 2C(\underline{o})(\lambda^2/\ell^2)[\ell/\lambda + \exp(-\ell/\lambda) - 1]$$

where λ is the integral scale of the underlying point semivariogram, in the vertical direction, and h is the modulus of the vertically oriented separation vector.

APPENDIX G

REGULARIZED SPHERICAL SEMIVARIOGRAM

For purely vertical separations, the three-dimensional, geometrically anisotropic spherical semivariogram is:

$$\gamma(0,0,h) = C(\underline{o})[(3/2)(h/a) - (1/2)(h/a)^3] \qquad (G.1)$$

The regularized form of (G.1) is dependent on the relative magnitudes of the vertical range, a, and the regularization length, ℓ. The vertical experimental semivariogram of log permeability measurements made at the Oracle site indicates that the vertical range is much greater than 2ℓ (approximately 35 m vs 7.6 m). Therefore, only the regularized form of (G.1) corresponding to $a \geq 2\ell$ is listed here (Huijbregts, 1971):

$0 \leq h \leq \ell$:

$$\gamma_\ell(0,0,h) = C(\underline{o})(h^2/a^2)[3a/2\ell - \ell/2a - (h/a)(a^2/2\ell^3) - (h^2/a^2)(a/4\ell) + (h^3/a^3)(a^2/20\ell^2)]$$

$\ell \leq h \leq a-\ell$:

$$\gamma_\ell(0,0,h) = C(\underline{o})[-\ell/2a + \ell^3/20a^3 + (h/a)(3/2 - \ell^2/4a^2) - h^3/2a^3]$$

$a-\ell \leq h \leq a$:

$$\gamma_\ell(0,0,h) = C(o)[1/2 - 3a/8\ell + a^2/10\ell^2 - 3\ell/4a + 3\ell^3/40a^3 + (h/a)(3/4 + a/\ell - 3a^2/8\ell^2 - \ell^2/8a^2) + (h^2/a^2)(-3a/4\ell + \ell/4a + a^2/2\ell^2) + (h^3/a^3)(-1/4 - a^2/4\ell^2) + h^4/8a^3\ell + h^5/40a^3\ell^2] \qquad (G.2)$$

$a \leq h \leq a+\ell$:

$$\gamma_\ell(0,0,h) = C(o)[1/2 - 3a/8\ell - a^2/10\ell^2 - 3\ell/4a + 3\ell^3/40a^3 + (h/a)(3/4 + a/\ell + 3a^2/8\ell^2 - \ell^2/8a^2) + (h^2/a^2)(-3a/4\ell + \ell/4a - a^2/2\ell^2) + (h^3/a^3)(-1/4 + a^2/4\ell^2) + h^4/8a^3\ell - h^5/40a^3\ell^2]$$

$\ell+a \leq h$:

$$\gamma_\ell(0,0,h) = C(o)[1 - \ell/2a + \ell^3/20a^3]$$

where h is the modulus of the vertically oriented separation vector.

APPENDIX H

ANISOTROPY RATIO ESTIMATES

Table H.1. Estimated Anisotropy Ratios for Non-Corrected Log Permeabilities, Exponential Semivariogram

		Ordinary Least-Squares	Weighted Least-Squares
Initial	g^*_{11}	0.34	0.33
	g^*_{22}	0.50	0.47
	g^*_{33}	0.22	0.23
	Total	1.06	1.03
Adjusted	g^*_{11}	0.32	0.32
	g^*_{22}	0.47	0.46
	g^*_{33}	0.21	0.22
	Total	1.00	1.00
	$\hat{L}_2$	0.72	0.73
	$\hat{L}_3$	1.4	1.4
	Ω	0.002	0.001

Table H.2. Estimated Anisotropy Ratios for Leakage-Corrected Log Permeabilities, Exponential Semivariogram

		Ordinary Least-Squares	Weighted Least-Squares
Initial	g_{11}^*	0.30	0.29
	g_{22}^*	0.47	0.44
	g_{33}^*	0.17	0.18
	Total	0.94	0.91
Adjusted	g_{11}^*	0.32	0.32
	g_{22}^*	0.50	0.48
	g_{33}^*	0.18	0.20
	Total	1.00	1.00
	$\hat{L}_2$	0.67	0.70
	$\hat{L}_3$	1.6	1.5
	Ω	0.003	0.001

Table H.3. Estimated Anisotropy Ratios for Leakage-Corrected Log Permeabilities, Spherical Semivariogram

		Ordinary Least-Squares	Weighted Least-Squares
Initial	g^*_{11}	0.27	0.27
	g^*_{22}	0.47	0.43
	g^*_{33}	0.13	0.14
	Total	0.87	0.84
Adjusted	g^*_{11}	0.31	0.32
	g^*_{22}	0.54	0.51
	g^*_{33}	0.15	0.17
	Total	1.00	1.00
	$\hat{L}_2$	0.62	0.65
	$\hat{L}_3$	1.8	1.6
	Ω	0.002	0.004

APPENDIX I

CHANGE OF BASIS

Let $\underline{e}_1$, $\underline{e}_2$, and $\underline{e}_3$ denote the standard unit normal basis vectors in R^3 which define the principal axes of a coordinate system, $\underline{x}$. Then we can write

$$\underline{x} = x_1\underline{e}_1 + x_2\underline{e}_2 + x_3\underline{e}_3 \tag{I.1}$$

where

$$\begin{aligned} \underline{e}_1 &= (1,0,0) \\ \underline{e}_2 &= (0,1,0) \\ \underline{e}_3 &= (0,0,1) \end{aligned} \tag{I.2}$$

Let $\underline{e}_1'$, $\underline{e}_2'$ and $\underline{e}_3'$ denote the same three vectors, whose coordinates are now expressed relative to the linearly transformed working coordinate system

$$\underline{x}' = \underline{A}\,\underline{x} \tag{I.3}$$

where $\underline{A}$ is nonsingular. The set $\underline{e}_1'$, $\underline{e}_2'$, $\underline{e}_3'$ is an orthogonal basis for R^3.

Suppose that the coordinates of this basis have been determined. Then any vector $\underline{x}'$ can be expressed as a linear combination of these vectors:

$$\underline{x}' = x_1\underline{e}_1' + x_2\underline{e}_2' + x_3\underline{e}_3' \tag{I.4}$$

Equation (I.4) can be derived by pre-multiplying both sides of equation (I.1) by $\underline{A}$. Equating the right-hand sides of expressions (I.3) and (I.4) gives (Noble and Daniel, 1977, pp. 274-275):

$$\underline{A} = [\underline{e}_1' \ \underline{e}_2' \ \underline{e}_3'] \qquad (I.5)$$

APPENDIX J

SYMBOLS

$\underline{A}$	matrix of semivariogram ranges, in principal directions; coordinate transformation matrix
a	range of semivariogram
a_i	range of semivariogram, in i^{th} principal direction
$\underline{B}$	scale tensor defined by (2.48) and (2.49)
b	a constant
C	spatial covariance function, generally expressed relative to principal coordinate system
C_ℓ	covariance function of $f_\ell(\underline{x})$
C_V	covariance function of volume averaged process, $f_V(\underline{x})$
$\overline{C}(V,V)$	same as $C_V(\underline{o})$
$\overline{C}(V,V')$	same as C_V
C_o	nugget constant
E	expectation operator
e	base of Napierian (natural) logarithm, $e \cong 2.71828183$
$\underline{e}_i$	i^{th} unit basis vector
$F(\ )$	some function
$\underline{F}$	wave number tensor defined by equation (3.37), expressed relative to principal coordinate system
F_{ii}	ii^{th} element of $\underline{F}$
$f(\underline{x})$	general spatial stochastic process; logarithm of local permeability

$f_\ell(\underline{x})$ $f(\underline{x})$ regularized by averaging over a vertical segment of length ℓ, centered at $\underline{x}$

$f_p(\underline{x})$ regularization of $f(\underline{x})$ by weight function $p(\underline{x})$

$f_V(\underline{x})$ volume averaged process $f(\underline{x})$

$f^*(\underline{x})$ measured values of $f(\underline{x})$

g gravitational acceleration, $g \cong 9.8066$ m/sec^2

g_{ii} F_{ii}/σ_f^2

$g(\underline{x})$ weight function

H hydraulic head

H_o ambient hydraulic head

H_w hydraulic head in wellbore

$\underline{h}$ spatial separation vector, expressed relative to principal coordinate system

$\underline{h}_i$ spatial separation vector corresponding to i^{th} data pair of a particular distance class

$\underline{I}$ identity matrix

i index; imaginary number $i = \sqrt{-1}$

$\underline{J}$ negative expectation of hydraulic gradient

J_j j^{th} element of vector $\underline{J}$

j index

K local scalar permeability

$\overline{\underline{K}}$ effective permeability tensor, expressed relative to general coordinate system

$\overline{\underline{K}^p}$ effective permeability tensor, expressed relative to principal coordinate system

$\overline{K^p_{ii}}$ effective permeability in i^{th} principal direction

$\underline{K}$ permeability tensor

K_{ij} ij^{th} element of $\underline{K}$

K_ℓ geometric mean of local scalar permeability

$\underline{k}$ wave number vector

k_i i^{th} element of $\underline{k}$

$\underline{L}$ matrix of anisotropy ratios

ℓ length of test zone, single-hole packer tests

lim limit

ln Napierian (natural) logarithm

MSE mean squared error

$N(\underline{h})$ number of data pairs in the distance class corresponding to $\underline{h}$

$P[f(\underline{x})]$ cumulative distribution function of $f(\underline{x})$

$p[f(\underline{x})]$ probability density function of $f(\underline{x})$

p water pressure

$p(\underline{x})$ weight function

Q volumetric injection rate

Q_{leak} volumetric leakage rate

$\underline{q}$ specific discharge

q_j j^{th} element of $\underline{q}$

R^n n-dimensional space

r distance; radial distance from wellbore axis

r_e effective radius of influence

r_w radius of wellbore

$S(\underline{k})$ spectral density (power spectrum)

$S_{ff}(\underline{k})$ spectral density of process $f'(\underline{x})$

$\underline{s}$ dummy variable

$\underline{t}$ dummy variable

t	time
$U(\underline{h})$	unit step (Heaviside) function
$\underline{u}$	unit vector
V	volume or domain
Var	variance
$\underline{x}$	location vector, expressed relative to principal coordinate system
x_i	i^{th} element of $\underline{x}$
Y	linear combination of $f(\underline{x})$
$\underline{y}$	unit vector of wave number domain, defined in (3.52)
$Z(\underline{k})$	complex orthogonal process
α	angle between hydraulic head fluctuation gradient and log permeability fluctuation gradient
γ	semivariogram of $f(\underline{x})$
γ_{f*}	semivariogram of $f^*(\underline{x})$
γ_{ℓ}	semivariogram of $f_{\ell}(\underline{x})$
γ_V	semivariogram of $f_V(\underline{x})$
$\gamma(V)$	local semivariogram of $f(\underline{x})$
γ_{ε}	semivariogram of $\varepsilon(\underline{x})$
$\gamma_{\varepsilon f}$	cross-variogram of $\varepsilon(\underline{x})$ and $f(\underline{x})$
γ^*	sample semivariogram of $f^*(\underline{x})$
$\Delta(\underline{h})$	distance tolerance assigned to separation vector $\underline{h}$
δ_{ij}	Kronecker delta
$\delta(\underline{x}-\underline{x}_i)$	Dirac distribution
$\varepsilon(\underline{x})$	measurement error
ε_*	difference between semivariogram and sample semivariogram

$\varepsilon(V)$	difference between semivariogram and local semivariogram
$\varepsilon_*(V)$	difference between sample semivariogram and local semivariogram
η	angle tolerance (window)
θ	angle, spherical coordinate
$\underline{\lambda}$	matrix of principal integral scales
λ_i	integral scale in i^{th} principal direction
$\lambda(\underline{u})$	integral scale in direction of $\underline{u}$
Π	product
π	pi $\cong$ 3.14159265
ρ	water density; radial distance in spherical coordinates of wave number domain
$\sum$	sum
σ^2	variance
σ_f^2	variance of local log permeability
σ_ε^2	variance of measurement error, $\varepsilon(\underline{x})$
ϕ	angle, spherical coordinate
Ω	estimation criterion
∇	gradient operator
$\nabla\cdot$	divergence operator
$(\ )^*$	complex conjugate; measured value; estimate
$(\ )'$	residual or fluctuation; relative to working coordinate system
$(\ )^T$	transpose
$(\ )^{-1}$	inverse
$\hat{}$	estimate
$\bar{}$	(overbar) ensemble average or expectation; effective value

$\cong$	"is approximately equal to"
$<<$	"is negligible in comparison to"
$\lvert\ \rvert$	absolute value (scalar); modulus (vector); absolute value of determinant (matrix)
$\underline{\quad}$	(underline) vector, tensor or matrix quantity

REFERENCES

Bakr, A. A., L. W. Gelhar, A. L. Gutjahr, and J. R. MacMillan, Stochastic analysis of spatial variability in subsurface flows, 1, Comparison of one- and three-dimensional flows, Water Resour. Res., 14(2), 263-271, 1978.

Banerjee, A. K., Geology of the Oracle granite, Ph.D. dissertation, University of Arizona, Tucson, 1957.

Benjamin, J. R., and C. A. Cornell, Probability, Statistics, and Decision for Civil Engineers, McGraw-Hill, New York, 1970.

Bras, R. L., and I. Rodriguez-Iturbe, Evaluation of mean square error involved in approximating the areal average of a rainfall event by a discrete summation, Water Resour. Res., 12(2), 181-184, 1976.

Christakos, G. C., On the problem of permissible covariance and variogram models, Water Resour. Res., 20(2), 251-265, 1984.

Cushman, J. H., Comment on "Three-dimensional stochastic analysis of macrodispersion in aquifers by L. W. Gelhar and C. L. Axness," Water Resour. Res., 19(6), 1641-1642, 1983.

Dagan, G., Models of groundwater flow in statistically homogeneous porous formations, Water Resour. Res., 15(1), 47-63.

Davis, P. J., and P. Rabinowitz, Numerical Integration, Blaisdell Pub. Co., Waltham, Mass., 1967.

Flynn, T. J., Water temperature as a groundwater tracer in fractured rock, M.S. thesis, University of Arizona, Tucson, 1985.

Gambolati, G., and G. Volpi, Groundwater contour mapping in Venice by stochastic interpolators, 1, Theory, Water Resour. Res., 15(2), 281-290, 1979.

Gelhar, L. W., Stochastic subsurface hydrology from theory to applications, addendum to Proceedings, International Symposium of the Stochastic Approach to Subsurface Flow, Int. Assoc. Hydraul. Res., Montvillargenne, France, 1985.

Gelhar, L. W., and C. L. Axness, Three-dimensional stochastic analysis of macrodispersion in aquifers, Water Resour. Res., 19(1), 161-180, 1983a.

Gelhar, L. W., and C. L. Axness, Reply, Water Resour. Res., 19(6), 1643-1644, 1983b.

Glezen, W. H., and I. Lerche, A model of regional fluid flow: Sand concentration factors and effective lateral and vertical permeabilities, J. Int. Assoc. Math. Geol., 17(3), 297-315, 1985.

Gutjahr, A. A., L. W. Gelhar, A. A. Bakr, and J. R. MacMillan, Stochastic analysis of spatial variability in subsurface flows, 2, Evaluation and application, Water Resour. Res., 14(5), 953-959, 1978.

Gutjahr, A. A., and L. W. Gelhar, Stochastic models of subsurface flow: Infinite versus finite domains and stationarity, Water Resour. Res., 17(2), 337-350, 1981.

Hsieh, P. A., S. P. Neuman, and E. S. Simpson, Pressure testing of fractured rocks--a methodology employing three-dimensional cross-hole tests, U.S. Nuclear Regulatory Commission Topical Report NUREG/CR-3213, 1983.

Hsieh, P. A., and S. P. Neuman, Field determination of the three-dimensional hydraulic conductivity tensor of anisotropic media, 1, Theory, Water Resour. Res., in press.

Hsieh, P. A., S. P. Neuman, G. K. Stiles, and E. S. Simpson, Field determination of the hydraulic conductivity tensor of anisotropic media, 2, Methodology and application to fractured rocks, Water Resour. Res., in press.

Hufschmied, P., Estimation of three-dimensional statistically anisotropic hydraulic conductivity field by means of single well pumping tests combined with flowmeter measurements, in Proceedings, International Symposium of the Stochastic Approach to Subsurface Flow, Int. Assoc. Hydraul. Res., Montvillargenne, France, pp. 100-116, 1985.

Huijbregts, Ch. J., Reconstitution du variogramme ponctuel á partir d'un variogramme expérimental regularisé, Rep. N-244, Centre de Morphologie Mathematique, Ecole des Mines de Paris, Fontainbleau, France, July 1971.

Jones, J. W., Structural, hydraulic, and geophysical properties of granite near Oracle, Arizona, M.S. thesis, University of Arizona, Tucson, 1983.

Jones, J. W., E. S. Simpson, S. P. Neuman, and W. S. Keys, Field and theoretical investigation of fractured crystalline rock near Oracle, Arizona, U.S. Nuclear Regulatory Commission Topical Report NUREG/CR-3736, 1985.

Journel, A. G., The deterministic side of geostatistics, J. Int. Assoc. Math. Geol., 17(1), 1-15, 1985.

Journal, A. G., and Ch. J. Huijbregts, Mining Geostatistics, Academic Press, New York, 1978.

Lumley, J. L., and H. A. Panofsky, The Structure of Atmospheric Turbulence, Wiley, New York, 1974.

Matheron, G., The Theory of Regionalized Variables and Its Applications, Ecole des Mines de Paris, Fontainbleau, France, 1971.

Neuman, S. P., Statistical characterization of aquifer heterogeneities: An overview, in Recent Trends in Hydrogeology. T. N. Narasimhan, ed., Geological Society of America, Special Paper, no. 189, pp. 81-101, 1982.

Neuman, S. P., and E. A. Jacobson, Analysis of nonintrinsic spatial variability by residual kriging with application to regional groundwater levels, J. Int. Assoc. Math. Geol., 16(5), 499-521, 1984.

Noble, B., and J. W. Daniel, Applied Linear Algebra, Prentice-Hall, New Jersey, 1977.

Priestley, M. B., Spectral Analysis and Time Series, v. 1, Academic Press, New York, 1981.

Silliman, S. E., Ph.D. dissertation, University of Arizona, Tucson, in preparation.

Vanmarcke, E. H., Random Fields: Analysis and Synthesis, MIT Press, Cambridge, 1983.

Winter, C. L., S. P. Neuman, and C. M. Newman, Prediction of far-field subsurface radionuclide dispersion coefficients from hydraulic conductivity measurements, U.S. Nuclear Regulatory Commission, Topical Report NUREG/CR-3612, 1985.